

Aggregation and post-translational modification of the parathyroid hormone and its agonistic activity towards the G-protein coupled PTH-receptors

Dissertation

zur Erlangung des akademischen Grades
doctor rerum naturalium
(Dr. rer. nat.)

vorgelegt der
Naturwissenschaftlichen Fakultät I
Biowissenschaften
der
Martin-Luther-Universität Halle-Wittenberg

von Mohanraj Gopalswamy

geboren am 19. März 1981 in Vellore, India

Gutachter:

1) Prof. Dr. Jochen Balbach

2) Prof. Dr. Hauke Lilie

3) Prof. Dr. Daniel Huster

Ort und Tag der öffentlichen Verteidigung: Halle (Saale), 28.08.2017

I dedicate this Thesis to

My father

My first Hero

Captain. K. Gopalswamy

My Chemistry teacher

My College time Hero

Dr. D. Gajapathy

My PhD guide

My Research life Hero

Prof. Dr. Jochen Balbach

and
My Family

Table of contents

Contents

1	Introduction	4
1.1	Membrane proteins	4
1.1.1	Peripheral membrane proteins.....	5
1.1.2	Integral membrane proteins.....	5
1.2	G-protein coupled receptors.....	6
1.2.1	Classification of GPCRs	8
1.2.2	Structural studies of GPCR	9
1.3	Parathyroid hormone.....	12
1.3.1	Secretion and storage of Parathyroid hormone	12
1.3.2	Biological function and clinical aspects of PTH.....	13
1.3.3	Structure and functional features of PTH and PTH1R.....	15
1.3.4	Extracellular domain structures.....	17
1.3.5	Mechanism of ligand-receptor interactions.....	19
2	Aim of the project.....	21
3	Materials and methods.....	23
3.1	Chemicals and enzymes	23
3.2	Column materials and columns.....	23
3.3	Stains, plasmids and antibiotics	23
3.4	Various materials and instruments.....	24
3.5	Culture media.....	24
3.6	Transformation by electroporation	25
3.7	SDS-Polyacrylamide Gel electrophoresis.....	26
3.8	Protein concentration determination	26
3.9	Expression, inclusion body preparation and purification of nPTH1R.....	27
3.9.1	Expression	27
3.9.2	Preparation of inclusion bodies.....	28
3.9.3	Inclusion body solubilization	28
3.9.4	Purification of inclusion bodies by IMAC	29
3.9.5	Refolding by pulse renaturation method	29
3.9.6	Hydrophobic interaction chromatography (HIC).....	29
3.9.7	Gel filtration chromatography	30
3.10	Expression and purification of ¹⁵ N-nPTH1R.....	30
3.11	Expression and purification of PTH	30
3.11.1	Expression of PTH (15-34)/(1-34)/(1-84).....	30
3.11.2	Purification of SUMO fusion proteins [PTH (15-34)/(1-34)/(1-84)]....	31
3.11.3	Purification of PTH (15-34) from SUMO fusion proteins.....	32
3.11.4	Purification of PTH (1-34) from SUMO fusion proteins.....	32
3.11.5	Purification of PTH (1-84) from SUMO fusion proteins.....	33
3.12	Expression and purification of ¹⁵ N-PTH, ¹⁵ N/ ¹³ C-PTH.....	33
3.13	Cell line, preparation of lysates and kinase assay.....	33
3.14	cAMP accumulation assay.....	34
3.15	PTH (1-84) fibril preparation and ThT kinetic assay	34

3.16	A β fibrils preparation.....	35
3.17	Fourier-transform infrared (FTIR) spectroscopy	35
3.18	Mass spectrometry and fibril core identification	35
3.19	Transmission electron microscopy (TEM)	35
3.20	Inhibition of fibril growth	36
3.21	Circular dichroism (CD) spectroscopy	36
3.22	Isothermal titration calorimetry (ITC)	37
3.22.1	Theory of receptor binding.....	37
3.22.2	Experimental conditions and parameters	38
3.23	NMR Spectroscopy	39
3.23.1	Sample preparations and measurements	39
3.23.2	NMR titration experiments	41
3.23.3	Pulse field gradient NMR diffusion experiment	42
3.23.4	NMR dynamic experiments	42
3.23.5	Theory of chemical exchange	43
3.24	Solid-state NMR spectroscopy	46
3.24.1	Membrane sample preparation.....	46
3.24.2	² H Solid-State NMR spectroscopy.....	46
3.24.3	¹³ C NMR spectroscopy	47
3.25	NMR experiments for phosphorylation studies	48
3.26	NMR experiments for inhibition of PTH fibrils	48
3.27	Surface Plasmon Resonance (SPR)	49
4	Results.....	50
4.1	The overexpression and purification of nPTH1R	50
4.2	Purification of PTH fragments.....	51
4.2.1	PTH (15-34)	51
4.2.2	PTH (1-34)	52
4.2.3	PTH (1-84)	53
4.3	Functional studies of purified nPTH1R.....	54
4.3.1	Unbound nPTH1R exist as monomer in solution	54
4.3.2	Interaction of ¹⁵ N-nPTH1R with unlabeled PTH (1-84).....	55
4.4	Characterization of PTH (15-34) (antagonist) Interaction with nPTH1R	57
4.4.1	PTH (15-34)-Receptor interaction studied by ITC and NMR	57
4.5	Interaction studies of PTH (1-34) (agonist) with nPTH1R.....	59
4.5.1	ITC studies of PTH (1-34)/nPTH1R complex	60
4.5.2	SPR studies of PTH (1-34)/nPTH1R complex.....	61
4.5.3	NMR interaction studies of PTH (1-34) to the nPTH1R	62
4.6	Competition binding between PTH (15-34) and PTH (1-34) to the nPTH1R	64
4.7	Interaction studies of full length PTH (agonist) with nPTH1R	67
4.7.1	PTH (1-84)/nPTH1R complex studied by CD	67
4.7.2	Thermodynamics of PTH (1-84)/nPTH1R binding by ITC.....	68
4.7.3	SPR analysis of PTH (1-84) binding to nPTH1R	69
4.7.4	Interaction of PTH (1-84) to the nPTH1R studied by NMR.....	70
4.7.5	Dynamic studies of PTH (1-84)/nPTH1R complex	74
4.8	Non-specific interaction of PTH (1-84) to the membrane	75
4.8.1	Interaction of PTH (1-84) to the membranes studied by CD and ITC..	76
4.8.2	Membrane interaction of PTH (1-84) studied by PFG-NMR	77
4.8.3	Identification of membrane binding region in PTH (1-84).....	78

4.9	Solid-state NMR spectroscopy for PTH-membrane interactions	80
4.9.1	Structural studies of PTH-membrane interaction by ¹³ C SSNMR.....	80
4.9.2	Dynamics of membrane upon PTH binding studied by ² H-SSNMR....	82
4.10	Two-step ligand transportation model for binding of PTH to the nPTH1R ...	84
4.11	Phosphorylation of PTH (1-84)	86
4.11.1	Phosphorylation visualized by autoradiography	86
4.11.2	Phosphorylation detected by mass spectrometry	87
4.11.3	Identification of phosphorylation site by NMR	87
4.11.4	Effect of phosphorylation studied my cAMP activity.....	89
4.12	Fibrillation of PTH (1-84).....	90
4.12.1	PTH (1-84) fibril formation	90
4.12.2	Structural characterization of PTH fibrils	91
4.12.3	Identification of the fibril core	93
4.12.4	Inhibition of PTH (1-84) fibril formation by EGCG	94
5	Discussion	97
5.1	Binding mechanism of PTH to the nPTH1R	97
5.1.1	PTH interaction to the membrane	99
5.1.2	PTH binding to the nPTH1R.....	101
5.2	Structural and functional studies of PTH phosphorylation.....	104
5.3	Systematic study of PTH fibril	106
6	Conclusion	109
7	Summary	111
8	Zusammenfassung	113
9	Appendix	116
9.1	CSI for PTH (15-34)	116
9.2	Interaction of PTH (15-34) to the nPTH1R studied by SPR	116
9.3	CD spectra and Heteronuclear NOE for PTH (1-34).....	117
9.4	CSI for full length PTH (1-84)	118
9.5	Binding of PTH (1-84) to the nPTH1R in the presence of POPG vesicle....	119
10	Abbreviation	120
11	Bibliography.....	121
12	Resume	133
13	Publications.....	134
14	Declaration (Erklärung)	136
15	Acknowledgements.....	137

1 Introduction

1.1 Membrane proteins

Cell is the fundamental unit of function in all organisms. All the living cells are surrounded by a cell membrane or plasma membrane. The cell membranes are essential for the integrity and function of the cell. The membrane acts as an insurmountable barrier for the continual flow ions and metabolites into or out of the cell to maintain many of life's processes. The plasma membrane is mainly composed of a bilayer of various lipids and specific proteins. The plant cell has a rigid cell wall and an animal cell membrane is a flexible lipid bilayer. The lipids in the cell's plasma membrane are chiefly phospholipids like phosphatidyl ethanolamine and cholesterol. The proteins which are attached to the cell membrane can vary depending on cell type and subcellular location. The fluid mosaic model of the cell membrane with embedded proteins and a lipid bilayer is shown in **Fig. 1.1** (Singer and Nicolson 1972; Lodish et al. 2000).

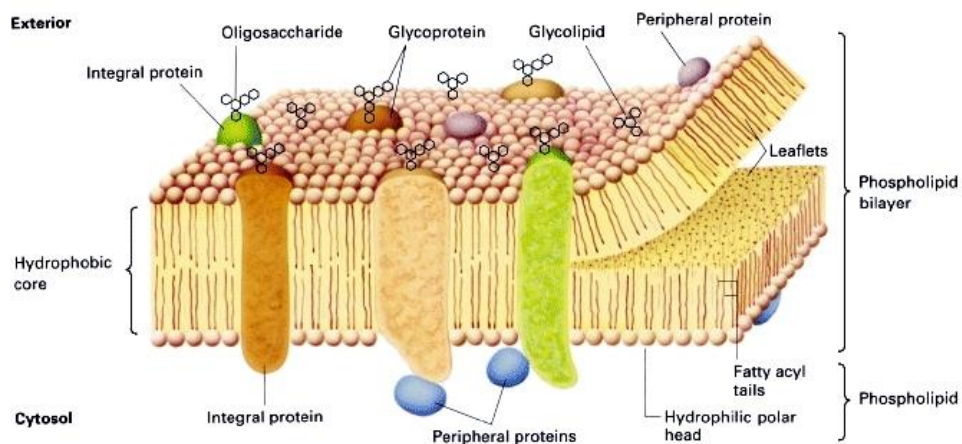


Fig. 1.1 Schematic diagram of typical membrane proteins in a biological membrane. Picture has taken from the text book, title: Molecular Cell Biology, by Lodish and co workers (Lodish et al. 2000)

The key to understanding the function of the cell membrane lies in the understanding of proteins in it. Some proteins are bound only to the membrane surface, whereas others have one region buried within the membrane and other regions are exposed interior and/or exterior face of the membrane. Protein or their domains on the extracellular membrane surface are generally involved in cell-cell signaling or interactions. Protein

domains are on the exterior face of the plasma membranes are involved in many functions, from anchoring cytoskeletal proteins to the membrane to triggering intracellular signaling pathways. In many of the cases, the basic function of membrane protein and their topology in the membrane can be predicted based on well-studied homology proteins. Membrane proteins are divided into two broad categories, integral (intrinsic) membrane proteins and other is peripheral (extrinsic) membrane proteins. This classification is based on the nature of the protein-membrane interactions (Lodish et al. 2000).

1.1.1 Peripheral membrane proteins

Peripheral membrane proteins (or extrinsic proteins) are proteins that do not penetrate the bilayer to any significant degree and are associated with the membrane, mainly through ionic interactions and hydrogen bonds between the membrane surface and the membrane embedded protein. They do not interact with the hydrophobic core of the phospholipid bilayer. Peripheral proteins are weakly associated with membrane surface and they can dissociate from the membrane by high salt concentrations and changes in pH. Cytoskeletal proteins such as spectrin, actin in erythrocytes and the enzyme protein kinase C are some of the peripheral proteins localized to the cytosolic face of the plasma membrane. This enzyme shuttles between the cytosol and the cytosolic face of the plasma membrane and plays a role in signal transduction. Certain proteins like extracellular matrix proteins are localized to the outer surface of the plasma membrane (Lodish et al. 2000).

1.1.2 Integral membrane proteins

Integral membrane proteins (or intrinsic proteins) are characterized by one or more hydrophobic domain(s) that are embedded in the phospholipid bilayer. The hydrophobic side chains of the integral membrane protein interact with fatty acyl groups of the membrane bilayer, thus anchoring the protein to the membrane. Polar domains of the integral membrane proteins flank these apolar segments. Most integral proteins span the entire phospholipid bilayer (Lodish et al. 2000). Furthermore, polypeptides with identical sequences can span the membrane differently (Ott and Lingappa 2002). The transmem-

brane proteins contain one or more membrane-spanning domains as well as domains, from four to several hundred residues long, extending into the aqueous medium on each side of the bilayer. Integral membrane proteins are classified into two classes based on the structure of the membrane spanning segments. Protein with transmembrane sections, which contain an α helical structure falls in the first category. The length of this helix is from 17 to 25 amino acid residues. For example, hormone receptors (as discussed later in detail), Na^+ , K^+ -ATPase, cytochrome oxidase and ion channels and gates contain α helix at the transmembrane segments. The other classes of transmembrane proteins contain only β sheets at the transmembrane segments. Mitochondrial outer membrane protein called porins or voltage-dependent anion channel (VDAC) is a well know example for β sheet structures. Solution NMR structure of VDAC reconstituted in detergent micelles forms a 19-stranded β barrel fold (Hiller et al. 2008). In contrast to an α helical or β sheets structures at the transmembrane segments some integral membrane proteins are anchored to the membrane leaflets by covalently bound fatty acids. In this case, the polypeptide chain faces towards the hydrophilic region and the bound lipids are embedded in the membrane bilayer. For example, Thy-1 protein and alkaline phosphatase are anchored by glycosylphosphatidylinositol, Ras protein is anchored through farnesyl and palmitoyl groups (Lodish et al. 2000).

1.2 G-protein coupled receptors

The superfamily of guanine nucleotide-binding protein (G-protein)-coupled receptors (GPCRs) or seven transmembrane receptors are the largest families of integral membrane proteins. This family consisting of approximately 1000 members exhibits the extraordinary structural diversity in natural agonist ligands. GPCRs play a major role in many physiological functions, including cell-cell communication, cell differentiation, metabolism or synaptic transmission. Indeed, GPCR constitutes approximately 50% of the human drugs currently marketed. The annual market revenue at 2013 was about 100 billion dollar and a market analyst predicts 114 billion dollars by 2018 (Ezer 2014). However, these drugs target only a small fraction (about 10%) of known GPCRs (De Amici et al. 2010). GPCRs mediate cellular actions to a diverse range of endogenous ligands (e.g., biogenic amines, peptides, glycoproteins, lipids, nucleotides, nucleosides,

ions, and proteases) and exogenous environmental agents, such as light, odors, and taste (**Fig. 1.2**). The agonist bound GPCR, leading to its interaction with heterotrimeric G proteins. The activated GPCR catalyses the exchange of GDP for GTP on the $G\alpha$ subunit and dissociates the $G\alpha$ and $G\beta\gamma$ subunits from each other and from GPCR. Activated $G\alpha$ subunits subsequently bind to and regulate the activity of effectors, which is typically an enzyme (e.g., adenylate cyclases) or ion channel (e.g., potassium and calcium channel) and produces small molecule second messengers such as cAMP, diacylglycerol, and inositol-1,4,5-trisphosphate (Gether 2000).

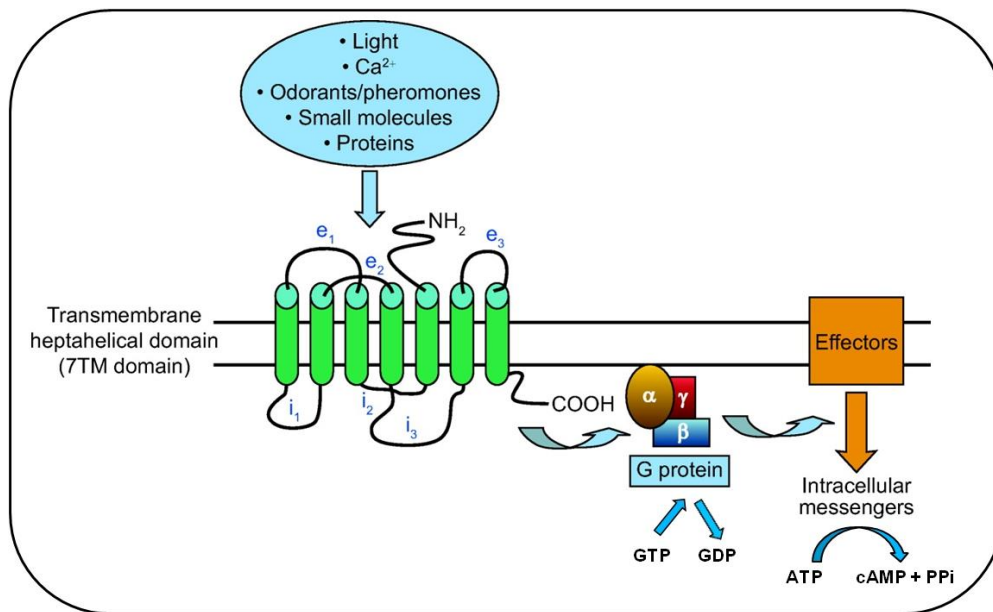


Fig. 1.2. The classical view of G protein-mediated signaling by GPCRs. All GPCRs possess seven transmembrane helices (7TM) and can comprise an extracellular N-terminal domain and an intracellular C-terminal domain. The 7TM are connected by three intracellular loops (i_1 - i_3) and three extracellular loops (e_1 - e_3). GPCRs are activated by many of endogenous ligands such as hormone, ions, lipids, proteins and exogenous stimuli like light, odors and taste. The activated receptor catalyses the exchange of GDP for GTP on the $G\alpha$ subunits and dissociates into a GTP-bound $G\alpha$ subunit and $G\beta\gamma$ heterodimer. Activated GTP-bound $G\alpha$ subunits bind to and regulate the activity of effectors such as adenyl cyclase that control intracellular messengers like cyclic AMP. The picture is modified from Bridges and co-worker (Bridges and Lindsley 2008).

The GPCR family exhibits conserved seven transmembrane helices (7TM), an extracellular N-terminal domain and an intracellular C-terminal domain. The 7TM are connected by three intracellular and three extracellular loops. The helical domain is embedded in the membrane which is generally hydrophobic in nature. The intracellular and extracellular loops, both N and C terminus are generally hydrophilic, and it is exposed to the water-rich environments. The length of the helices is varied from 17 to 25 amino acids

long, while the loops and terminus can vary widely in length up to hundreds of amino acids.

1.2.1 Classification of GPCRs

The signaling functions of a large variety of extracellular stimuli are mediated through GPCRs. Sequencing of the human genome has revealed nearly 1000 human genes that encode G protein-coupled receptors. GPCRs generally consist of a single polypeptide chain of the length of 400 to 3000 amino acids. This contains the variable size of the extracellular N-terminal domain from 7 to 3000 amino acids, an intracellular C-terminal domain from 12 to 400 amino acids, three endoloops and three exoloops to the size of each 5 to 250 amino acids (Ruiz-Gomez et al. 2010). Except for the highly conserved 7TM helical domain, all other domains vary substantially among GPCRs. The superfamily of GPCRs has been classified into six families (family A to F) based on sequence similarity and functional roles (Kolakowski 1994). The most common division is into three main families (or classes): A, B, and C. The rhodopsin-like or β -adrenergic receptor-like family (class A), glucagon receptor-like or secretin receptor-like (class B), metabotropic glutamate receptors (class C).

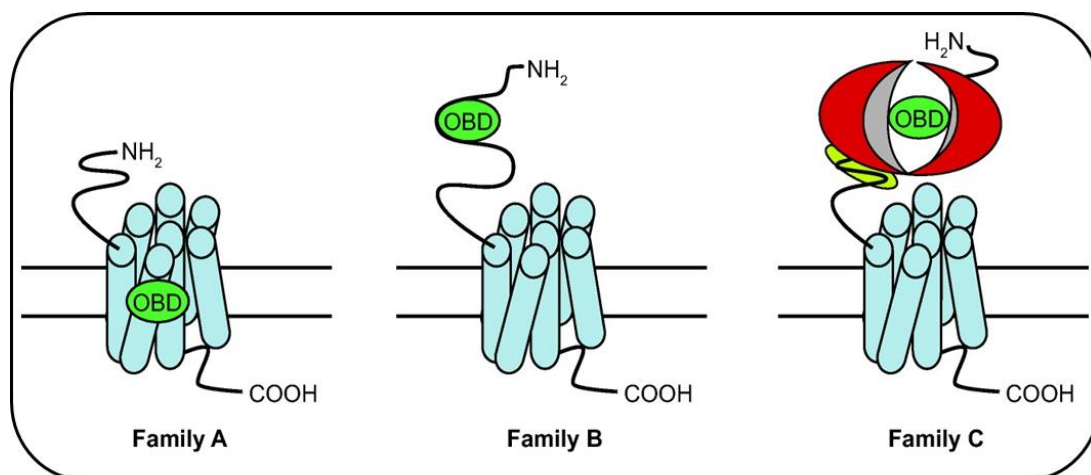


Fig. 1.3. Schematic diagram of the three major families of GPCRs. The orthosteric binding domain (OBD) of each class of GPCRs is shown in green. The OBD is located at 7TM, N-terminal domain and the extracellular Venus-flytrap like domain for Class A, B and C GPCRs, respectively.

These major families are readily identified by their ligand binding domain, the family B has a large extracellular N-terminal domain and family C has a long extracellular N-terminal “Venus-flytrap” like domain. The orthosteric binding domain (OBD) is located

at the 7TM for class A GPCRs, whereas the OBD is located in the N-terminal domain of class B. For class C it is located within the extracellular Venus flytrap-like domain shown in **Fig. 1.3**. Class A or rhodopsin-like receptors contain approximately 675 receptors which include 375 olfactory receptors. This family is by far the largest, comprises receptors for odorants, small molecules such as catecholamines, lipid-like substances, some peptides, glycoproteins, and nucleotides. The receptor-activating ligands of class A family typically dock within the heptahelical transmembrane bundle at the level of the lipid bilayer.

1.2.2 Structural studies of GPCR

First high-resolution crystal structure of GPCR, that of bovine rhodopsin (pdb code 1F88) was solved by Palczewski and colleagues in 2000 (Palczewski et al. 2000). This structure confirmed that the existence of a canonical 7TM alpha-helical bundle which is arranged in an anticlockwise manner when seen from the extracellular side of the cell membrane. Furthermore, these crystal studies show that several of conserved amino acids within the rhodopsin family involved in interhelical networks that play a critical role in the stabilization and activation of rhodopsin (Palczewski et al. 2000). At the beginning, the crystal structure of bovine rhodopsin provided a framework for pharmacophore-based drug design for the entire GPCR family. However, this structure fails to provide information about the molecular mechanism of G protein coupling homologs, because the receptor was locked into its rigid state by an inverse agonist, 11-cis-retinal.

After rhodopsin structure, seven years later next GPCR structure, human β 2-adrenergic receptor was solved by Cherezov, Kobilka and coworkers (Cherezov et al. 2007; Rasmussen et al. 2007). Brian K. Kobilka received the Nobel Prize in Chemistry 2012 for unraveling the molecular studies of GPCR. Generally, GPCRs exhibit conformational flexibility in the absence of ligands, which making them notoriously difficult to crystallize. Kobilka and coworkers circumvented this problem by replacing intracellular loop 3 with the rigid structural domain of T4 lysozyme (pdb code 2RH1) or by making a complex with Fab fragment (pdb 2R4R). Both of β 2-adrenergic receptors were solved in the presence of partial inverse agonist, carazolol, which is again locked in an inactive state

like 11 *cis* retinal for rhodopsin. These two model template structure for GPCRs diverge primarily in the transmembrane helix (TM) 1, TM3, TM4, TM5 and TM6 regions. A major difference was seen in TM1, that is, a proline-induced kink in the TM1 was present in rhodopsin and was absent in β 2-adrenergic receptor (β 2AR) (Tesmer 2010).

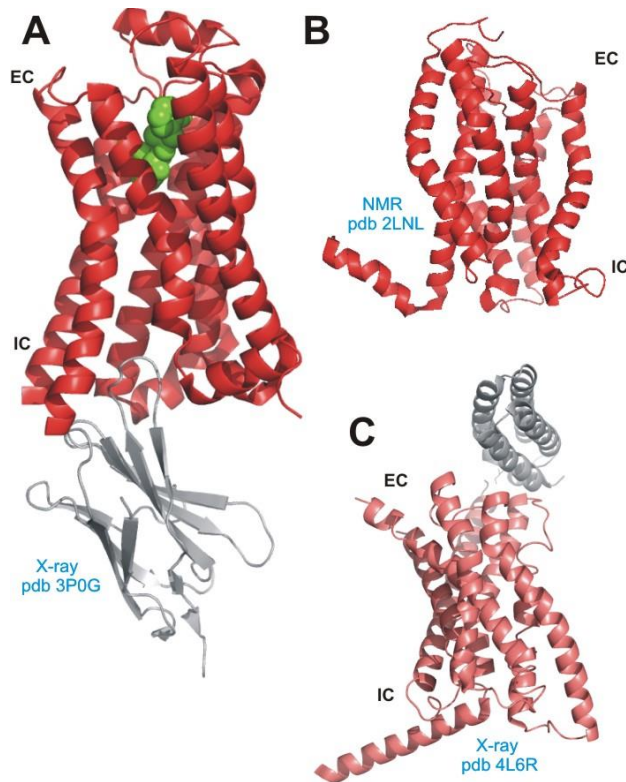


Fig. 1.4. Structure of 7TM domain of GPCR. (A) Crystal structure of nano-body (NP80) stabilized (in gray) BI-167107, an agonist (in green) bound to human β 2 adrenoceptor (in red), the active conformation of class A GPCR (pdb 3P0G). (B) NMR structure of human chemokine receptor CXCR1 in DMPC liquid crystalline phospholipid bilayers (pdb 2LNL). (C) X-ray crystal structure of class B GPCR of human glucagon receptor (red) fused to the thermally stabilized apocytochrome b562 RIL (gray).

Unlike the structural determination of inactive GPCRs either with the antagonist or inverse agonist, the active state of GPCR requires both agonist

and G α subunits. Due to the biochemical challenges on working with agonist-receptor-G protein complex Rasmussen and coworkers used camelid antibody fragment that behaves like G protein. This functional antibody or a nano-body (Nb80) preferentially binds to and stabilizes the active conformation of GPCR shown in **Fig. 1.4A**. There are subtle differences in the binding groove between agonist and antagonist/inverse bound states. The major difference between the active and inactive state of GPCR is coming from TM6, with an 11.4 Å outside movement of the helix. In addition to that, significant structural changes were seen in the cytoplasmic regions of TM5 and TM7 that reflect binding on Nb80 and G protein (Rasmussen et al. 2011).

First solution NMR structure of GPCR was solved by Gautier and group members in 2010. Seven helical TM receptor sensory rhodopsin II was determined in detergent diheptanoylphosphatidylcholine (DHPC). The protein-detergent complex was estimated

to be 70 kDa. The overall topology of solution NMR structure has a close agreement with crystal structure with root mean square deviation of 1.23 Å for backbones (Gautier et al. 2010). Other NMR structure of human GPCR was reported for chemokine receptor CXCR1 in liquid crystalline phospholipid (DMPC) bilayers (Park et al. 2012) shown in **Fig. 1.4B**. Recently many crystal structures were determined for GPCRs by modifying receptor either mutation, fusion with T4 lysozyme or addition of antibody. However, NMR structure was solved without any modification of its primary sequence and under physiological condition. Compared to the crystal structure of CXCR4, NMR structure is significantly similar. But the notable difference for CXCR1 is a well-defined helix at the C terminus that is absent in the crystal structure. This helix has amphipathic amino acids that align along the membrane surface, revealed that bilayers may have stabilization effect of its conformer (Park et al. 2012). More recently backbone dynamics of β 1-adrenergic receptor (AR) in complex with six ligands and the apo form were studied by NMR. The efficacy of antagonist, inverse agonist and agonist ligands and their allosteric motion towards TM (mainly TM5) were analysed by using TROSY (transverse relaxation-optimized spectroscopy) spectra of selectively ^{15}N labeled variant of β 1AR (Isogai et al. 2016).

High resolution crystal structure of human glucagon receptor that belongs to class B GPCR family was resolved that shown in **Fig. 1.4C**. The glucagon receptor is a potential drug target for type 2 diabetes. Secretin-like family lack protein sequence conservation with known structures of class A family. The receptor was fused to the thermally stabilized apocytochrome b562RIL (gray in **Fig. 1.4C**) and crystallized alone with the antagonist ligand NNC0640. Helical bundles of 7TM are conserved between class A and B families (**Fig. 1.4**). However the major difference was observed for the TM1 that is longer (about 16 Å) towards EC than any known structure of class A GPCRs. This may facilitate glucagon binding and define the orientation of ECD. Another significant difference was seen at the C-terminus, where helix 8 is tilted approximately 25° away from the membrane compared to the known structures (Siu et al. 2013).

Till December 2016, 172 structures were solved including class A, class B and orphan family receptors (www.gpcrdb.org). Some of them are, rhodopsin (28 structures), hu-

man β 2-adrenergic-receptor (15 structures), Turkey β 1-adrenergic-receptor (14 structures), human α 1 adenosine receptor (11 structures), human chemokine receptor, human dopamine receptor³, Human histamine receptor 1, human M3 muscarinic acetylcholine receptor, human opioid receptor, human nociceptin/orphanin FQ receptor, human protease-activated receptor 1, Neurotensin receptor, human chemokine receptor type 1, human M2 muscarinic acetylcholine receptor, sphingosine 1-phosphate receptor, corticotrophin releasing factor receptor 1, human glucagon receptor, human smoothed receptor (2structures), 5-hydroxytryptamine receptor, CCR5 chemokine receptor (Palczewski et al. 2000; Cherezov et al. 2007; Rasmussen et al. 2007; Huang et al. 2013; Jianyi Yang and Zhang 2014).

1.3 Parathyroid hormone

Parathyroid glands secrete parathyroid hormone (PTH) that regulates calcium homeostasis. The parathyroid glands were discovered in the 19th century. In 1880, Sandström was the first to described that the function of the glands was distinct and a separate entity from thyroid (Boothby 1921). After a long 25 years intense debate about the function of parathyroid glands, in 1925 J. B. Collip revealed the principle physiological role of glands in calcium regulation by extracting active parathyroid glands from oxen (Collip 1925). From 1925 to late 1970s metabolic studies were performed to understand the implications of an excess or deficiency of the parathyroid hormone.

1.3.1 Secretion and storage of Parathyroid hormone

Human parathyroid hormone produced as a prepropeptide (**Fig. 1.5**) containing 115 amino acids. The 25 amino acid presequence or signal peptide is cleaved by signal peptidase within the endoplasmic reticulum and converted into pro-PTH. The 84 amino acid mature PTH is produced after trafficking into Golgi apparatus. Then the mature



Fig. 1.5. Primary sequence of human PTH. The Pre or signal sequence (in black), pro region (in blue) and mature PTH (in green).

PTH is stored into secretory granules and, depending on the concentration of calcium PTH is released into the blood (Datta et al. 2007). It has been reported that peptide and hormones found in the pituitary secretory granules of the endocrine system are stored in the form of functional amyloids. Furthermore, few hormones like glucagon, insulin and PTH tend to form amyloid fibrils under certain *in vivo* and *in vitro* conditions (Kedar et al. 1976; Maji et al. 2009). Often, mutations result in the accumulation of a conformationally defective protein in the ER which contributes to diseases such as Alzheimer's, Parkinson's, Huntington's, or type 1 diabetes (Mattson et al. 2001). C18R mutation in the pre sequence of pre-pro-PTH disrupts the hydrophobic core of the signal sequence leading to intracellular accumulation and causes the familial isolated hypoparathyroidism (Ahn et al. 1986). Investigation on storage of peptide hormones may help to understand hormone release and also cell apoptosis.

1.3.2 Biological function and clinical aspects of PTH

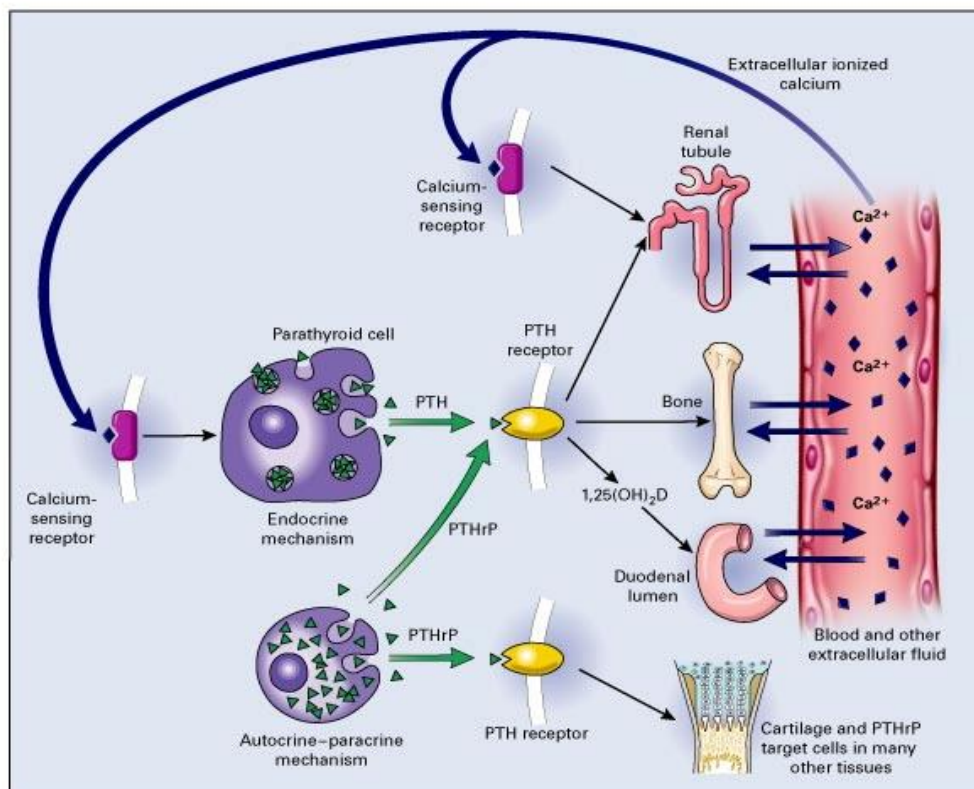


Fig. 1.6. Calcium homeostasis in blood. Production of PTH and PTHrP is shown on the left, and their biochemical process (blue double side arrows) shown on the right. PTH is rapidly secreted from parathyroid gland in response to decrease in calcium in the blood (long blue arrow). Both hormone binds and activated (green arrow) by PTH receptor (yellow). PTH regulates calcium concentration from bone, kidney and intestine. Phosphate homeostasis of PTH are not shown in the picture. PTHrP regulate cell proliferation and differentiation programs in developing tissues (Marx 2000).

Osteoporosis is a progressive skeletal disease in which bones become thin, weak, brittle, and prone to fracture. The World Health Organization (WHO) declares osteoporosis to be second largest diseases next to cardiovascular diseases as a critical health problem (Piscitelli et al. 2008). Calcium and other minerals help strengthen and protect bones. PTH is the primary regulator of calcium and phosphate in the bones (**Fig. 1.6**). Calcium-sensing receptor on the surface of the parathyroid gland cells was capable of sensing small changes in the serum calcium concentration. Within seconds, PTH secretion is stimulated by the action of low calcium level. The set point for PTH secretion is 1 mmol per liter (Marx 2000). PTH thereby regulates large calcium fluxes across bone, kidneys, and intestines (small blue arrows in **Fig. 1.6**). In the kidney, PTH reduces calcium excretion by increasing calcium reabsorption in the renal tubule. Furthermore, PTH also prevents phosphate reabsorption in the kidney to maintain phosphate homeostasis. PTH act both anabolic (to stimulate bone formation) and catabolic (release calcium from bone) action on bones. The other important function of PTH is the conversion of inactive vitamin D to its most active vitamin D (Gensure et al. 2005). Like PTH, PTH related peptide (PTHrP) binds and activates same the PTH1R (see more on section 1.3.3). Along with calcium and phosphate regulation, PTHrP plays a vital role in organ development, tissue proliferation and muscle tone (**Fig. 1.6**) (Guerreiro et al. 2010).

Primary hyperparathyroidism is caused due to high serum parathyroid hormone and hypercalcemia. This causes bones to release calcium constantly leads to Osteoporosis. Furthermore, over production of PTH or degradation production of PTH influence the mean arterial blood pressure (Lehmann et al. 2009). Inadequate production of PTH reduces the calcium level in the blood (hypocalcemia) and causes hypoparathyroidism (Kim and Keating 2015). About 13% of total American population is affected by chronic kidney disease and PTH is implicated as one of the causes of this disease (Naud et al. 2012). Bioengineered PTH (1-84) is approved by FDA in 2007 and EMA in 2013 for hypoparathyroidism (Kim and Keating 2015). In 2002, the FDA approved PTH (1-34) and in 2006, EMA approved PTH (1-84) has drugs for the treatment of osteoporosis (Piscitelli et al. 2008). Other forms of truncated PTH, PTH (1-31), PTH (1-36) and PTH (1-38) have been studied for the treatment of osteoporosis (Pietrogrande 2010; Kim and

Keating 2015). Understanding structural features of PTH are important to discover new therapeutic drugs.

1.3.3 Structure and functional features of PTH and PTH1R

Parathyroid hormone (PTH) receptor 1 (PTH1R) and 2 (PTH2R) belong to the class B subfamily of GPCRs and function as agonist receptors for peptide hormones including PTH, PTH related peptide (PTHrP) and tuberoinfundibular peptide (TIP) (**Fig. 1.7A**). Both PTH1R and PTH2R contain a large N-terminal domain (NTD) with 6 highly conserved cysteine residues, 7 transmembrane helices (TM), and a large C-terminal domain. The TMs are connected by 3 intracellular and 3 extracellular loops (**Fig. 1.7B**). Both receptors share about 50% sequence identity (Grauschopf et al. 2000). When extracellular agonists bind to the receptors they switch from the inactive to the active form. The signaling cascade, *via* heterotrimeric G proteins, modulates the flow of secondary messengers, including inositol trisphosphate, diacylglycerol, cGMP or cAMP (Gilman 1987). These secondary messengers activate the intracellular signaling pathways, which in turn modulate cell function, including the skeletal, endocrine, and cardiovascular or nervous systems (Gensure et al. 2005).

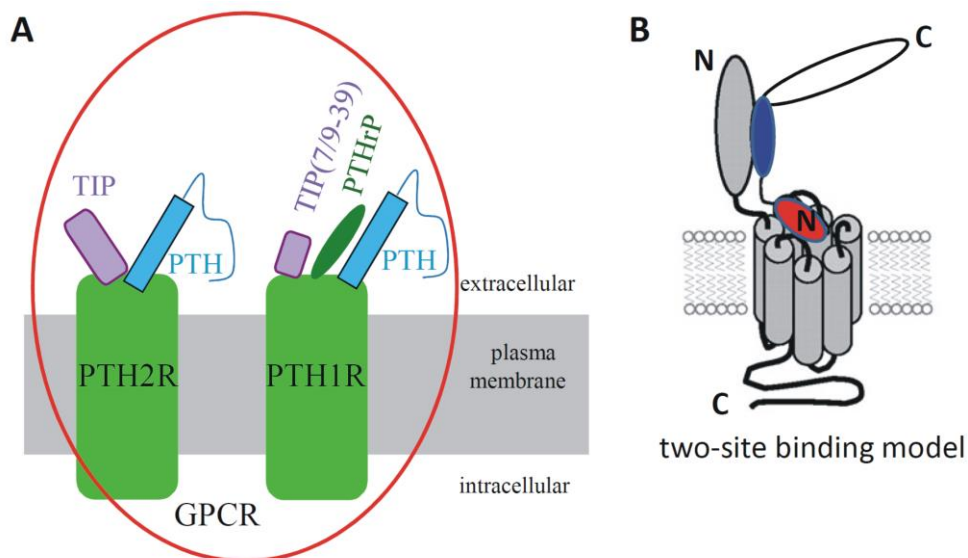


Fig. 1.7. Ligands and receptors in the PTH signaling system and its binding mode. (A) PTH and PTHrP bind and activate the same PTH1R. PTH and TIP bind and activate the same PTH2R. N-terminal truncated TIP peptide act as an antagonist for PTH1R. (B) Proposed two-site binding model based on mutation and cross-linking data. N-terminus of the PTH peptide (~1-10) binds to TM of PTH1R, the middle part (~15-34) interacts with ECD-PTH1R. The function of C-terminus of PTH (~40-84) is not known.

PTHrP has been identified from certain malignant tumors and released to blood stream at high concentration with the majority of the patients with malignancy associated hypercalcemia. In human, PTHrP is produced as one of three isoforms of 139, 141 or 171 amino acids (Burtis 1992). PTH and PTHrP are known to act on PTH1R in kidney and bone to conserve calcium. PTH (18nM) and TIP binds (0.59 nM) and stimulates another receptor, PTH2R, expressed in the human brainstem (Hoare and Usdin 2000; Goold et al. 2001). However, PTHrP do not respond to PTH2R and TIP ligand do not act on PTH1R. Interestingly, N-terminal truncated TIP ligand, TIP (7-39) or TIP (9-39) is a high affinity (6nM) antagonist for the PTH1R, while losing much of its affinity for the PTH2R (**Fig. 1.7A**) (Hoare and Usdin 2000). PTH (7-34) (45nM), PTHrP (7-36) (65nM) and several analogs of these peptides are PTH1R antagonists (Gardella et al. 1996). Hence, the receptor selectivity is confined to the N-terminus.

The shorter analogues of PTH/PTHrP (1 to 34 residues) bind and stimulate PTH1R in an analogous manner to the “two-site model” (**Fig. 1.7B**), also shown for other class B GPCRs (Mann et al. 2008). This model is mainly based on mutational and crosslinking studies. According to this model, N-terminal domain of PTH1R (nPTH1R) binds to the C-terminal part of PTH (1-34) (blue in **Fig. 1.7B**) and N-terminal part of PTH (1-34) (red in **Fig. 1.7B**) interact with the transmembrane helix to activate the receptor (Gardella and Juppner 2001; Gensure et al. 2005).

The function of GPCRs is modulated by receptor activity-modifying proteins (RAMPs1, -2, -3). All three human RAMP proteins (~160 amino acids) consist of a large NTD (**Fig. 1.8**), and a single TM and a small C-terminal tail. It has been reported that PTH1R selectively interact with RAMP2, while the PTH2R selectively interacts with RAMP3 (Kuwasako et al. 2009). But the detailed molecular mechanism is not known.

Sequence homology between PTH (1-34) and PTHrP (1-34) contain 11 identical residues, whereas TIP shares 2 identical residues with PTH and PTHrP in the sequence alignment (Gensure et al. 2005). NMR and X-ray studies have been carried out for these ligands in the range of buffers, micelles, and trifluoroethanol (TFE). NMR and CD studies exhibit nascent structure in water, which are stabilized by micelles or TFE. The N-

terminus (~1-10 residues), C-terminus (~15-34 residues) of the peptide ligands forms an α -helix and these two helical regions are linked by a flexible hinge region. However, X-ray data for PTH (1-34) exhibit a long helix with a slight bend in the middle (Oldenburg et al. 1996; Barden et al. 1997; Pellegrini et al. 1998; Jin et al. 2000; Mason et al. 2005).

1.3.4 Extracellular domain structures

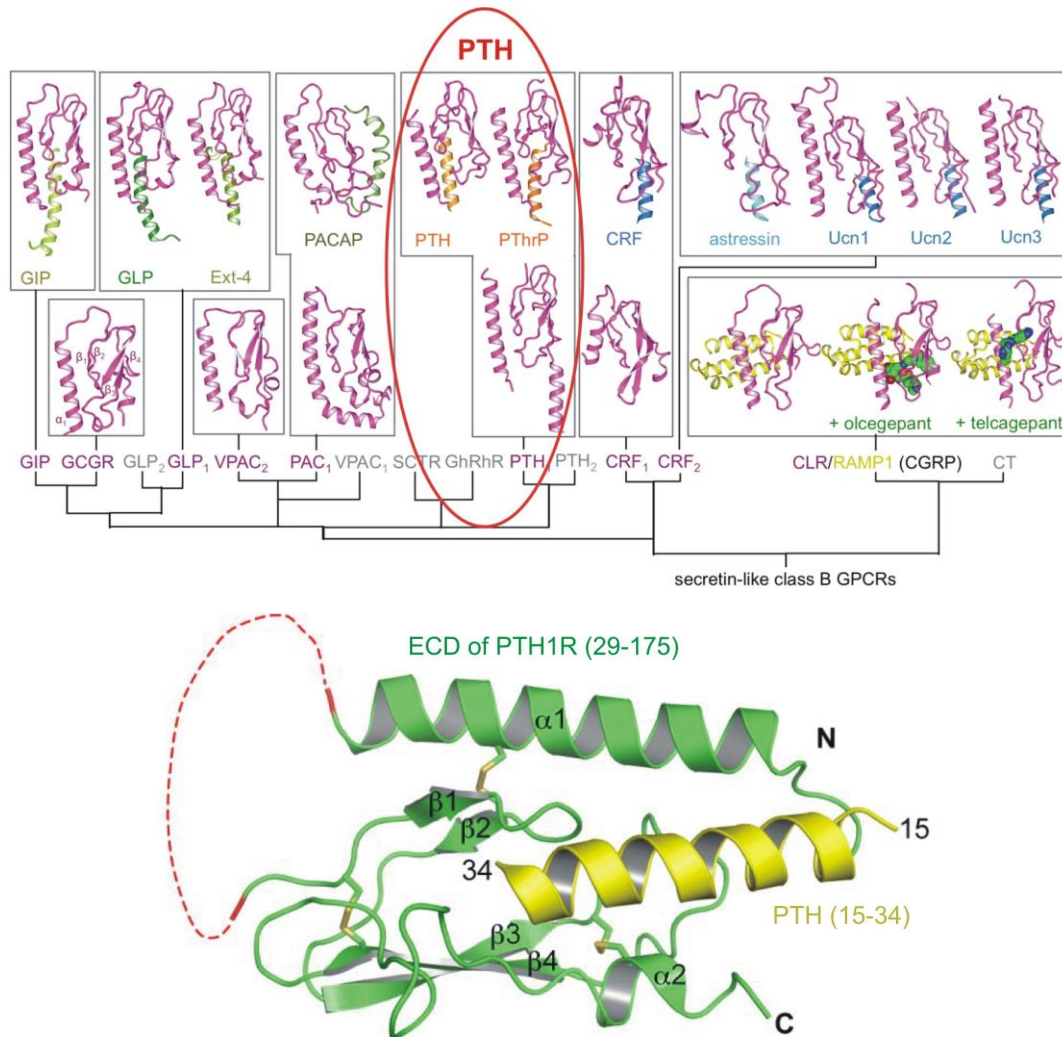


Fig. 1.8. Structures of class B GPCR ECDs and their ligands bound to the ECDs. Upper panel: The C-terminal region of the peptide interacts with the extracellular domain of class B GPCRs. Available X-ray and NMR structures of ECDs (magenta) and in complexes with their cognate peptide hormones (different colors), also ECDs in complexes with RAMP (yellow) proteins (upper). Structures for PTH/PTHrP family are shown inside the red circle. All nine known N-terminal domain complex structures of the class B GPCRs exhibits an α - β - β - α fold with conserved residues containing 3 disulfide bonds. Lower panel: A representative crystal structure for PTH (15-34) ligand (yellow) bound to ECD of PTH1R (green) showing the α - β - β - α fold and the disulfide bonds depicted as sticks. The dashed line represents a disordered loop region (Pioszak and Xu 2008; Holtenstein et al. 2014).

All members of the class B GPCR family have a large N-terminal domain that is about 120 to 180 amino acids long. Ligands that activate these receptors are peptide hormones with a length of about 26 to 110 amino acids. The basic signal transduction starts when the peptide ligand binds to the extracellular domain of the receptor. In the past 10 years, 9 different ligand-ECD complex structures have been solved by both X-ray and NMR techniques. The N-terminal domain of the receptors and either in complex with their cognate peptide ligands (gastric inhibitory polypeptide (GIP), glucagon-like peptide (GLP), exendin-4, pituitary adenylate cyclase-activating polypeptide (PACAP), corticotropin-releasing factor (CRF), stressin, urocortin (Ucn), vasoactive intestinal polypeptide, PTH and PTHrP, Vasoactive intestinal polypeptide (VIP), calcitonin (CT), PTH and PTHrP) or in complex with RAMP proteins was shown in **Fig. 1.8** (Grace et al. 2007; Sun et al. 2007; Pioszak and Xu 2008; Runge et al. 2008; Parthier et al. 2009; Pal et al. 2010; Pioszak et al. 2010; Kumar et al. 2011; Siu et al. 2013; Culhane et al. 2015). Most of the complexes were crystallized along with the fusion-tag due to the high disorder regions in the ECDs. Many of these peptide hormones are disordered, however they adopt α helical conformations in the ECD bound form. All these structures reveal that the N-terminal domain contains an α - β - β - α fold with the helical segment of the peptide hormone primarily interacting in the middle layer as a “hotdog in a bun” (Parthier et al. 2009). Furthermore, all the ECDs are stabilized by 3 disulfide bonds (depicted as a stick in **Fig. 1.8**). However, there are a few differences between the various ECD structures, which may give a hint to the ligand specificity. For example, the N-terminal α -helix is absent in the solution NMR structure of the N-terminal domain of the CRF 2 receptor (Grace et al. 2004) and it is conserved in most X-ray structures. The same N-terminal helix is shorter in the CRF 1 receptor (Pioszak and Xu 2008).

The N-terminal 34 residue fragments of PTH or PTHrP is sufficient enough to bind and activate the PTH1R. It is known that the N-terminal part of a peptide ligand (residues 1-14) interacts with the TM domain and the C-terminal part of the ligand (residues 15-34) binds to the nPTH1R (Gensure et al. 2005). The N-terminal domain of the PTH1 receptor (29-187) was crystallized with fusion tag (maltose binding protein) in the absence and in complex with PTH (15-34) or PTHrP (12-34) (Pioszak and Xu 2008; Pioszak et al. 2009; Pioszak et al. 2010) (**Fig. 1.8**). Like other extracellular domains of class B

GPCR, nPTH1R has a conserved α - β - β - α fold. This fold is believed to be stabilized by the 3 disulfide bonds and the 5 conserved residues (Asp113, Trp118, Pro132, Gly152, and Trp154) throughout the class B GPCR family. Analytical ultracentrifugation experiments showed that the nPTH1R in solution is a monomer (Grauschopf et al. 2000), but it is a dimer in the X-ray studies (Pioszak et al. 2010). In the dimer structure, the endogenous peptide binding groove is occupied by the C-terminal fragment of ECD. However, mutations at Arg-179, Val183, L187 residues which are present at the peptide binding site disrupt the dimer and this mutant monomer retained wild-type PTH binding and cAMP activity (Pioszak et al. 2010). PTH (15-34) and PTHrP (12-34) exhibit similar binding affinities for the nPTH1R. Both the ligands are disordered in free form and adopt an α helix in the ECD bound state. These two different ligands bind at the same binding groove of the ECD with subtle changes in the local conformation. However, the notable differences are at the C-termini of the ligand. PTH forms a continuous α helix from residues L15 to F34, whereas PTHrP helix extends from I15 to I31. Another difference is that PTHrP helix gently curves in respect to the helical axis (Pioszak and Xu 2008; Pioszak et al. 2009).

1.3.5 Mechanism of ligand-receptor interactions

Earlier in 1986, Sargent and Schwyzer derived a model for catalysis of ligand-receptor interaction. They proposed multiple sequential steps rather than direct ligand-receptor interactions. It includes surface accumulation of charged ligands, ligand-membrane interactions, and ultimately binding to the receptor itself (Sargent and Schwyzer 1986; Schwyzer 1986). Ligand binding to the membranes leads to the conformational change of the ligand and this is believed to be the bioactive conformation of the ligand, then it binds to the target receptor. This model was also proposed for other class B GPCR ligands like VIP, PACAP, and PTH. Earlier in 1974, it was shown that the VIP ligand interacts to the isolated liver-cell membranes of a rat with the dissociation constant of 0.17 nM and stimulates the activity of adenylate cyclase in these membranes (Desbuquois 1974). Furthermore, VIP in phospholipid micelles (with ethylene glycol and distearoyl phosphatidylethanolamine (DSPE)) showed ~3 fold more potent vasodilation relative to that evoked by aqueous VIP alone (Onyuksel et al. 1999). The solution

NMR structure of PACAP in the membrane and its receptor (PACAP receptor) partly confirmed a two-step model (Inooka et al. 2001). In the case of PTH, a nonspecific interaction of PTH to the membrane induces an α helix confirmation, followed by two-dimensional diffusion leading to highly specific, ligand-receptor interaction (Pellegrini et al. 1998a). There are several other examples in the literature reported that the ligand interaction to the membrane alters the structural and/or functional properties (Moroder et al. 1993; Onyuksel et al. 1999; Yamamoto et al. 2008).

Several structures of GPCRs or extracellular domains in complex with their cognizant ligand have been reported. Despite this detailed structural and functional knowledge on receptor and ligand interactions a clear cut mechanism of the mode of ligand interaction with its receptor remains elusive. Whether the ligand directly interacts with the receptor (one step binding model) or first interacts with the membrane followed by guiding towards the extracellular domain (the two-step binding model).

2 Aim of the project

Parathyroid glands were discovered in the late 19th century. The physiological role of these glands in calcium regulation was revealed in 1900-1925. The consequences of deficiency and excess of PTH hormone (Hypo-, Hyperparathyroidism respectively) was studied in late 1950. In late 1970s amino acid sequence of PTH from several species were determined. During the last three decades, rapid advance in understanding the physiology, pathophysiology and therapeutic significance of PTH. However, the following questions are not addressed completely.

1) Osteoporosis is a major healthcare problem, causes more than 9 million fractures every year. In 2002, the FDA approved PTH (1-34) and in 2006, EMA approved PTH (1-84) has drugs for the treatment of osteoporosis. Also, bioengineered PTH (1-84) was approved by FDA in 2007 and EMA in 2013 for hypoparathyroidism. The biological action of PTH occurs by binding and activating PTH1R. But the detailed molecular mechanism is not fully elucidated. The aim is to elucidate the molecular mechanism by studying receptor binding in vitro and activation in vivo by PTH of different length (15-34, 1-34 and 1-84).

2) In 1986, the two-step binding model was proposed for the hormone-receptor interaction. Accordingly, the hormone binds to the cell membrane first, followed by the binding to the target receptor. However, the two-step binding model is not yet experimentally approved. Here, PTH and ECD of PTH1R will be taken as a model system for receptor binding and studied in a membrane mimicking environment with the aim to prove or disprove the two-step binding model. Since PTH is used as a drug, the interaction of the hormone with the membrane is crucial for its efficacy.

3) PTH undergoes posttranslational modifications during maturation. Apart from full length PTH, 10-20% of modified PTH was identified in blood circulation. In 1984, phosphorylation of PTH has been identified from human and bovine parathyroid gland. But there is no information available about the exact site of modification and the effect of phosphorylation on receptor signaling cascade. In this thesis, phosphorylation sites

should be identified, and modified/unmodified PTH used to test the regulation of PTH1R and PTH2R activation.

4) Hormones are stored at high concentration in cytoplasmic granules in endocrine tissues. Amyloid deposits have been found in the parathyroid glands and in parathyroid adenomas. Furthermore, amyloids are associated with neurological and other diseases. In early 1976, the formation of fibrils from PTH (1-84) was reported, however, without a detailed molecular characterization. In this thesis, a detailed characterization of *in vitro* generated amyloid fibrils from human PTH (1-84) is planned with the aim to test the hypothesis that PTH amyloids can be classified as functional amyloids.

3 Materials and methods

3.1 Chemicals and enzymes

GuaHCl, Coomassie Brilliant Blue G, Brain lipids-Folch fraction 1, Dnase I, Lysozyme (Sigma-Aldrich, Munich, Germany), IPTG (Gerbu, Gaiberg, Germany), Reduced and oxidized Glutathione (Applichem, Mannheim, Germany), ^{15}N Ammonium chloride, ^{13}C glucose, D_2O , d_{38} -DPC (Cambridge Isotopes, Cambridge, USA), POPC, POPG, DMPC, DMPG (Avanti polar lipids, USA), All other chemicals were purchased from Carl Roth, Karlsruhe, Germany unless otherwise specified.

3.2 Column materials and columns

C18 preparative RP-HPLC column (VP 250/10 Nucleosil 500-5 C18 PPN, Macherey-Nagel), Ni-Sepharose Fast Flow, Phenyl Sepharose 6 Fast Flow (high sub) 5ml, HiLoad 16/60 Superdex 75 prep grade, Superdex peptide 10/300 GL, Hiload 26/60 Superdex 30 prep grade (GE Healthcare, Munich, Germany)

3.3 Stains, plasmids and antibiotics

E. coli Rosetta (DE3) and *E. coli* BL21 codonPlus-RIL (Novagen, Darmstadt, Germany). Rosetta cells are derivatives of BL21 strains design to enhance the expressions of eukaryotic proteins. BL21 C+ RIL strains have been optimized for expression of AT rich genomes. Both stains carry T7 promoters, suitable for protein production with pET vectors (induction with IPTG).

Glycerol stock of pET15b plasmid containing cDNA of nPTH1R in Rosetta (DE3) cells and pETSUMOPHTH plasmids were kindly provided by Eva Bosse-Dönecke, Group of Prof. Rainer Rudolph, MLU, Halle

Rosetta (DE3) - pET15bnPTHR1 - Ampicillin (300 $\mu\text{g}/\text{ml}$) and kanamycin (50 $\mu\text{g}/\text{ml}$)
BL21 C+ - pETSUMOPHTH - Chloramphenicol (25 $\mu\text{g}/\text{ml}$) and kanamycin (50 $\mu\text{g}/\text{ml}$)

3.4 Various materials and instruments

Dialysis membranes and clamps	- Spectrum (CA, USA)
Micropipettes and tips, Eppi, GelPrep kit	- Eppendorf (Hamburg, Germany)
Concentrator Vivaspin 15R	- Sartorius (Aubagne Cedex, France)
Quartz cells	- Hellma (Mühlheim, Germany)
NMR tubes (5mm)	- New Era (Vineland, USA)
Prepacked pierce [®] gels SE250	- Thermo Fischer Scientific (Germany)
Äkta FPLC, Äkta Purifier	- GE-Healthcare (Munich, Germany)
HPLC	- Gynkotec (Germering, Germany)
Autoclave VX-95	- Systec (wettenberg, Germany)
Fermenter, and Centrifuge	- New Brunswick Scientific (Germany)
Centrifuge – Sorvall RC5B plus	- Thermo Fischer Scientific (Germany)
Ultra pure water system GenPure (UF)	- TKA (Niederelbert, Germany)
Freeze dryer - Alpha 1-4 LSC	- Christ (Osterode, Germany)
Shaking incubator – Innova 40 and 43	- New Brunswick Scientific (Germany)
Sonicator - W-250D	- Branson (Dietzenbach, Germany)
Homogenizer – Emulisiflex 05	- Avestin (Canada)
Homogenizer – Ultra-Turrax T18 basic	- Ika (Staufen, Germany)
CD spectrophotometer J-815	- Jasco (Groß-Umstadt, Germany)
UV/Visible spectrophotometer V-650	- Jasco (Groß-Umstadt, Germany)
VP-ITC titration calorimeter	- MicroCal (Northampton, MA, USA)
NMR spectrometer – Avance III	- Bruker (Karlsruhe, Germany)
Surface Plasmon Resonance T-100	- Biacore AB (Uppsala, Sweden)

3.5 Culture media

Ultra pure water was used to prepare the culture media. The medium was sterilized by heating with 121 °C for 15min at 101 kPa. ¹³C-glucose, antibiotics and other minerals were sterile filtered with 0.22 µm filter (Dr. Ilona Schubert Laborfachhandel, Leipzig, Germany) and added prior to the inoculation.

The following chemicals were calculated to prepare one liter of culture media.

dYT medium	- 16 g pepton, 10 g yeast extract, 5 g NaCl
Agar plate	- dYT with 1.5% of Agar-Agar
5 x M9	- 85 g Na ₂ HPO ₄ · 12H ₂ O, 15 g KH ₂ PO ₄ , 2.5 g NaCl, 5 g ¹⁵ NH ₄ Cl
TS2	- 100 mg ZnSO ₄ · 7H ₂ O, 30 mg MnCl ₂ · 4H ₂ O, 300 mg H ₃ BO ₃ , 200 mg CoCl ₂ · 6H ₂ O, 20 mg NiCl ₂ · 6H ₂ O, 10 mg CuCl ₂ ·2H ₂ O, 900 mg Na ₂ MoO ₄ · 2H ₂ O, 20 mg Na ₂ SeO ₃ .
Minimal medium (M9)	- 200 ml 5xM9, 2 ml-TS2, 1 ml-1M MgSO ₄ , 1 ml-100 mM CaCl ₂ , 1ml-10mM Fe(III)-citrate, 20ml-10 % ¹³ C-glucose (2g/l), 5ml BME Vitmin complex (Sigma, steinhein, Germany)
Antibiotics	- Ampicillin (300 µg/ml), chloramphenicol (25 µg/ml) and kanamycin (50 µg/ml)

dYT media was used to express unlabeled proteins and peptide. The minimal medium was used to express ¹⁵N and ¹³C/¹⁵N labeled proteins and peptides.

3.6 Transformation by electroporation

Introducing DNA into cells is called as electroporation. Electroporation (Potter et al. 1984) was performed using BTX-ECM399 (Harvard apparatus, USA) apparatus. One to two micro liter of pETSUMOPHTH plasmid vector DNA and 40ul of *E. coli* BL21 codonPlus-RIL competent cells were allowed to sit on ice for 5-10 min. The DNA and cells were mixed and transferred into the 0.2cm electroporation cuvette (Peqlab, UK). The electrical pulse (2.5 kV voltages, 25 µF capacitance and 500Ω resistance) were delivered for 5msec. Immediately after the pulse, 600 µl of dYT medium was added and transferred to the eppendorf tube. The mixture was then incubated at 37 °C for 1 hour. Fifty micro liter of incubated medium was plated on an agar plate containing kanamycin and chloramphenicol antibiotics and left overnight at 37 °C. Next day, a single colony was picked and used for expression.

Glycerol stock solution of pET15bnPTHR1 transformed Rosetta (DE3) cells were kindly provided by Eva Bosse-Dönecke, Group of Prof. Rainer Rudolph, MLU. Halle

3.7 SDS-Polyacrylamide Gel electrophoresis

Electrophoresis is a separating or resolving technique on the basis of protein size with the influence of an applied electric current (Lodish et al. 2000). A good separation of proteins can be achieved by varying the pore size of cross-linked polyacrylamide. Tricine-SDS-PAGE (1-100kDa) was used to resolve peptides (Schagger and von Jagow 1987; Schagger 2006). Tricine-SDS-PAGE was carried out using Hoefer electrophoresis- SE250 apparatus (San Francisco, CA, USA) at a current of 25mA for stacking gel and 45mA for resolving gel. The sample was prepared by mixing protein (10-50 μ g) with Roti[®]-Load1 buffer (4:1 ratio) and heated to 95 °C for 5min. The gel was stained with Coomassie Brilliant Blue G and destained with methanol (5%,v/v), acetic acid (10%,v/v) solution. The following chemical components were used for electrophoresis.

Separation gel (12.5% SDS)	4.17 ml Acrylamide rotiphorese [®] , 3.27 ml Gel buffer, 2.85 ml ddH ₂ O, 4.5 μ l TEMED, 83.3 μ l 10% (w/v) APS
Separation gel (15% SDS)	5 ml Acrylamide rotiphorese [®] , 3.26 ml Gel buffer, 1.65 ml ddH ₂ O, 4.5 μ l TEMED, 83.3 μ l 10% (w/v) APS
Stacking gel	1.2 ml Acrylamide rotiphorese [®] , 1.5 ml Gel buffer, 3.25 ml ddH ₂ O, 4.0 μ l TEMED, 50 μ l 10% (w/v) APS
Gel buffer	3M Tris/HCl, 0.3% (w/v) SDS, pH 8.45 at 25 °C
Anode buffer	200mM Tris/HCl, pH 8.9 at 25 °C
Cathode buffer	100 mM Tris/HCl, pH 8.23 at 25 °C, 0.1% (w/v) SDS, 100 mM Tricine

Pierce[®] prepacked gel (4-20% SDS) were used for peptides. Electrophoresis was carried out with 80mA, Tris (12.1 g/l)-HEPES (23.8 g/l)-SDS (1 g/l) as a running buffer. Sample preparation, Staining and destaining were performed with the above procedure.

Protein ladder Roti[®]-Mark was used as a standard for SDS-PAGE.

3.8 Protein concentration determination

The concentration of PTH and PTH1R were determined by measuring absorption at 280nm with a UV/Visible spectrophotometer. One cm quartz cuvette was used and con-

centration was calculated by Beer-Lambert law (Hammes 2007). The extinction coefficients of protein calculated from ExPASy proteomic tool-ProtParam (Gill and von Hippel 1989) were given. nPTH1R - $37930 \text{ M}^{-1}\text{cm}^{-1}$, PTH (15-34)/(1-34)/(1-84) – $5500 \text{ M}^{-1}\text{cm}^{-1}$ (Hennig 2010).

3.9 Expression, inclusion body preparation and purification of nPTH1R

All the purification procedures were performed at 4-8 °C unless otherwise mentioned. All the buffers were filtered (0.2 µm) and degassed prior to use.

3.9.1 Expression

nPTH1R was expressed (**Fig. 3.1**) with 6xHis-tag at the N-terminus in the *E. coli* Rosetta (DE3). All cultivations described here were carried out at 37 °C with ampicillin (300 µg/ml), chloramphenicol (25 µg/ml) resistance. Glycerol stock of Rosetta cells was picked and cultured in 5ml dYT medium. Fresh grown cells were transferred to 100ml dYT medium and cultivated overnight. The 4 liter dYT medium was inoculated with overnight culture, at initial OD₆₀₀ of 0.05. The cells were allowed to grow (240-280 rpm shaking speed) until the cell density reached an OD₆₀₀ of 0.7-1.2. Induction was done by 1mM IPTG for 4-5 hours. Cells were harvested by centrifugation at 7000 rpm, 4 °C for 10 min and stored frozen at -80 °C.

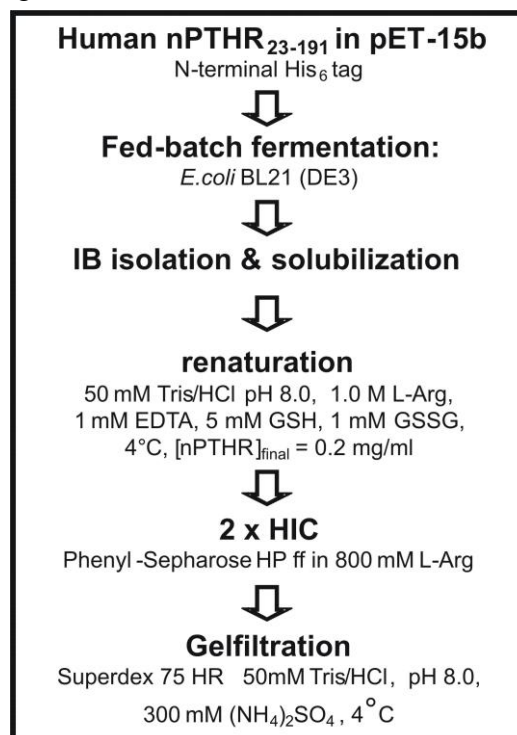


Fig. 3.1 Schematic representation of different steps involved in nPTH1R purification

3.9.2 Preparation of inclusion bodies

nPTH1R was over expressed as an inclusion bodies (IBs). IB preparation and purifications were followed as described in the dissertation of Ulla Grauschopf and Julia Hennig (Grauschopf et al. 2000; Grauschopf 2000a; Hennig 2010).

<u>Buffer I</u>	<u>Triton buffer</u>	<u>Wash buffer</u>
100 mM Tris/HCl	60 mM EDTA	100 mM Tris/HCl
1 mM EDTA	6% Triton X-100	20 mM EDTA
pH 7.00	150 mM NaCl	pH 7.00
	pH 7.00	

Frozen cell pellets were thawed on ice and resuspended in buffer I with the help of ultra-turrax homogenizer. Lysozyme (1mg/ml) was added and stirred for 30-40 min. Cells were disrupted by high pressure cell dispersion (three times at 500-1000 bar) or by sonication (two min at 35-40% intensity for 30ml of cell lysate). DNase I (5 μ g/ml) and MgCl₂ (3mM) was added for DNA digestion and stirred for 30 min at room temperature. A half volume of Triton buffer was added to the mixture and stirred for 30-40 min. Insoluble IB was separated by centrifuging at 20,000 rpm for 30 min. IB was washed by Triton and wash buffer mixed solutions (1:3 ratio) for two times. Triton was removed by washing IB with wash buffer for three times. Centrifugation was done during each wash step to separate IBs. Purity was checked by SDS-PAGE. IB was stored at -20 °C until use.

3.9.3 Inclusion body solubilization

Inclusion bodies were solubilized (1 g of IBs in 10 ml of buffer) by Ultra-turrax homogenizer or stirring at room temperature for 2-3 hours in 6 M guanidinium chloride (GdmCl), 100 mM Tris/HCl, 1mM EDTA and freshly prepared 100 mM DTT at pH 8.00 (Lilie et al. 1998). Insoluble materials were removed by centrifuge (20000 rpm, 30 min). Solubilized protein was dialyzed (3.5 kDa MWCO) against 4 M GdmCl at pH 2-3 until the DTT was removed.

3.9.4 Purification of inclusion bodies by IMAC

IBs were purified with Ni²⁺- immobilized metal affinity chromatography (IMAC).

<u>Ni-equilibration buffer</u>	<u>Ni-wash buffer</u>	<u>Ni-elution buffer</u>
4 M GdmCl	4 M GdmCl	4 M GdmCl
100 mM Tris/HCl	100 mM Tris/HCl	100 mM Tris/HCl
pH 8.00	pH 6.30	pH 4.00

The pH of dialyzed protein solution was increased to pH 8.00 by adding 4M NaOH and applied to the previously equilibrated Ni column. Column was washed with five column volumes of Ni-wash buffer. Elution was done by linear gradient from 0 to 100% in 100 min or by step gradient to 100%. Elution fractions were concentrated to 10mg/ml.

3.9.5 Refolding by pulse renaturation method

Renaturation buffer was prepared containing 50mM Tris/HCl or sodium phosphate, 1M L-arginine, 1mM EDTA, 5mM GSH, 1mM GSSG and pH 8.00. The volume of refolding buffer was prepared based on protein concentration and guanidine concentration (0.2 mg/ml and 0.1M end concentrations respectively) in the refolding solution. The protein solution was applied in four pulses with 6 hours gap between the pulses. Each pulse contains less than 50 µg/ml of protein solution. Refolding solution was stirred gently for 10 min and incubated over 3 days at 4 °C (Grauschopf et al. 2000).

3.9.6 Hydrophobic interaction chromatography (HIC)

Prior to the hydrophobic interaction chromatography (Phenyl Sepharose) refolding solution was concentrated to 100-150 ml using Vivaflow 200 membrane (10 kDa MWCO, Viva Science, Hannover, Germany).

<u>HIC-equilibration buffer</u>	<u>HIC-elution buffer</u>
50mM Tris/HCl	50mM Tris/HCl
1M ammonium sulfate	L-arginine
L-arginine	pH 8.00
pH 8.00	

1 M ammonium sulfate powder was added to the concentrated protein solution and incubated for 30 min. Part of incorrectly folded protein was removed by centrifugation (20000 rpm, 30 min). The supernatant was applied to the equilibrated HIC column. The column was washed with equilibrium buffer until UV absorption below 100 mAU. Protein was eluted with either linear gradient from 1 M to 0 M ammonium sulfate or step gradient. After step gradient, 300mM ammonium sulfate was added. Elution fractions were concentrated to 1-2 mg/ml (Vivaspin, 10 kDa MWCO).

3.9.7 Gel filtration chromatography

Final purification was performed on a Superdex 75 prep grade Gel filtration column in 50mM Tris/HCl or sodium phosphate, 300mM ammonium sulfate, pH 8.00 at 1 ml/min flow rate. Elution fractions were stored at -20 °C for further use.

3.10 Expression and purification of ¹⁵N-nPTH1R

For uniform enrichment of the protein with ¹⁵N isotopes, *E. coli* Rosetta (DE3) cells were grown in M9-minimal medium (section 3.5) containing ¹⁵NH₄Cl (1 g/l) as sole nitrogen source (Cambridge Isotopes). The isotopic labeled protein, expression, and purification were essentially the same as unlabeled nPTH1R as described in section 3.9.

3.11 Expression and purification of PTH

All the purifications were carried out at 4-8 °C unless otherwise specified. All the buffers used here were filtered (0.2µm) and degassed. The purity of all the fragments was confirmed by SDS-PAGE and mass spectrometry. Samples were stored at -20 °C. Protease inhibitor cocktail was added in each step of purification to avoid degradation.

3.11.1 Expression of PTH (15-34)/(1-34)/(1-84)

All three PTH fragments were expressed (**Fig. 3.2**) as a SUMO fusion protein with 6xHis-tag at the N-terminus in the *E. coli* BL21 codonPlus-RIL (Bosse-Doenecke et al.

2008). Expressions were carried out in four liter dYT medium at 37 °C in chloramphenicol (25µg/ml) and kanamycin (50µg/ml) resistance. Cells were grown as described earlier in section 3.9.1. At an OD₆₀₀ of 0.8-1.2, protein expression was induced with 1mM IPTG and further allowed to grow for 3½ hours. Cells were harvested by centrifugation at 7000 rpm, 10min, 4 °C and stored at -80 °C.

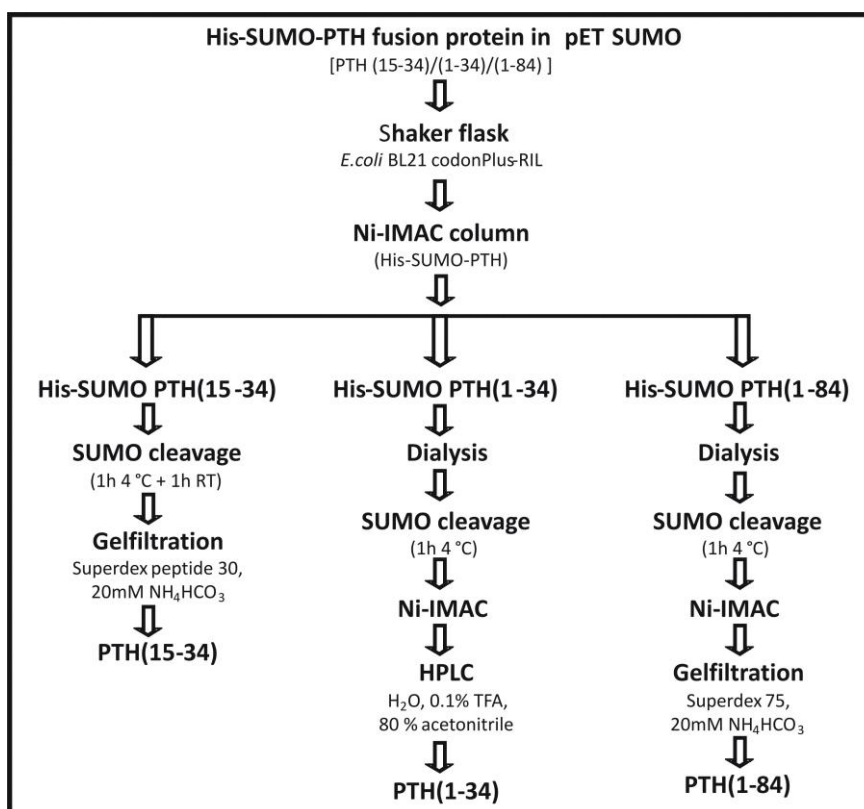


Fig. 3.2 Flow scheme for the recombinant production of different PTH fragments

3.11.2 Purification of SUMO fusion proteins [PTH (15-34)/(1-34)/(1-84)]

SUMO fusion protein was purified in Ni-IMAC at 4-8 °C unless otherwise indicated.

Lysis buffer

50mM Na₂HPO₄

300mM NaCl

10mM Imidazole

pH 8.00

Elution buffer

50mM Na₂HPO₄

300mM NaCl

500mM Imidazole

pH 8.00

Cell pellets were resuspended in ice-cold lysis buffer (1 g of cells in 4 ml of lysis buffer). Lysozyme (1 mg/ml), DNase I (5 µg/ml) and MgCl₂ (2 mM) were added and stirred for 30 min. Cells were disrupted as described earlier in section 3.9.2. Cell debris was removed by centrifugation at 20000 rpm, 30 min. Supernatant was applied in to the Ni column (flow rate 2ml/min). Bound protein was washed with five column volumes of lysis buffer and eluted with 50% step gradient.

3.11.3 Purification of PTH (15-34) from SUMO fusion proteins

Purified SUMO fused PTH (15-34) peptides were pooled and SUMO-buffer (lysis buffer with 2% IGEPAL) was added to the volume of 1:10 ratio. A recombinantly expressed Ulp1-SUMO protease (50-150µg/ml) (Mossessova and Lima 2000) was added to the ratio of 1:100 and incubated for an hour at 4 °C, followed by at room temperature for 30 min to an hour. Digestion or cleavage reaction was monitored by SDS-PAGE. After cleavage, His-tagged SUMO, low molecular weight compounds, and other contaminants were removed by Gel filtration peptide column (Superdex peptide 10/300 GL or Hiload 26/60 Superdex 30 prep grade from GE Healthcare) equilibrated with 20mM ammonium hydrogen carbonate (pH was not adjusted). Peak fractions were pooled and lyophilized.

3.11.4 Purification of PTH (1-34) from SUMO fusion proteins

Digestion of SUMO fusion proteins of PTH (1-34) was carried out same as described in section 3.11.3 with the exception that the incubation time was one hour at 4 °C. After the digestion, the cleaved His-tagged SUMO was removed by a second Ni column step and flow through was collected. The peptide in the flow through was separated by Reverse-phase HPLC on C18 column. The column was equilibrated in solvent A (dd H₂O and 0.1% TFA). 1-4 ml of protein solutions (3-10 mg) were injected with the flow rate 4.5 ml/min. The peptide was eluted with solvent B (80% acetonitrile, 0.1% TFA), gradient elution from 30% to 55% over 55 min. UV detection was at 280 nm and 215 nm. Peak fractions were collected manually and lyophilized.

3.11.5 Purification of PTH (1-84) from SUMO fusion proteins

Cleavage reaction and removal of SUMO by Ni affinity column were carried out as specified in section 3.11.3 and 3.11.4. The flow through from the second Ni step then applied to a HiLoad 16/60 Superdex 75 prep grade gel filtration column equilibrated with 20mM ammonium hydrogen carbonate (pH was not adjusted). Pooled peak fractions were lyophilized and stored.

3.12 Expression and purification of ^{15}N -PTH, $^{15}\text{N}/^{13}\text{C}$ -PTH

For generating isotopically labeled PTH peptides (all three PTH (15-34)/(1-34)/(1-84) fragments), the SUMO fusion proteins were expressed in *E. coli* BL21 codonPlus-RIL cells growing in M9-minimal medium supplemented with $^{15}\text{NH}_4\text{Cl}$ (1 g/l) for uniform ^{15}N labeling, both $^{15}\text{NH}_4\text{Cl}$ and ^{13}C -glucose (2 g/l) for double labeling, as sole nitrogen and carbon source (Cambridge Isotope Laboratories), respectively. The expression and purification were same as described above in the section 3.11, with the exception that the induction time was 4-5 hours.

3.13 Cell line, preparation of lysates and kinase assay

Human embryonic kidney 293 (HEK 293) cells were cultured in Dulbecco's modified Eagle medium (DMEM) supplemented with 10% heat inactivated (56 °C for 30 minutes) fetal bovine serum (FBS) and 5% sodium pyruvate. The cells were grown at 37 °C in a humidified chamber with 5% CO_2 . HEK 293 cells were lysed in the presence of protease inhibitor, 2x kinase assay buffer (20 mM MOPS pH 7.5, 15 mM MgCl_2 , 10 mM EGTA, and 2 mM DTT) and phosphatase inhibitors (0.25 mM activated Na_3VO_4 , 0.5 mM NaF, 15 mM β -glycerophosphate). Lysed cells were collected by centrifuged at 12000 rpm for 15 minutes at 4 °C and the clear supernatant was used for the kinase reaction. Kinase assays were performed by incubating 30 μg PTH (1-84) with lysate (1-2 mg/ml total protein concentration), ^{32}P ATP (5 μCi ^{32}P - γ -ATP and cAMP(5 μM). This

reaction mixture was incubating for 3 h at 37 °C. After the reaction samples were analyzed by 15% SDS PAGE and detected by autoradiography.

3.14 cAMP accumulation assay

HEK 293 cells stably expressing PTH1R/PTH2R were prepared as previously published (Mann et al. 2008). HEK 293 cells were washed twice with PBS and harvested by centrifugation (3000g). Then the cells were diluted to a density of 6.67×10^5 cells/ml in stimulation buffer (HBSS, 5 mM HEPES, 0.1% BSA, pH 7.4). Alexa Fluor® 647-anti cAMP antibody was diluted into adequate cell suspension at 0.005% (v/v) and the suspension seeded at a density of 4×10^3 cells/well into a 96 well plate (6 µl/well). PTH (1-84) was diluted to the desired concentration using stimulation buffer containing 1 mM IBMX. Cells were treated with 6 µl of a single concentration of peptide hormone per well and these experiments were performed in triplicate. Receptor stimulation was carried out at 37 °C for 30 minutes and then the reaction was terminated by the addition of 12 µl detection mix containing 0.00044% (v/v) Eu-W8044 labeled streptavidin and 0.00133% (v/v) biotin-cAMP. Plates were incubated at room temperature for 1 hour. Afterward, fluorescence measurements were taken using a VICTOR X4 2030 plate reader (PerkinElmer Life and Analytical Sciences). All experiments were performed in triplicate and repeated independently three times. GraphPad Prism 6.01 was used for data analysis.

3.15 PTH (1-84) fibril preparation and ThT kinetic assay

Formation of PTH fibrils was achieved by dissolving 10 mg/ml concentration of recombinant purified PTH (1-84) in 50 mM borate buffer, pH 9.0 and followed by incubation at 65 °C. ThT kinetics was performed in borate buffer and individual aliquots were prepared and incubated. The reaction was stopped by dilution with an addition of pre-cooled buffer at 4 °C. The kinetics was followed over 3 h of incubation time. The kinetic samples were finally diluted to 35 µM of PTH (1-84) and Thioflavin T (ThT) was added in equal molar ratio. ThT fluorescence was monitored by an excitation wave-

length of 450 nm. For the EM analysis, the PTH (1-84) samples were incubated at least for 1h.

3.16 A β fibrils preparation

A β peptides were recombinantly expressed and purified according to reported procedure (Christopeit et al. 2005). A β (1-40) fibrils were grown in 50 mM HEPES buffer at pH 7 by dissolving 50 μ M of the peptide followed by incubation at 37 °C (Haupt et al. 2011).

3.17 Fourier-transform infrared (FTIR) spectroscopy

FTIR spectra for PTH (1-84), PTH (1-84) fibrils and A β (1-40) fibrils were recorded with a Tensor 27 FTIR spectrometer (Bruker, Germany) equipped with a BIOATR II cell. The MCT detector was cooled with liquid nitrogen. 15 μ l of the samples (protein concentration: 5 mg/ml) were placed onto the crystal of the ATR cell and measured at room temperature. Collected spectra were averages of 64 scans at 4 cm^{-1} resolution.

3.18 Mass spectrometry and fibril core identification

The fibrils were prepared as mentioned in 3.15 section. These fibrils were mixed with chymotrypsin in the 1:100, enzyme to fibril (w/w) (Sarell et al. 2013) ratio in 25 mM Tris-Cl, 50 mM NaCl at pH 7.8 and then incubated at 37 °C. Tosyllysine chloromethyl ketone hydrochloride (TLCK) treated MS grade chymotrypsin was used. The fibrils were dissociated into monomers by adding hexafluoro-2-propanol in 1:1 ratio (v/v). Samples at a different time point were analyzed by MALDI-TOF or ESI-MS-MS. For the mass spectrometry, samples were desalted by Pierce C18 Tips prior to analysis.

3.19 Transmission electron microscopy (TEM)

PTH fibril sample prepared at section 3.15 were diluted to 50 μ M and a 5 μ l droplet of fibril samples were pipetted onto a formvar carbon-coated copper grid (Ted Pella Inc.)

and washed three times with 50 μ l of water drops. The water was carefully removed with filter paper between washes. Grids were then stained with 50 μ l of 2 % (w/v) uranyl acetate which was then removed and air dried. Specimens were examined using Zeiss 900 transmission electron microscope and it was operated at an acceleration voltage of 80 kV.

3.20 Inhibition of fibril growth

The inhibition of PTH (1-84) fibril growth was monitored by transmission electron microscopy using 3000-30000x magnification. For the EM analysis, 10 mg/ml of PTH (1-84) was dissolved with and without epigallocatechin gallate (EGCG) in 50 mM borate buffer to the molar ratio of 1:2.4 and 1:10 (protein: EGCG). Inhibition was monitored at different time points from 1 to 48 h.

3.21 Circular dichroism (CD) spectroscopy

Far ultraviolet (UV) CD spectra were carried out on a Jasco J-815 CD spectrometer equipped with a Peltier thermostatted cell holder and Peltier ETC-505T temperature controller. Far-UV CD spectra (190-260 nm) were recorded at 20-25 °C at a protein concentration of 5-20 μ M in CD buffer (10 mM sodium phosphate, 150 mM sodium sulfate, and pH 6.0) using a 1 mm path length quartz cuvette with the following parameters (Yang et al. 1986): 100 nm/min scanning rate, 1 sec response time, 0.2 nm data pitch, 1 nm bandwidth, 10-20 accumulation. The spectra were smoothed by the software provided by JASCO.

Preparation of vesicles: The lipids (POPC, POPG, DMPG, and Brain lipids from bovine) were dissolved in chloroform and dried overnight to remove CHCl_3 . The dried lipid film was resuspended in CD buffer followed by vortexing. After 2-3 freeze-thaw cycles, the lipid was extruded with 100nm polycarbonate filters (Avanti Polar Lipids) to prepare large unilamellar vesicles (LUVs) (Hope et al. 1985; Mills et al. 2008).

CD sample for the lipid interactions was prepared by mixing PTH (1-84) and lipid vesicles to the final concentration of 10-20 μM and 1 mM (protein: lipid ratio of 1:50-100) respectively. The micelles interactions were carried out by mixing 10-20 μM of PTH (1-84) with 100 mM SDS/100mM DPC. The PTH (1-84)-lipid or micelle mixtures were equilibrated for at least an hour before acquiring spectra. Protein spectra were corrected with the corresponding buffer or buffer containing micelles/liposomes and converted to mean residue weight ellipticity $(\theta)_{\text{MRW}}$ [$\text{deg cm}^2/\text{dmole}$] (Schmid 1997) with

$$(\theta)_{\text{MRW}} = \frac{(\theta)_{\text{mdeg}}}{10\text{cnd}} \quad 3.1$$

where $(\theta)_{\text{mdeg}}$ is the observed ellipticity in millidegrees, c is the protein concentration in moles per liter, d is the path length in cm, and n is the number of amino acid residues.

3.22 Isothermal titration calorimetry (ITC)

3.22.1 Theory of receptor binding

A. J. Clark (1937) was the first who formulated the receptor occupancy theory (Rang 2006). This quantitative model describes receptor binding with the following assumptions: binding is reversible, all the receptor molecules are equivalent and independent, the active chemical agent does not undergo degradation or participate in other reactions, and only exists in either a free form or bound to the receptor (Spiegel 2003). When a ligand (L) interacts with the receptor (M), binding follows the law of mass action.



$$K_a = [\text{ML}] / [\text{M}] [\text{L}] \quad 3.3$$

In this equation (Eq.3.3) K_a is the association rate constant, $[\text{L}]$, $[\text{M}]$ and $[\text{ML}]$ are the concentrations of the free ligand, free receptor, and the receptor-ligand complex respectively. In the ITC experiment, the binding equilibrium is measured directly by determining the heat evolved (exothermic) or absorbed (endothermic) on the association of a ligand with its binding partner. The amount of heat (Q) evolved or taken up by addition

of ligand can be represented by the equation (Pierce et al. 1999; Lewis and Murphy 2005)

$$Q = V_0 \Delta H_b [M]_t K_a [L] / (1 + K_a [L]) \quad 3.4$$

where V_0 is the volume of the cell, ΔH_b is the enthalpy of binding per mole of ligand, $[M]_t$ is the total receptor concentration including bound and free fractions. For the macromolecule containing multiple ligand binding sites that are non-interacting, the cumulative heat of binding can be described by

$$Q = V_0 [M]_t \sum n_i \Delta H_i K_{ai} [L] / (1 + K_{ai} [L]) \quad 3.5$$

To determine the stoichiometry (n), K_a and ΔH_b equation 3.5 is described in terms of the binding constant and total ligand concentration $[L]_t$ to obtain the quadratic:

$$Q = (n[M]_t \Delta H V_0) / 2 \left\{ X - \sqrt{X^2 - 4[L]_t / (n[M]_t)} \right\} \quad 3.6$$

$$X = 1 + [L]_t / (n[M]_t) + 1 / (nK_a [M]_t)$$

where

The values of K_a , n and ΔH can be obtained from fitting program for nonlinear least squares analysis. From the value of K_a , the absolute temperature (T) and the gas constant ($R = 8.3144 \text{ J mol}^{-1} \text{ K}^{-1}$) the Gibbs free energy (ΔG) and the entropy (ΔS) can be determined from the following equations (Perozzo et al. 2004; Salim and Feig 2009)

$$\Delta G^0 = -RT \ln(K_a) \quad \Delta G = \Delta H - T\Delta S \quad 3.7 \quad 3.8$$

3.22.2 Experimental conditions and parameters

The ITC experiments were performed using a MicroCal VP-ITC titration microcalorimeter (MicroCal Northampton, USA). Titration of PTH (15-34)/(1-34)/(1-84) (250-350 μM) into a nPTH1R solution (20-30 μM) was performed at 15-25 $^\circ\text{C}$ in 20 mM sodium phosphate, 300mM Na_2SO_4 , pH 6.0 (ITC buffer). The experiments were carried out with the following parameters: 25-29 total numbers of injections, 10 μl volume of each injection, 20 sec duration of injection, 250-500 sec delay between the injections, 307 rpm constant stirring speed. PTH and the nPTH1R were dialyzed overnight in the same

buffer and the solutions were degassed under vacuum prior to use. The heat of dilution was measured by titrating PTH into a buffer under identical conditions.

For lipid ITC experiments, liposomes were prepared using the same technique as described in section 3.21 with minor modifications: lipid film was dissolved in ITC buffer. The micelles were prepared by dissolving detergents (concentration above the critical micelle concentration value) into the ITC buffer.

ITC experiment for the binding of PTH (1-84) to the nPTH1R in liposomes was carried out with the same conditions as described above. Additionally, 1 mM of POPC or 2.5 mM of DMPC was provided in both cell and the syringe. The binding of PTH (1-84) with liposomes or micelles were performed by taking PTH (1-84) of concentration of 50-100 μ M in a cell and liposomes (0.5-2 mM) or micelles (10-40 mM) in the syringe. Titrations were carried out with the same parameter as described above.

Data analysis: Baseline correction and peak integration, curve fit (Eq. 3.5 and 3.6) were done by Origin software provided by MicroCal, Inc. From the value of K_a , T , n , R , and ΔH_b , the value of ΔG (Eq. 3.7) and ΔS (Eq. 3.8) were calculated.

3.23 NMR Spectroscopy

All the NMR data were acquired at 25 °C on Bruker Avance III spectrometers operating at ^1H frequencies of 600 MHz (14.1 T) and 800 MHz (18.8 T) both equipped with z-axis gradient triple resonance probes. The 800 MHz spectrometer was equipped with a cryoprobe. Spectra were processed by NMRPipe (Delaglio et al. 1995) and analyzed using NMRView software (Johnson and Blevins 1994).

3.23.1 Sample preparations and measurements

NMR Samples were prepared in 10 mM Bis-tris or 20 mM sodium phosphate, 300mM Na_2SO_4 , 0.02 % NaN_3 , 10% (v/v) D_2O and pH 5.2-6.0 (NMR buffer) and until or oth-

erwise mentioned, in 5mm NMR sample tube. These same buffer conditions were used for previously reported ECD structure (Grace et al. 2007).

a) Backbone assignment of PTH ligands: Sequence-specific resonance assignments of PTH ligands were obtained from the following 2D HSQC (Heteronuclear single quantum correlation) (Vuister and Bax 1992; Mori et al. 1995) and TROSY (Transverse relaxation optimized spectroscopy) (Pervushin et al. 1997) based 3D experiments (Kay et al. 1990; Clore and Gronenborn 1991; Grzesiek and Bax 1992; Salzmänn et al. 1998) and the sample concentrations:

370 μ M- 15 N-PTH (15-34)	- 15 N-NOESY-HSQC (120msec and 288, 56, 1024), 15 N-TOCSY-HSQC (100msec and 288, 56, 1024)
450 μ M 13 C/ 15 N PTH (15-34)-	HNCA (48,48,1024), HNCACB (104, 48, 1024)
900 μ M 15 N-PTH (1-34)	- 15 N-NOESY-HSQC (150msec and 320, 64, 1024), 15 N-TOCSY-HSQC (120msec and 320, 64, 1024)
150 μ M 15 N-PTH (1-84)	- 15 N-NOESY-HSQC (120msec and 352, 64, 1024), 15 N-TOCSY-HSQC (80msec and 336, 64, 1024)
210 μ M 13 C/ 15 N PTH (1-84)	- HNCA (48, 64, 1024), HNCACB (128, 64, 1024)
All PTH samples	- 15 N-FHSQC (256, 1024), 13 C-CT-HSQC (512, 1024)

Mixing time (in milliseconds) and a total number of data points being acquired (F_1 - 1 H or 13 C, F_2 - 15 N and F_3 - 1 H nuclei respectively) were given in the parenthesis. The water suppression was achieved with either WATERGATE (Water suppression by gradient tailored excitation) sequence (Piotto et al. 1992) or water flip-back pulses (Grzesiek and Bax 1993a) or with pulse field gradient (Schleucher et al. 1994). The quadrature detection was obtained by States-TPPI (Time proportional phase increments) (States et al. 1982; Marion et al. 1989) and/or echo/anti-echo (Schleucher et al. 1993) methods. The 1 H carrier is set to the water frequency (4.7 ppm). Typical spectral widths were 34-65 ppm in F_1 (13 C), 15-30 ppm in F_2 (15 N) and 13 ppm in F_3 (1 H). NMR data were collected over 48-90 hours for 3D and 1-3 hours for 2D.

c) Membrane interaction of the PTH ligands: Liposomes (POPC, POPG, DMPC, DMPG and Brain lipids from bovine) and micelles (SDS, DPC, and LDAO) were pre-

pared as described earlier in section 3.21. The binding of PTH (1-84) by liposomes or micelles were monitored by HSQC spectra, taking ^{15}N -PTH (1-84) or $^{13}\text{C}/^{15}\text{N}$ -PTH (1-84) of the concentration of 75-150 μM in 5mm NMR tube and liposomes (2-5 mM) or micelles (100-200 μM) were added. The assignment of d_{38} -DPC (200 mM) bound $^{13}\text{C}/^{15}\text{N}$ -PTH (1-84) (200 μM) was done by ^{15}N -NOESY-HSQC (120msec), ^{15}N -TOCSY-HSQC (80msec), HNCA and HNCACB experiments. The assignment of d_{38} -DPC (200 mM) bound ^{15}N -PTH (1-34) (650 μM) was confirmed (Scian et al. 2006) by ^{15}N -NOESY-HSQC (120msec), ^{15}N -TOCSY-HSQC (80msec) experiments.

3.23.2 NMR titration experiments

The interaction of PTH to the nPTH1R was monitored by collecting ^{15}N -FHSQC (Mori et al. 1995) or ^{15}N -TROSY-HSQC (Pervushin et al. 1997) of the following samples:

185 μM - ^{15}N -PTH (15-34)	353 μM nPTH1R	1 : 1.91
750 μM - ^{15}N -PTH (1-34)	1.42 mM nPTH1R	1 : 1.47
113 μM - ^{15}N -PTH (1-84)	178 μM nPTH1R	1 : 1.58

Unlabeled nPTH1R was added to the ^{15}N -PTH samples in 8-12 steps and the spectrum was recorded in each step with 256(^{15}N), 1024 (^1H) data points. Perturbation of backbone ^1H and ^{15}N chemicals shifts (Grzesiek et al. 1996) or the intensity change upon complex formations (Feeney et al. 1979) were quantified using Eq 3.9 & 3.10, respectively

$$\Delta_{\text{av}} = [(\Delta\delta_{\text{HN}}^2 + \Delta\delta_{\text{N}}^2/25)/2]^{1/2} \quad 3.9$$

$$I = I_0 - [I_0 ((M_t + nL_t + K_d) - ((M_t + nL_t + K_d)^2 - (4 M_t nL_t))^{1/2}) / 2M_t] \quad 3.10$$

Where (Eq 3.9) $\Delta\delta_{\text{av}}$ is the weighted average amide chemical shift changes, $\Delta\delta_{\text{HN}}$ and $\Delta\delta_{\text{N}}$ are the chemical shift perturbation for proton and nitrogen, respectively. In the equation 3.10, I_0 is the observed initial intensity, I is the change in intensity upon complex formation, $[L]_t$, and $[M]_t$ are the total ligand and receptor concentrations. Assuming a 1:1 ligand:receptor ratio (Grauschopf et al. 2000; Pioszak and Xu 2008), the dissociation constant (K_d) are determined by nonlinear fitting program Grafit (Erithacus software, UK).

3.23.3 Pulse field gradient NMR diffusion experiment

PTH (1-84) in either lipid or micelle sample were prepared as described in section 3.23.1. The translational diffusion experiments of PTH (1-84) under these conditions were carried as described earlier (Wilkins et al. 1999; Balbach 2000) at 25 °C. The strength of the gradient (G) was calibrated using known water diffusion coefficient and the temperature was calibrated using methanol (Price et al. 1999; Berger and Braun 2004; Cavanagh et al. 2007). The diffusion coefficient (D) of the samples were deter-

mined (Equ. 3.11) by fitting the $R_h = (4.75 \pm 1.11) N^{0.29 \pm 0.02}$ intensity (I) of the NMR signals as a function of gradient strength (Price et al. 1999)

$$I = S \exp(-\gamma^2 G^2 \delta^2 D (\Delta - \delta/3))$$

where S is the pre-exponential factor, γ is the gyromagnetic ratio (^1H - 2.678×10^8 T/m), δ is the duration of the gradient pulse (6 msce), Δ is diffusion time (80-120 msec). The hydrodynamic radius (R_h) of the protein was calculated using the equation 3.12 (Wilkins et al. 1999), where N is the number amino acids of the globular protein.

3.23.4 NMR dynamic experiments

a) Heteronuclear ^1H - ^{15}N NOEs (^1H - ^{15}N NOE)

The sensitivity-enhanced pulse schemes were used to measure ^1H - ^{15}N nuclear Overhauser enhancement effects (NOEs) (Kay et al. 1989; Grzesiek and Bax 1993c). The experiments were recorded with proton saturation of 3-5 sec. The ^1H - ^{15}N NOE values were calculated from the ratio of cross-peak intensities in two spectra collected from with (I_{sat}) or without (I_{eq}) amide proton saturation (Feng et al. 1998)

$$^1\text{H}-^{15}\text{N NOE} = I_{\text{sat}} / I_{\text{eq}} \quad 3.13$$

b) Fast (millisecond) amide proton exchange

The newMEXICO (Measurement of Exchange rates in Isotopically labeled Compounds) experiment was used to measure fast (millisecond) amide protons exchange rates (Gemmecker et al. 1993; Koide et al. 1995; Mori et al. 1995). The experiment was recorded with mixing times of 10 msec to 250 msec.



$$I / I_{\text{ref}} = k_{\text{ex}} [\exp(-R_{1w}t) - \exp(-(R_{1\text{NH}} + k_{\text{ex}})t)] / (R_{1\text{NH}} + k_{\text{ex}} - R_{1w}) \quad 3.15$$

In the equation 3.14, $\text{NH}_{\text{closed}}$ and NH_{open} are the closed and open state of the protein and the corresponding rate constants are k_{cl} and k_{op} . The intrinsic rate constant (k_{int}) are determined from model compound studies (Bai et al. 1993). The amide proton exchange rates (k_{ex}) were calculated by using the equation 3.15 (Mori et al. 1997; Weininger 2009), where I is the measured peak intensity of a given amide at mixing time t , I_{ref} is its intensity in the reference spectrum, $R_{1\text{NH}}$ and R_{1w} are the longitudinal relaxation of a given amide proton and water ($R_{1w}=0.42 \text{ s}^{-1}$), respectively. Assuming EX2 exchange mechanism ($k_{\text{cl}} \gg k_{\text{int}}$), the protection factor (PF) and the apparent free energy 3.16 can be calculated by using (Equ. 3.16) (Bai et al. 1994)

$$k_{\text{ex}} = k_{\text{op}} k_{\text{int}} / k_{\text{cl}} = K_{\text{op}} k_{\text{int}} \quad \text{PF} = 1 / K_{\text{op}} \quad \Delta G = RT \ln(\text{PF})$$

3.23.5 Theory of chemical exchange

The chemical exchange phenomena were first introduced by Gutowsky and coworkers in 1953 (McConnell 1958; Kaplan 1980). The line shapes of the NMR spectra are defined by the rotation (T_2) of the molecule and chemical exchange process. The primary focuses of this section concern the effect of chemical exchange in proteins. Chemical exchange refers to any process (for example, conformational flexibility, chemical reactions, formation of intermolecular complexes) in which groups of nuclei exchange reversibly between two or more different environments in which its NMR parameters (e.g., chemical shift (δ), coupling constant (J) and relaxation rates (T)) differs (Evans 1995).

The theory of chemical exchange in NMR (Wennerström 1972) can be explained by considering the simplest (spin system without scalar coupling interactions) exchange equilibrium between two conformers or chemical states, A and B.



where k_1 and k_{-1} are the rate constants for the forward and reverse reactions, respectively. NMR is sensitive to detect such process (e.g., intra or intermolecular, or ligand-

$$\frac{d}{dt} \begin{bmatrix} [A](t) \\ [B](t) \end{bmatrix} = \begin{bmatrix} -k_1 & k_{-1} \\ k_1 & -k_{-1} \end{bmatrix} \begin{bmatrix} [A](t) \\ [B](t) \end{bmatrix}$$

binding) even when the system is in equilibrium. The rate law for this system can be written as (Cavanagh et al. 2007)

for N first order chemical reaction between N chemical

$$dA(t)/dt = KA(t) \quad 3.19$$

species, the equation is

In this equation (3.19) the matrix element of the rate matrix K are expressed as

$$K_{ij} = -\sum_{j=1}^N k_{ij} \quad \text{and} \quad K_{ij} = k_{ij} \quad (i \neq j), \quad \text{for the reaction } A_i \xrightarrow{k_{ij}} A_j$$

McConnell equation: The Bloch equation describes equation 3.17 as considering only in the two extreme limits of slow and fast exchange. In the case of an intermediate region, (exchange rates contribute to relaxation) the modified Bloch (McConnell) equation must be applied (McConnell 1958). For simple two-site exchange (Eq. 3.17), with $\delta_A \neq \delta_B$ and $T_{2A}=T_{2B}=T_2$, but with no spin-spin coupling, McConnell equations written as:

$$\begin{aligned} dM_{Ax}/dt &= \gamma (M_{Ax}B_0 + M_{Az}B_1 \sin \omega t) - (M_{Ax}/T_2) - (M_{Ax}/\tau_A) + (M_{Bx}/\tau_B) \\ dM_{Ay}/dt &= \gamma (M_{Az}B_1 \cos \omega t - M_{Ax}B_0) - (M_{Ay}/T_2) - (M_{Ay}/\tau_A) + (M_{By}/\tau_B) \\ dM_{Bx}/dt &= \gamma (M_{By}B_0 + M_{Bz}B_1 \sin \omega t) - (M_{Bx}/T_2) - (M_{Bx}/\tau_B) + (M_{Ax}/\tau_A) \\ dM_{By}/dt &= \gamma (M_{Bz}B_1 \cos \omega t - M_{Bx}B_0) - (M_{By}/T_2) - (M_{By}/\tau_B) + (M_{Ay}/\tau_A) \end{aligned} \quad 3.21$$

Where B_0 is the static magnetic field, B_1 is the applied radio frequency field, ω is the Larmor frequency, $M_{A,B,x,y,z}$ is the exception value for the bulk magnetization along a particular Cartesian axis in the rotation frame, τ_A (or $1/k_1$) and τ_B (or $1/k_{-1}$) are the lifetimes of the nucleus in each site. The solution to the McConnell equations is rather complex, which include the following parameters: the equilibrium site populations (p_A and p_B), the rate constants, $k_{ex} = (k_1 + k_{-1})$ or $k_{ex} = (k_1/p_A + k_{-1}/p_B)$ and the chemical shift difference between the magnetically distinct sites ($\Delta\delta = \delta_A - \delta_B$).

The relationship between $\Delta\delta$ and k_{ex} defines the regimes of the chemical exchange time-scale (Kempf et al. 2004):

$$\begin{aligned} k_{ex} > \Delta\delta &\quad \rightarrow \quad \text{fast exchange} \\ k_{ex} \sim \Delta\delta &\quad \rightarrow \quad \text{intermediate exchange or coalescence} \\ k_{ex} < \Delta\delta &\quad \rightarrow \quad \text{slow exchange} \end{aligned}$$

Typical spectra (Cavanagh et al. 2007) reflecting exchange at different rates relative to the chemical shift (Jeener et al. 1979) are depicted in **Fig. 3.3**. Two different cases are considered in this picture: the first (a-f) is the symmetric unimolecular exchange spectra with equal populations ($p_1 = p_2 = 0.5$) and the second (g-l) is skewed population with $p_1 = 3p_2$. When there is no exchange, two resolved resonances (f and l) are observed with resonance frequencies δ_A and δ_B , and relaxation delay constant ρ_1 and ρ_2 (longitudinal relaxation of A and B). As the rate of exchange increases, the lines broaden (spectra e and k), coalescence when $k_{ex} \sim \Delta\delta$ (spectra c and i) and sharpen into a single average peak (spectra b and h) at population-weighted average shift ($\delta_{obs} = p_1\delta_A + p_2\delta_B$). The resonance lineshape becomes increasingly narrow until it reaches the limit as the k_{ex} tends to ∞ .

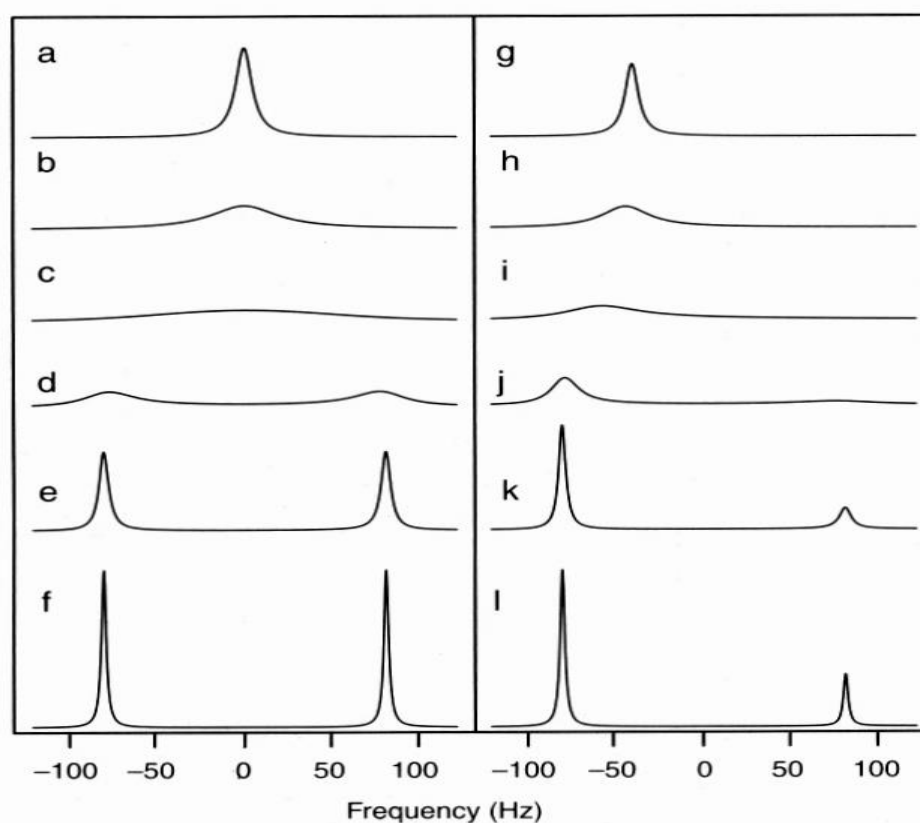


Fig. 3.3 The spectral consequences of chemical exchange for two-site system. Cavanagh and coworker simulated the spectra with the following parameters, $\Delta\delta/2\pi = 180$ Hz, $\rho_1 = \rho_2 = 10s^{-1}$. In (a-f), $p_1 = p_2 = 0.5$; in g-l, $p_1 = 3p_2$ and the calculated exchange rates, k_{ex} , equal to (a,g) 10000 s^{-1} , (b,h) 2000 s^{-1} , (c,i) 900 s^{-1} , (d,j) 200 s^{-1} , (e,k) 20 s^{-1} , and (f,l) 0 s^{-1} (Cavanagh et al. 2007).

Generally, a rule of thumb is that the interaction with $K_d < 10 \mu M$ are in slow exchange, K_d between 10 -100 μM are often in intermediate exchange and $K_d > 100 \mu M$ are in fast

exchange (Cavanagh et al. 2007). The proteins system fall under intermediate exchange regime are particularly challenging, because of line broadening effect, even the resonances may disappear from the NMR spectrum (Bhattacharya et al. 2010).

3.24 Solid-state NMR spectroscopy

3.24.1 Membrane sample preparation

The phospholipids (either POPC-d₃₁ or DMPC-d₆₇) were co-dissolved with PTH (1-34) in an organic solvent, dried under vacuum (10 mbar), and then dissolved in cyclohexane. After freezing in liquid nitrogen, the samples were lyophilized under a vacuum of approximately 0.1 mbar. Subsequently, the sample was hydrated to 50 weight percent with deuterium-depleted H₂O, freeze-thawed, stirred, and gently centrifuged for equilibration. The sample with POPC-d₃₁ was then transferred to a 5-mm glass vial and finally sealed with Parafilm for NMR measurements while the DMPC-d₆₇ sample was transferred to a MAS rotor for solid-state NMR experiments.

Membrane sample for PTH (1-84) was prepared using the same method as described in section 3.21. The peptide to the DMPC-d₆₇ was 1:50 molar ratios. The sample was incubated for 4 hours including 3 freeze-thaw cycles to enable binding of the peptide to the inner leaflet of the membrane and subsequently centrifuged (1.5 hours, 79 000 × g). The pellet was lyophilized and hydrated with 50 weight percent H₂O. Finally, the sample was transferred to a MAS rotor.

3.24.2 ²H Solid-State NMR spectroscopy

²H NMR spectra were acquired with a widebore Bruker Avance 400 NMR spectrometer operating at a resonance frequency of 61.4 MHz for ²H (magnetic field strength of 9.4 T). A double-channel solids probe equipped with a 5-mm solenoid coil was used.

The ^2H NMR spectra were accumulated with a spectral width of ± 250 kHz using quadrature phase detection, a phase-cycled quadrupolar echo sequence (Davis et al. 1976) with two $6.0 \mu\text{s}$ $\pi/2$ pulses separated by a $60 \mu\text{s}$ delay, and a relaxation delay of 0.5 s. A phase-cycled inversion-recovery quadrupolar echo pulse sequence was used to measure the relaxation times for the decay of Zeeman order (T_{1Z} ; spin-lattice relaxation time). A relaxation delay of 1.5 s was used and all other parameters were the same as for recording the ^2H NMR spectra. The signals were left-shifted after acquisition to initiate the Fourier transformation beginning at the top of the quadrupolar echo. An exponential line broadening not exceeding 50 Hz was applied.

The ^2H NMR powder-type spectra were de-Packed using the algorithm of McCabe and Wassall (McCabe and Wassall 1995), and order parameter profiles were determined from the observed quadrupolar splittings ($\Delta \nu_Q$) according to:

$$|\Delta \nu_Q^{(i)}| = \frac{3}{2} \chi_Q \left| S_{\text{CD}}^{(i)} \right| \left| P_2(\cos \theta) \right| \quad 3.22$$

Here $\chi_Q = e^2qQ/h$ represents the quadrupolar coupling constant (167 kHz for ^2H in the C– ^2H bond) and θ is the angle between the bilayer director axis and the main external magnetic field and P_2 is the second Legendre polynomial. For the de-Packed ^2H NMR spectra $\theta = 0^\circ$ and hence $P_2(\cos \theta) = 1$. The segmental order parameter is described by

$$S_{\text{CD}}^{(i)} = 1/2 \left\langle 3 \cos^2 \beta_i - 1 \right\rangle \quad 3.23$$

and depends on the angle β between the C– ^2H bond vector and the bilayer director axis where the brackets indicate an ensemble or time average. Details of the order parameter determination have been described in the literature (Huster et al. 1998). The Pake doublets were assigned starting at the terminal methyl group, which exhibits the smallest quadrupolar splitting. The methylene groups were assigned consecutively according to their increasing quadrupolar splittings.

3.24.3 ^{13}C NMR spectroscopy

The ^{13}C MAS NMR measurements were carried out on a Bruker Avance 750 Spectrometer (Bruker BioSpin GmbH, Rheinstetten, Germany) operating at a resonance frequen-

cy of 749.7 MHz for ^1H and 188.5 MHz for ^{13}C . A double-resonance MAS probe equipped with a 4 mm spinning module was used. The carbon magnetization was excited by either cross polarization (via ^1H), direct polarization or via an INEPT transfer (Morris and Freeman 1979; Gross et al. 1995). Typical pulse lengths were for 5 μs ^{13}C 90° pulse and 4 μs for the ^1H 90° pulse. ^{13}C CP MAS spectra were acquired with CP contact time of 700 μs . For heteronuclear decoupling, a ^1H radio-frequency field strength of 65 kHz was applied using the TPPM decoupling sequence (Bennett et al. 1995). ^{13}C chemical shifts were referenced externally relative to TMS (Morcombe and Zilm 2003). These NMR experiments were carried out at a temperature of 303 K and a MAS frequency of 7 kHz.

3.25 NMR experiments for phosphorylation studies

To phosphorylated PTH (1-84) HEK 293 cell lysate was used. The lysate was obtained (section 3.13) in the presence of kinase assay buffer, protease and phosphatase inhibitors. The NMR experiment was carried out by mixing lysate (15-20 mg/ml) with 30 μM of ^{15}N labeled PTH (1-84), 100 μM ATP, and 5 μM cAMP. This reaction mixture was incubated for 3 h at 37 $^\circ\text{C}$. Afterward, the reaction samples were dialyzed using a 1 kDa cut-off membrane in NMR buffer at 4 $^\circ\text{C}$ for 17 h in order to remove the unincorporated ATP and small molecules. The same samples were used for 1D ^{31}P NMR.

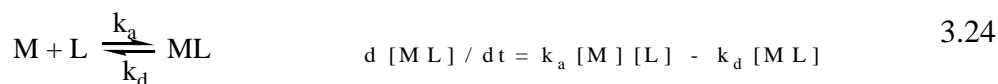
3.26 NMR experiments for inhibition of PTH fibrils

To identify the interaction sites of EGCG to monomer PTH (1-84), 50 μM of ^{15}N -PTH (1-84) were titrated with EGCG to the molar ratio of 1:1 and 1:5, respectively, and monitored by 2D ^1H - ^{15}N HSQC experiments. The NMR titration was carried out in 10 mM BisTris, 300 mM Na_2SO_4 , 0.02 % NaN_3 , pH 5.3 and at 25 $^\circ\text{C}$.

3.27 Surface Plasmon Resonance (SPR)

Surface Plasmon resonance (SPR) was carried to study the association (k_a) and dissociation (k_d) rate constants (Eq 3.17) for the interaction of PTH ligands to the nPTH1R. The experiment was performed on Biocore[®] T100 (Uppsala, Sweden) in 50 mM sodium phosphate, 150mM NaCl, pH 7.8 at 20 °C. The primary amine group of nPTH1R was chemically biotinylated using a kit instructed by company manufactures (Biotinylation kit-21335, Thermo Fisher Scientific, Germany). The biotinylated nPTH1R was immobilized on Biocore sensor chip-SA. Different concentration (0.1-50 μ M) of PTH ligands were injected over the flow rate of 30 μ l/min. Regeneration of the sensor chip surface was achieved by injecting 50 μ l of glycine buffer, pH 2.5 (Sigma-Aldrich, Munich, Germany). The activity of the regenerated chip was verified by repeating same data points. Data were analyzed by fitting to the 1:1 single site binding model provided by the company manufacturer (Kuziemko et al. 1996; Grauschopf et al. 2000).

When a ligand (L) interact with the receptor (M) the rate equation can be written as



Where k_a and k_d are the association and dissociation rate constants, respectively, [L], [M] and [ML] are the concentrations of the free ligand, free receptor, and the receptor ligand complex respectively. Since the signal from the biosensor R is proportional to the amount of complex and the maximum signal (R_{max}), when all the sites are occupied, is proportional to the initial concentration of L, so equation 3.24 can be rewritten as

$$d R / dt = k_a (R_{max} - R) [M] - k_d R \quad R = R_0 e^{-k_d (t - t_0)} \quad 3.25$$

Where R_0 is a response at an arbitrary starting time t_0 . The association and dissociation rate constants were obtained from the above integrated equations using biocore software.

4 Results

4.1 The overexpression and purification of nPTH1R

PTH regulates the calcium and phosphate level in blood by acting at the PTH1R. Biophysical studies to investigate the molecular mechanism of this interaction required large protein samples. Recombinant unlabeled and ^{15}N labeled ECD of PTH1R were expressed in *E. coli* from the expression vector pET15b. The nPTH1R was present (**Fig. 4.1A**) in the insoluble fraction after expression at 37 °C (lane 2). IBs were isolated from the cell lysates and extensively washed to remove soluble protein (lane 3). Further purification of IBs was done on Ni-IMAC under denatured conditions (lane 4) to prevent precipitation and aggregation. The denatured protein was then rapidly diluted to the protein end concentration of 0.2 mg/ml in a refolding buffer containing 1M L-Arginine, 5mM GSSG and 1mM GSH and pH 8.0. Renatured protein was then purified by the ammonium sulfate salt precipitation method, HIC (lane 5) and a gel filtration chromatography (lane 6) (Grauschopf et al. 2000). The native protein migrates at 21.6 kDa on the SDS-PAGE gel (indicated by the arrow), consistent with the calculated molecular weight by the ExPASy tool. The final yield was 105 mg from 4 liters of rich culture media (70 g wet weight of cells, 6.8 g of IBs and refolding yield was 35%). To carry out NMR experiments, ^{15}N labeled nPTH1R was purified with the same protocol as described for unlabeled protein (section 3.9 and 3.10) that yielded 36.6 mg from 4 liters of M9 culture media (**Fig. 4.1B**).

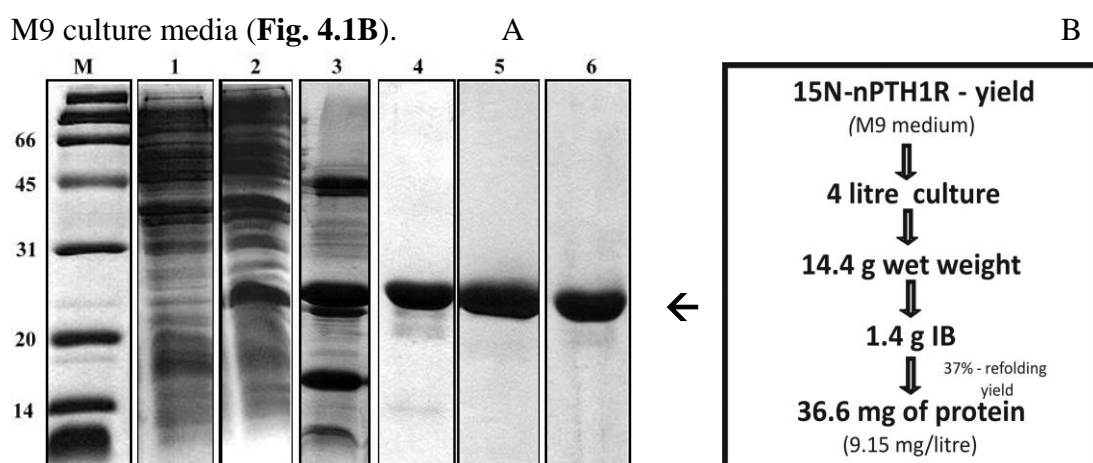


Fig. 4.1. SDS-PAGE results for the expression, renaturation and purification of nPTH1R. (A) Coomassie-stained gel showing, Lanes: M, molecular weight marker in kDa; 1, whole bacteria lysates (before induction) ; 2, four hours after 1mM IPTG induction; 3, IB preparation; 4, elute of from Ni-IMAC column for the sample from lane 3; 5, elute from the HIC column; 6, elute of nPTH1R from gel filtration column. Arrows refer to the protein of 21.6 kDa (B) ^{15}N -nPTH1R was expressed in 4 litre of M9 minimal media and 14.4 g of cells were harvested. Cells was lysed by sonication. The cell pellets were washed by 2% Triton-100 and 1.4 g of IBs were obtained. After refolding, HIC and gelfiltration chromatography, 36.6mg of pure nPTH1R (9.15 mg/liter) were obtained.

4.2 Purification of PTH fragments

All three PTH fragments namely PTH (15-34), PTH (1-34), PTH (1-84) expressed (un-labeled and ^{15}N and/or ^{13}C labeled) as a SUMO fusion protein in BL21 codonPlus-RIL at 37 °C. SUMO fusion tag has been reported to enhance expression and solubility (Marblestone et al. 2006). PTH fragments were purified using Ni-IMAC, followed by a cleavage of fusion part, then purified by HPLC or gel filtration chromatography. A detailed protocol for expression and purification of different PTH fragments from SUMO fusion protein is mentioned in section 3.11. The efficiency of the cleavage reactions and purity of the peptide fragments were checked by SDS-PAGE gel (figures were shown below) and confirmed by MALDI-TOF mass spectrometry (**Table 4.1**).

4.2.1 PTH (15-34)

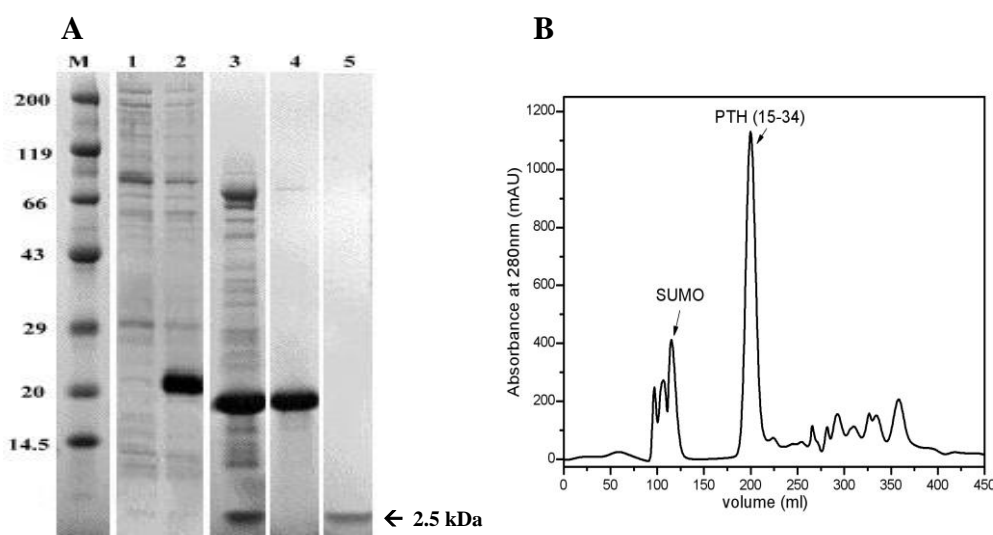


Fig. 4.2. SDS-PAGE analysis (4-20%) and gel filtration profile for the purification of PTH (15-34). (A) Lane M, protein molecular weight marker (kDa); lane 1, before induction; lane 2, after induction with 1mM IPTG; lane 3, fusion protein purified after the first Ni IMAC column, cleaved by SUMO protease and cleaved product applied on gel; lane 4, SUMO fraction from the gel filtration column; lane 5, PTH (15-34) fraction from the gel filtration column, corresponds to molecular weight of 2.5kDa show by arrow mark. (B) The chromatogram obtained for the final gel filtration step of PTH (15-34). Peptide was eluted between the elution volume of 189 and 212 ml with the flow rate of 2.5 ml/min on S-30 peptide column.

Small peptides are difficult to express in bacterial systems due to their size. Use of the SUMO fusion expression system (Bosse-Doenecke et al. 2008), leads to the successful overexpression (**Fig. 4.2**) of the fusion protein (lane 2). The soluble fusion protein was

purified by Ni-IMAC using imidazole gradient. The fusion part was cleaved (see section 3.11.3) by Ulp1 SUMO protease (lane 3). The PTH (15-34) was separated from the cleavage product by a gel filtration chromatography (lane 4 and 5). Purified peptide was confirmed by MALDI-TOF mass spectrometry. One liter of culture yielded 1-4 mg of peptide in the rich or M9 medium. To avoid degradation all the purification steps were carried out continuously. Alternatively samples can be frozen at -20 °C.

4.2.2 PTH (1-34)

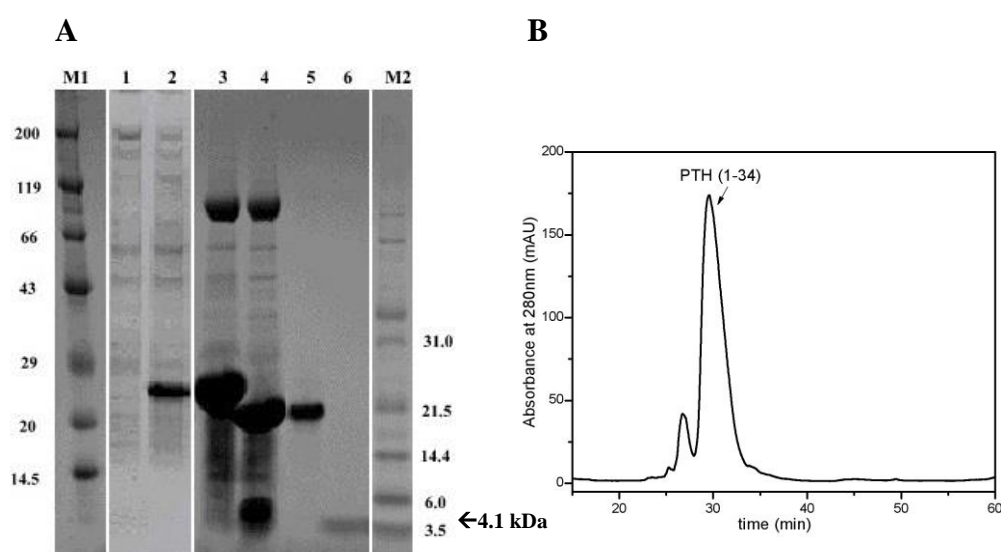


Fig. 4.3. SDS-PAGE (4-20%) of the different stage of purification of PTH (1-34). (A) lane 1, uninduced; lane 2, after induction by 1mM IPTG; lane 3, elute of His₆-SUMO-PTH (1-34) from first Ni-IMAC; lane 4, SUMO protease cleavage protein samples; lane 5, elute of His₆-SUMO from second Ni-IMAC; lane 6, purified PTH (1-34) after elution from RP-HPLC; lanes M1 and M2, lower molecular weight protein markers. (B) RP-HPLC trace of PTH (1-34), measured absorbance at 280 nm versus time. The peak at 39% buffer B corresponds to peptide.

The active fragment of human parathyroid hormone, consisting of the N-terminal amino acids 1 to 34, was produced as a SUMO fusion protein from the culture supernatant of BL21 codonPlus-RIL. Results were shown in **Fig. 4.3**. His₆ tagged fusion proteins were purified using Ni-IMAC by eluting with 250mM Imidazole concentration (lane 3). The fusion protein was digested with the SUMO protease to the ratio of 1: 100 (volume of protease to the fusion protein) at 4 °C for an hour. The fusion protein was found to be cleaved completely (lane 4). The mixture of the cleavage reaction reapplied to the Ni-IMAC to remove His₆ tagged SUMO (lane 5). The flow through from the second Ni-IMAC was applied on RP-HPLC and PTH (1-34) was eluted (lane 6) at 40% of buffer B

(**Fig. 4.3B**). The typical yield was 4-10 mg of peptide per liter of bacterial culture (both M9 and dYT culture). During HPLC purification of PTH (1-34), the other byproducts were obtained with the defined fragments, PTH (1-33), PTH (1-30), PTH (1-27), PTH (1-25), and PTH (1-24). To accomplish this, the purification steps were carried out continuously and protease inhibitor cocktail was added in each step of purification.

4.2.3 PTH (1-84)

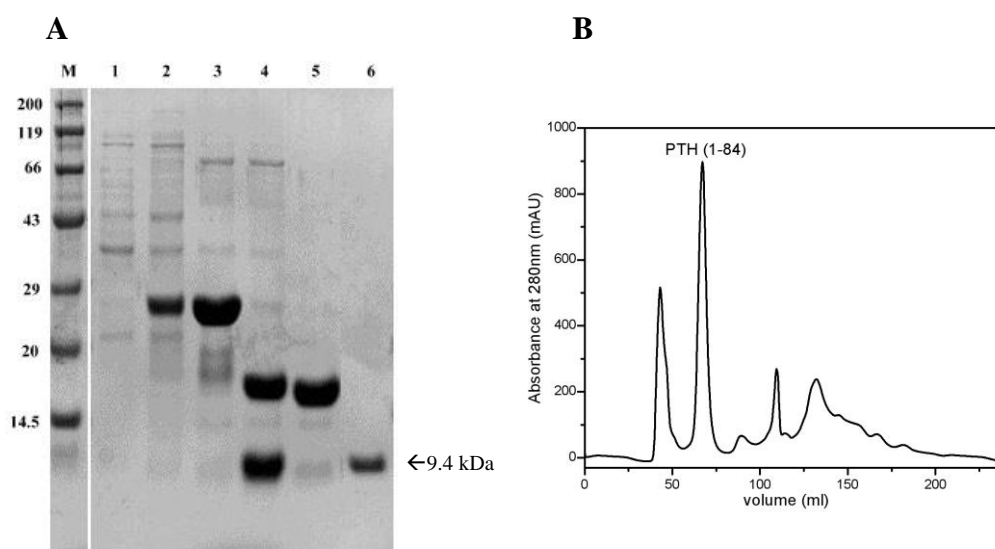


Fig. 4.4. SDS-PAGE (12.5%) analysis and gel filtration chromatogram of purified PTH (1-84). (A) lane M, protein molecular weight marker in kDa; uninduced; and induced by 1mM IPTG (lanes 1 and 2); lane 3, fusion protein purified by Ni-IMAC; lane 4, PTH (1-84) released from fusion protein, cleaved by SUMO protease; lane 5, His₆ tagged SUMO were separated from cleavage mixture by second Ni-IMAC; lane 6, PTH (1-84) were purified from the flow through of lane 5 by gel filtration chromatography. (B) Gel filtration chromatogram of PTH (1-84) was monitored by absorption at 280 nm. The feeding samples were taken from the flow through of second Ni-IMAC.

The full-length PTH was expressed in BL21 codonPlus-RIL using the pETSUMOPHTH expression vector. Results were shown in **Fig. 4.4**. The N-terminal His₆ tagged SUMO fusion protein was found in the soluble fraction after cell lysis in a French Press or sonication (lane 2). The fusion protein was purified on a Ni⁺ loaded IMAC sepharose resin (lane 3). Cleavage of PTH (1-84) from the His-SUMO-PTH (1-84) fusion protein (see 3.11.5) was carried out by incubating fusion protein with partially purified SUMO proteases in SUMO buffer (lane 4). The cleavage product was loaded on a Ni-IMAC and His₆ tagged SUMO were separated from cleavage mixture (lane 5). Flow through from the second Ni-IMAC was collected and applied on gel filtration Superdex 75 column. The detailed chromatography profile of the purified PTH (1-84) (lane 6) was shown in

Fig. 4.4B. The final yield was 20-50mg of PTH (1-84) per liter of dYT or M9 culture media.

Table 4.1. Mass spectrometry (MALDI-TOF) results of purified PTH fragments.

<i>PTH fragments</i>	<i>Observed molecular weight</i>	<i>Predicted molecular weight*</i>
PTH (15-34)	2542.8 Da	2542.9 Da
PTH (1-34)	4120.2 Da	4117.8 Da
PTH (1-84)	9426.7 Da	9424.7 Da

* Molecular weight predicted with an amino acid sequence using ExPASy-ProtParam tool.

4.3 Functional studies of purified nPTH1R

4.3.1 Unbound nPTH1R exist as monomer in solution

The human nPTH1R was expressed and purified for biophysical studies. Pioszak and coworker have shown that the crystal structure of the unliganded nPTH1R was a dimer (Pioszak et al. 2010). However, Grauschopf and coworker showed it was a monomer in solution by analytical ultracentrifugation method (Grauschopf et al. 2000). To address this question, pulse field gradient (PFG) NMR diffusion measurements were performed (see 3.23.3).

Fig. 4.5. NMR intensity at different gradient strengths in PFG NMR experiment of nPTH1R (80 μ M), in a buffer containing 20mM NaH₂PO₄, 300mM Na₂SO₄, 10% D₂O and pH 6.0. The red line represents a nonlinear, least-square fit of equation 3.11 of the data (integral between 0.5 and 2.5 ppm). The measured D value is $(1.13 \pm 0.01) \times 10^{-10}$ m²/s and corresponding R_h = 20.34 Å (Equ. 3.12.)

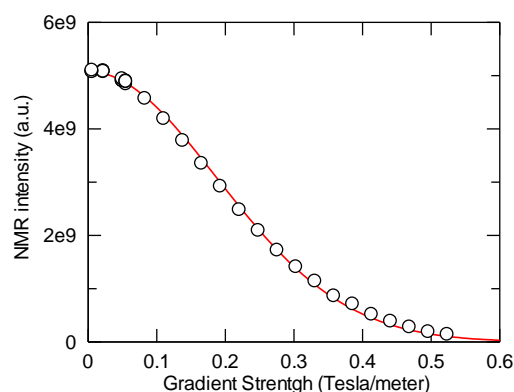


Table 4.2 Diffusion constant and hydrodynamic radii of nPTH1R.

<i>nPTH1R state</i>	<i>D (m²/s)</i>	<i>R_h (Å)^a</i>	<i>R_h (Å)^b</i>
monomer (189 aa)	$1.13 \pm 0.01 \times 10^{-10}$	20.34 ± 0.18	21.7

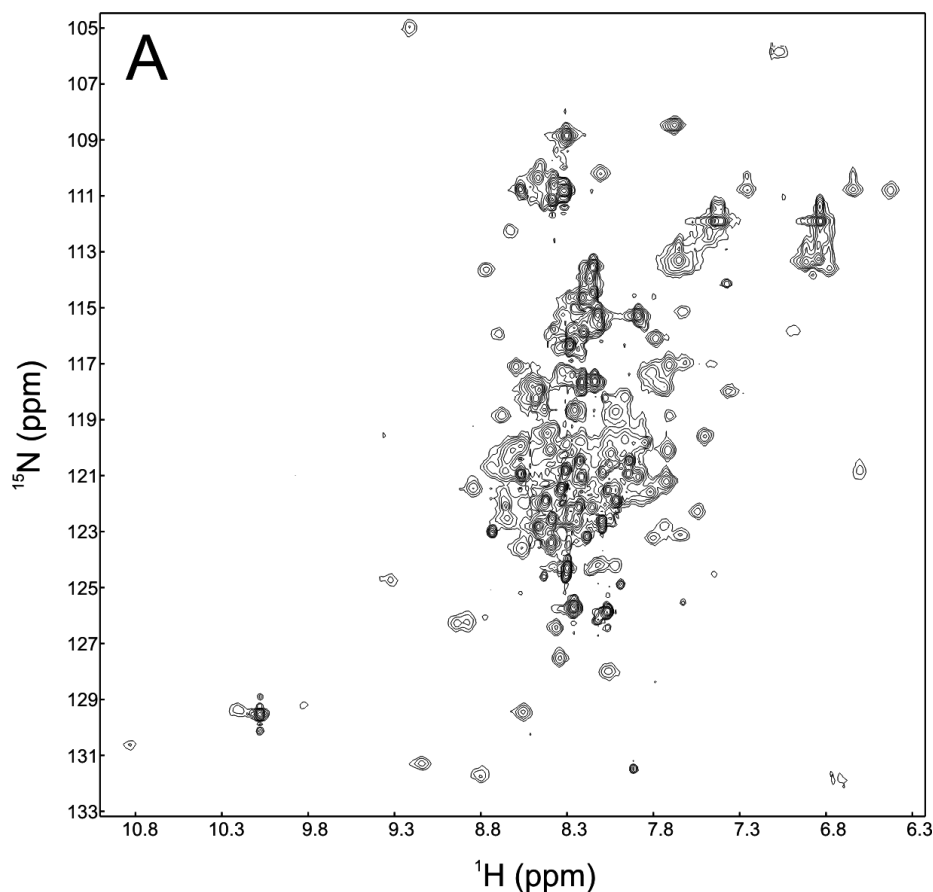
^a The observed R_h value, calculated using Stoke-Einstein equation.

^b R_h calculated using the empirical formula (see 3.12). aa: amino acids.

Through the diffusion experiment the effective hydrodynamic radii (R_h) of nPTH1R was calculated from the measured diffusion constant (D) (**Fig. 4.5**) using Stoke-Einstein equation (Wilkins et al. 1999). The results were shown in **Table 4.2**. The experimental result is in excellent agreement with the predicted hydrodynamic radii, indicating that the purified nPTH1R is a monomer in solution under NMR conditions.

4.3.2 Interaction of ^{15}N -nPTH1R with unlabeled PTH (1-84)

Parathyroid hormone 1 receptor consists of a large N-terminal extracellular domain, additionally to the intracellular and 7 TM domain. It has been shown in the literature that C-terminal portion of PTH (1-34) interact with the nPTH1R to impart a strong binding while signaling and activation are results from the interaction of an N-terminal portion of the peptide with juxtamembrane domains (**Fig. 1.7**). These observations are so called “two-site binding model”, which were based on results obtained by a large number of mutations and photochemical cross-linking studies (Hoare et al. 2000). In order to understand molecular level of PTH-nPTH1R interaction and nPTH1R recognition of other ligands, ^{15}N -nPTH1R has been refolded and purified (section 3.9).



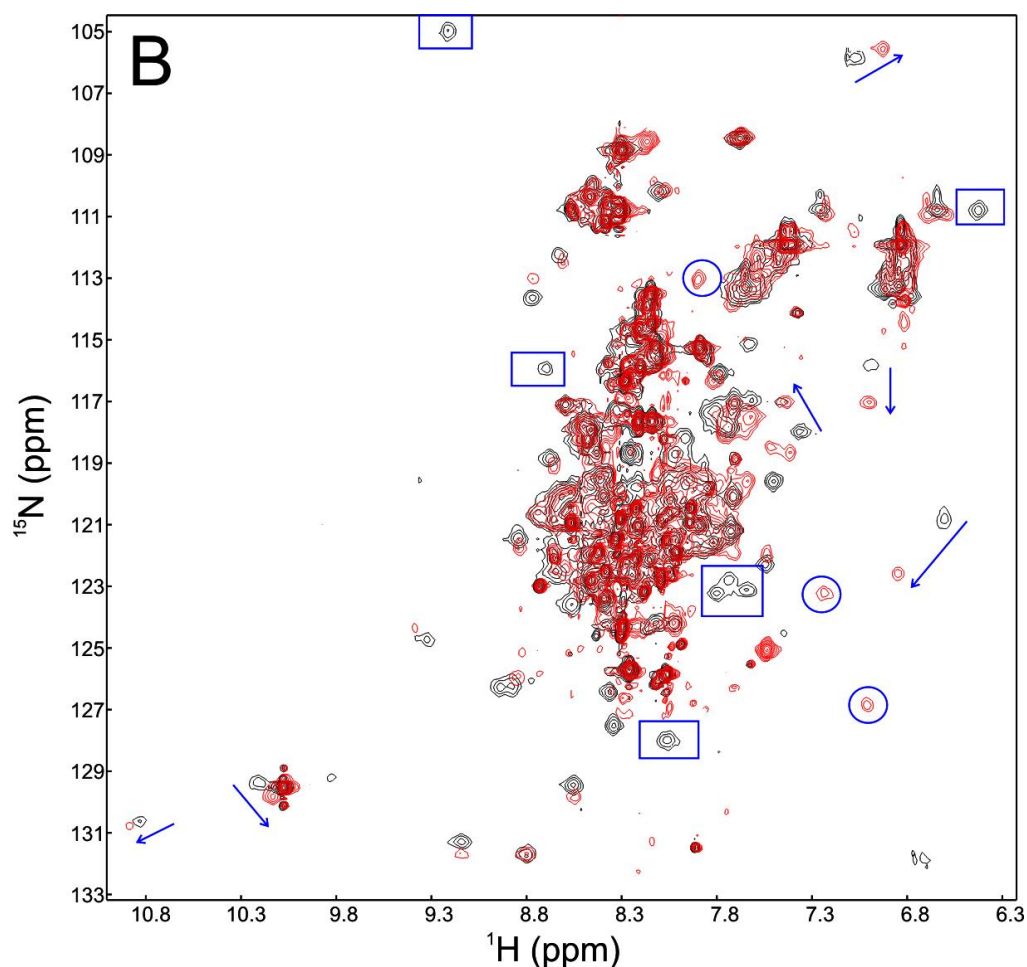


Fig. 4.6. 2D.¹⁵N-HSQC spectra of unliganded nPTH1R and complex with PTH (1-84) measured at 25 °C. (A) ¹⁵N-HSQC spectra of free ¹⁵N-labeled nPTH1R (270 μM). (B) Overlay of unbound nPTH1R in black contours and bound to unlabeled PTH (1-84) in red contours (nPTH1R to the ligand ratio of 1:1.7). Significant changes were observed in the backbone amides of nPTH1R upon binding. Some examples were illustrated by symbols. Arrow marks for peaks which disappear and appear at new chemical shift value, square for disappearance of free form and circle for appearance of new peak upon complex formation.

¹⁵N-HSQC spectrum obtained for well-folded free nPTH1R (270 μM) is shown in **Fig. 4.6A**. (measured in a buffer containing 20 mM NaH₂PO₄, 300 mM Na₂SO₄, pH 6.0, 10% D₂O at 25 °C). Overall, limited chemical shift dispersion was seen along the ¹H dimension between 8 and 8.5 ppm. These residues correspond to approximately 50% of the unstructured residues (see the CD spectra of nPTH1R in **Fig. 4.16**) in good agreement with the CD analysis. Some backbone resonances were broad, indicating the conformational instability with the time scale of a microsecond to millisecond range. The changes in temperature or pH failed to improve the quality of the spectrum. This result is consistent with spectra obtained for ECD of corticotrophin-releasing factor 1 recep-

tor, the other members of the class B GPCR receptor family (Grace et al. 2007; Grace et al. 2010) and the crystal structure of nPTH1R (Pioszak and Xu 2008).

To examine the effect of PTH (1-84) binding to nPTH1R, NMR titrations were performed. An Overlay of the ^{15}N -HSQC spectrum of ^{15}N -nPTH1R in the absence (black) and the presence (red) of unlabeled PTH (1-84) at 1:1.7 stoichiometry ratio shown in **Fig. 4.6B**. Simultaneously ^{15}N -TROSY-HSQC was also recorded and results were same as a ^{15}N -HSQC spectrum. Following agonist binding, significant chemical shift perturbation (symbols) was observed. Some cross peaks first disappeared (square) and appeared at different chemical shifts (circle). Some new cross peaks are also seen. This implies that the intermolecular interaction is in the slow exchange timescale ($k_{\text{ex}} < \Delta\delta$). The number of cross peaks in the bound form is larger than the free form which indicates that the bound nPTH1R is more structured than the unbound form. Also, the change in the tryptophan fluorescence of nPTH1R upon addition of ligand (Henze 2016) was confirmed by chemical shift perturbation of tryptophan side chains at 10.2 ppm and 10.8 ppm.

4.4 Characterization of PTH (15-34) (antagonist) Interaction with nPTH1R

The two-site activation model of PTH1R gets supported by the observation that the N-terminal 15 to 34 residues, the minimum length of PTH are capable of binding to the nPTH1R. However, it failed to activate the receptor (Pioszak and Xu 2008). In order to understand the structural basis for the binding of the antagonist to the nPTH1R in solution biophysical studies were carried out using purified labeled and unlabeled PTH (15-34) (section 3.11).

4.4.1 PTH (15-34)-Receptor interaction studied by ITC and NMR

Using HNCA, HNCACB, ^{15}N -NOESY-HSQC, and ^{15}N -TOCSY-HSQC experiments, all the amide resonances were assigned in the ^{15}N -HSQC spectrum of ^{15}N -PTH (15-34) (**Fig. 4.7**). The chemical shift index (CSI) method (Wishart et al. 1995) predicts α helix

for all the residues in the peptide (**Fig. 9.1**), which are in good agreement with the literature reported for solution structure of PTH (1-34) (Marx et al. 2000)

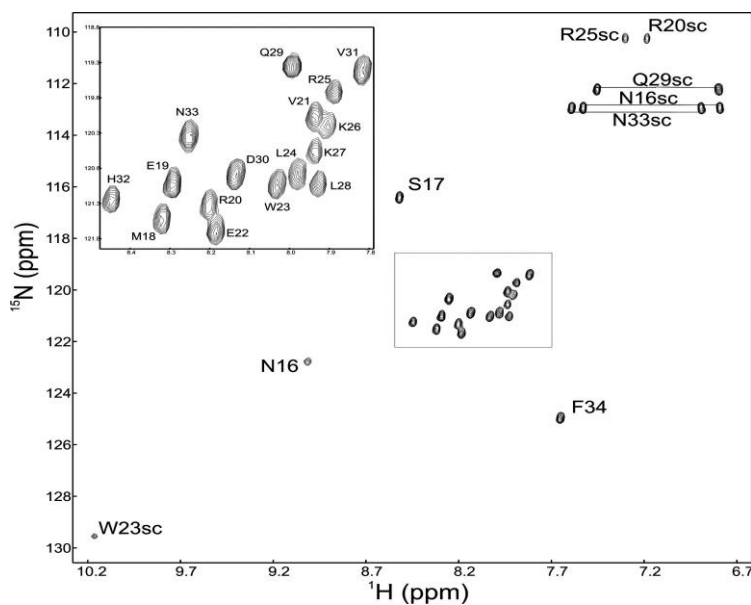


Fig. 4.7. 2D ^{15}N -HSQC spectrum of PTH (15-34). Inserted panel are expansion of the region shown in the box. Assignments were shown in single letter code. Spectrum measured at 25 °C in 20 mM sodium phosphate, 300 mM Na_2SO_4 , 0.02% NaN_3 , 10% D_2O , and pH 6.0. Arginine side chains were folded in the spectrum along the 15N dimension..

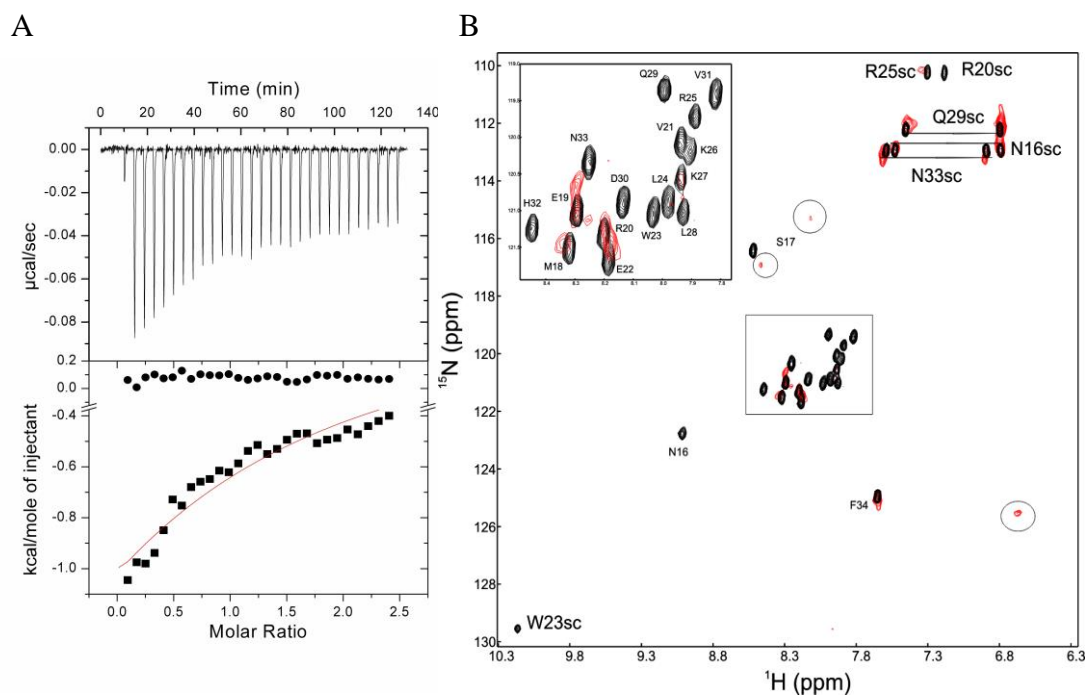


Fig. 4.8. Binding studies of PTH (15-34) with nPTH1R by isothermal titration calorimetry and NMR. **A.** PTH (15-34) (251 μM) was titrated into nPTH1R (23 μM), measured at 20 °C. The negative deflections are indicative of an exothermic reaction. The bottom panel shows the derived binding isotherm and the heat of dilution control experiment. The red line is the best fit to the experimental data assuming 1:1 binding model, K_d of $80 \pm 12 \mu\text{M}$ was calculated. **B.** ^{15}N HSQC of unbound (black) ^{15}N -PTH (15-34) and its bound form (red) with unlabeled nPTH1R (1:2 molar equivalent, ligand to ECD ratio). Most of the cross peaks disappeared and some new peaks appeared (shown by circle) upon complex formation.

The binding of PTH (15-34) with nPTH1R was first studied by ITC experiment. Experimental conditions and parameters were explained in section 3.22.2. PTH (15-34) exhibited an exothermic interaction with nPTH1R, whereas no heating of binding was detected when peptide titrated to the buffer (**Fig. 4.8A**). These data indicates that the PTH peptide interacts to the receptor domain. A dissociation constant (K_d) of $80 \pm 12 \mu\text{M}$ was calculated. K_d of $61 \pm 12 \mu\text{M}$ was calculated using surface plasmon resonance experiments (**Fig. 9.2**). This corresponds to an about 20 fold reduced affinity compared to the PTH (1-34/84) (see below).

To characterize this weak interaction, NMR titration experiments with unlabeled nPTH1R were conducted at 25 °C by collecting HSQC spectra on ^{15}N -PTH (15-34). In the apo form, all the NH signals were visible (black in **Fig. 4.8B**). But in the complex, most of the cross peaks disappeared (red in **Fig. 4.8B**). This indicates binding of PTH (15-34) to the nPTH1R and loss of intensity was due to the decrease in overall tumbling of the peptide and most probably reaching the intermediate exchange regime ($k_{\text{ex}} \sim \Delta\delta$) of peptide and receptor domain. Residues S17, N33, F34 and side chains NHs were still visible with slightly different chemical shift than in the apo form. These residues were corresponds to the N and C-terminal region of the peptide. A couple of peaks reappeared at different chemical shift values (circle). Changes in buffer conditions, pH and temperature failed to improve the quality of spectra. These observations revealed that all the residues in the PTH (15-34) interact with the nPTH1R and nicely correlate with the published crystal structure (Pioszak and Xu 2008).

4.5 Interaction studies of PTH (1-34) (agonist) with nPTH1R

Recombinant PTH (1-34) has been used as a drug (Forteo[®], Eli Lilly) for the treatment of osteoporosis and was approved by FDA in 2002. At present, only a single anabolic agent, PTH (1-34), is available to treat osteoporosis (Yasothan and Kar 2008). PTH (1-34), an agonist, has been shown to bind with high affinity PTH1 receptor. Based on the mutational studies on PTH1R, the two-site binding model has been proposed. A C-terminal portion of PTH (1-34) binds to the large amino-terminal extracellular domain

of the receptor and N-terminal portion of the ligand binds to the juxtamembrane domain (Hoare et al. 2000). To obtain more structural details of the complex, PTH (1-34) and nPTH1R was recombinantly expressed and interaction studies were performed.

4.5.1 ITC studies of PTH (1-34)/nPTH1R complex

ITC measurements were used to investigate the thermodynamics of binding of PTH (1-34) to the nPTH1R. The ligand was titrated into a solution of nPTH1R and the resulting heat change and binding data are shown in **Fig. 4.9**. The binding process was an exothermic reaction and accompanied by a loss of entropy (**Table 4.3**). This revealed that complex becomes more structured and thus increasing the overall order of the system. Dissociation constant (K_d) of 4.2 μM and a binding stoichiometry of 1:1 were obtained from the best fit to the experimental data. This K_d value is in good agreement with the literature value (K_d of 6 μM) obtained by others (Monaghan et al. 2007; Pioszak and Xu 2008). A control titration of PTH (1-34) into buffer was performed and subtracted from the real experimental data to account for the heat of dilution.

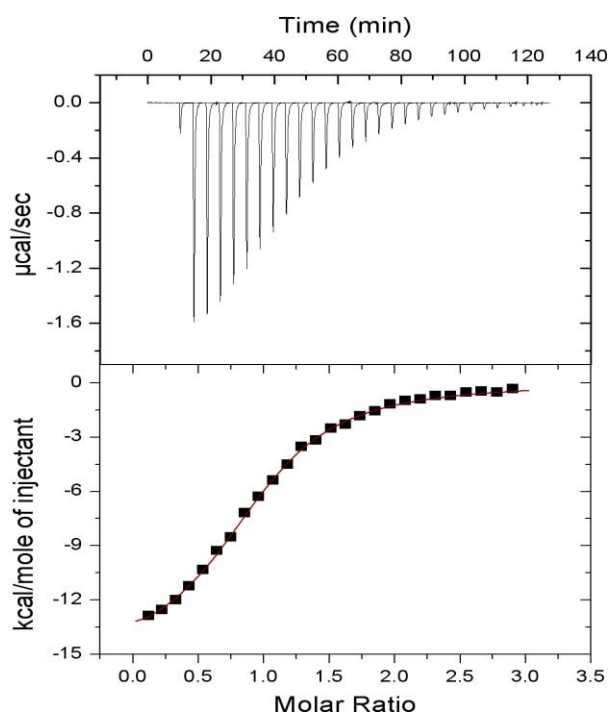


Table 4.3. Thermodynamic parameters derived from ITC data for PTH (1-34)/nPTH1R complex

n	0.942 ± 0.01
K_a	$2.37 \pm 0.088 \times 10^5 \text{ M}^{-1}$
ΔH	$-15.33 \pm 0.16 \text{ kcal mol}^{-1}$
ΔS	$-27.7 \text{ cal K}^{-1} \text{ mol}^{-1}$
ΔG	$-7.208 \text{ kcal mol}^{-1}$
K_d	$4.22 \pm 0.15 \times 10^{-6} \text{ M}$

Fig. 4.9. ITC profile for the binding of PTH (1-34) to the nPTH1R. Top panel: Heat flow versus time profile resulting from injection of 10 μl aliquots containing 400 μM PTH (1-34) into a solution of 28 μM nPTH1R in 20 mM sodium phosphate buffer, 300 mM sodium sulfate, pH 6.0 and measured at 20 $^\circ\text{C}$. Bottom panel: Plots of the heat change as function of ligand to the nPTH1R molar ratio, shown after subtraction of background heats determined in ligand to buffer experiments. The red line is the best fit to the experimental data assuming 1:1 binding model. The calculated thermodynamic parameters are given on the right side (Table 4.3).

4.5.2 SPR studies of PTH (1-34)/nPTH1R complex

Surface plasmon resonance (SPR) measurements were used to investigate the kinetic mechanism of PTH (1-34) interaction to the nPTH1R. In this experiments, chemically modified biotinylated nPTH1R was immobilized on the surface of the Biocore sensor chip SA. PTH (1-34) was injected with increasing concentration (0.2 - 45 μM) at a constant flow of 30 $\mu\text{l}/\text{min}$ on the surface. The mass of the bound molecules on the surface was monitored in terms of response unit RU. The resulting sensorgrams are shown in **Fig. 4.10A**.

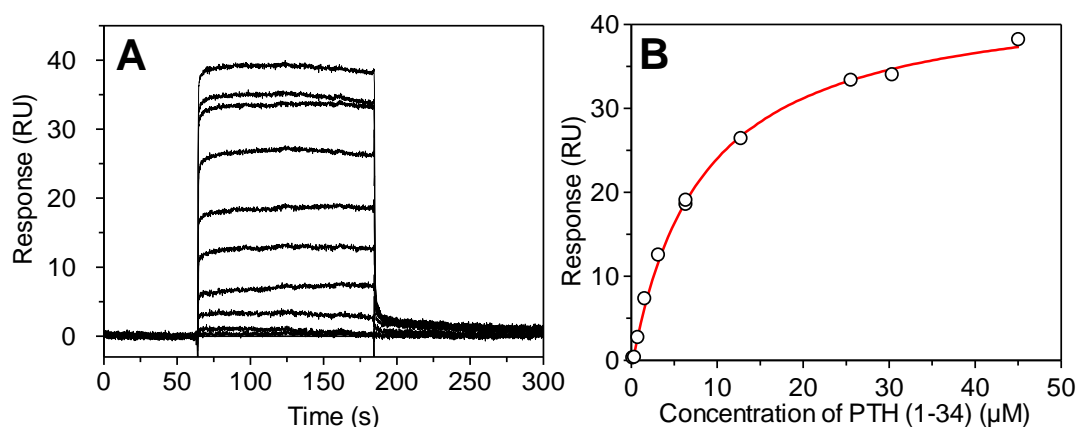


Fig. 4.10. Kinetics of PTH (1-34)-nPTH1R binding studied by SPR. **A.** Sensorgrams showing serial injections of PTH (1-34) at a concentration of (from bottom to top) 0.2, 0.4, 0.8, 1.6, 3.2, 6.4, 12.8, 25.6, 30.4, 45.1 μM immobilized nPTH1R on the sensor chip SA. The experimental data are fitted globally to a 1:1 single site binding model, yielding k_a and k_d of $(9.578 \pm 0.21) \times 10^3 \text{ M}^{-1}\text{s}^{-1}$ and $1.75 \pm 0.02 \times 10^{-2} \text{ s}^{-1}$, respectively. **B.** steady-state values (circle) were plotted against concentration of PTH (1-34). The red line represents the fit of the data to the steady-state model. The obtained K_d value was $8.03 \pm 0.57 \mu\text{M}$. Experiment was performed at 20 $^\circ\text{C}$ in 50 mM sodium phosphate, 150mM NaCl, pH 7.8.

The apparent association and dissociation rate constants were estimated by global fitting to the data to a single site binding model. The the association and dissociation rate constants were $(9.578 \pm 0.21) \times 10^3 \text{ M}^{-1}\text{s}^{-1}$ and $1.75 \pm 0.02 \times 10^{-2} \text{ s}^{-1}$, respectively. Affinity analysis was done by plotting the steady-state values against the concentration of PTH (1-34) (**Fig. 4.10B**) resulted in K_d of $8.03 \pm 0.57 \mu\text{M}$. This value is in good agreement with the binding affinity obtained by ITC experiment ($4.22 \mu\text{M}$), suggesting that immobilized and free nPTH1R interact with PTH (1-34) very similarly.

4.5.3 NMR interaction studies of PTH (1-34) to the nPTH1R

NMR interaction studies were performed on recombinantly produced isotope labeled (^{15}N and/or ^{13}C) PTH (1-34). The ^{15}N -HSQC spectrum of ^{15}N -PTH (1-34) is shown in **Fig. 4.11**. All the backbone and side chain resonances in the spectra were assigned by using standard 2D and 3D NMR experiments and confirmed with previously assigned chemical shift values (Marx et al. 2000; Scian et al. 2006). The spectra measured at pH 6.0 yield sharp cross peaks, however, most of the NH signals was not visible at pH 7.5. This topology is consistent with the CD spectra and heteronuclear ^1H - ^{15}N NOE correlation map (^1H - ^{15}N NOE value of 0.33) of the peptide, which revealed that the peptide is unstructured with a certain propensity of a helical conformation (**Fig. 9.3**).

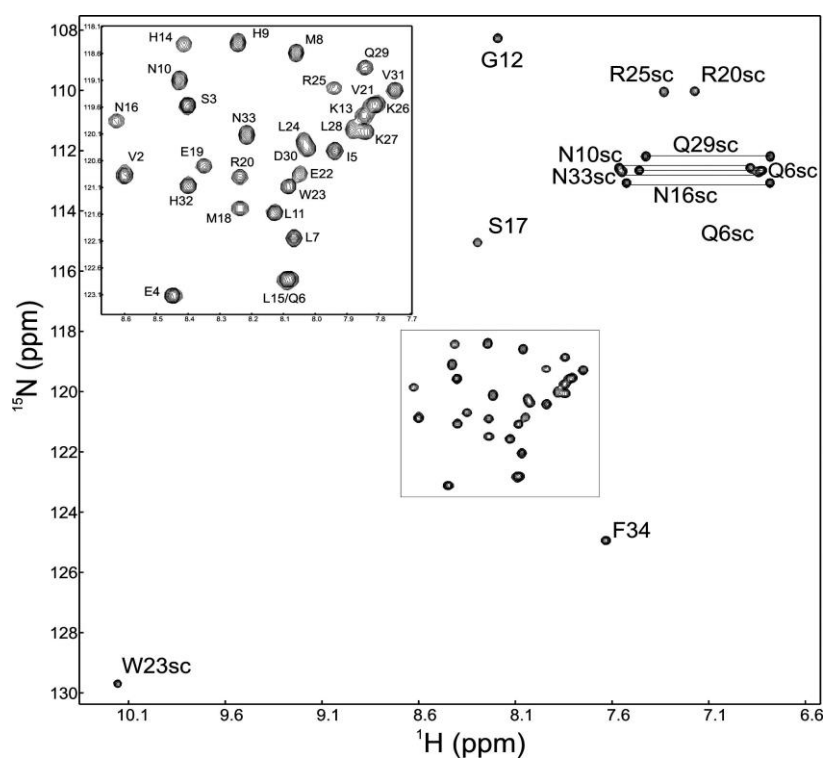


Fig. 4.11. 2D ^{15}N -HSQC spectrum of PTH (1-34). Inserted panel are expansion of the region shown in the box. Spectrum measured at 25 °C in 20 mM sodium phosphate, 300 mM Na_2SO_4 , 0.02% NaN_3 , 10% D_2O , and pH 6.0. Arginine side chains were folded in the spectrum. The amino acid side chains are denoted by amino acid number and followed by sc.

NMR is a powerful technique to investigate conformational and dynamic changes upon protein-protein interactions in solution. Therefore, NMR titration experiments were performed with ^{15}N -PTH (1-34) and unlabeled nPTH1R1. The amide resonance of ^{15}N -PTH (1-34) was detected at ^{15}N -HSQC spectrum. The spectrum of ^{15}N -PTH (1-34) in the free

(black in **Fig. 4.12**) and bound state (red in **Fig. 4.12**) shown significant differences in the chemical shifts and the line width of the resonances of individual residues. About half of the resonances got broadened beyond detection limits possibly because of reaching the intermediate exchange regime in the bound state. These resonances belong to the C-terminal half of PTH (1-34) and comprise Glu19-Phe34 plus some of its N-terminal half. Val2-Gly12 plus Leu15 and Met18 show detectable resonances in the bound state without or with only small changes in the chemical shifts.

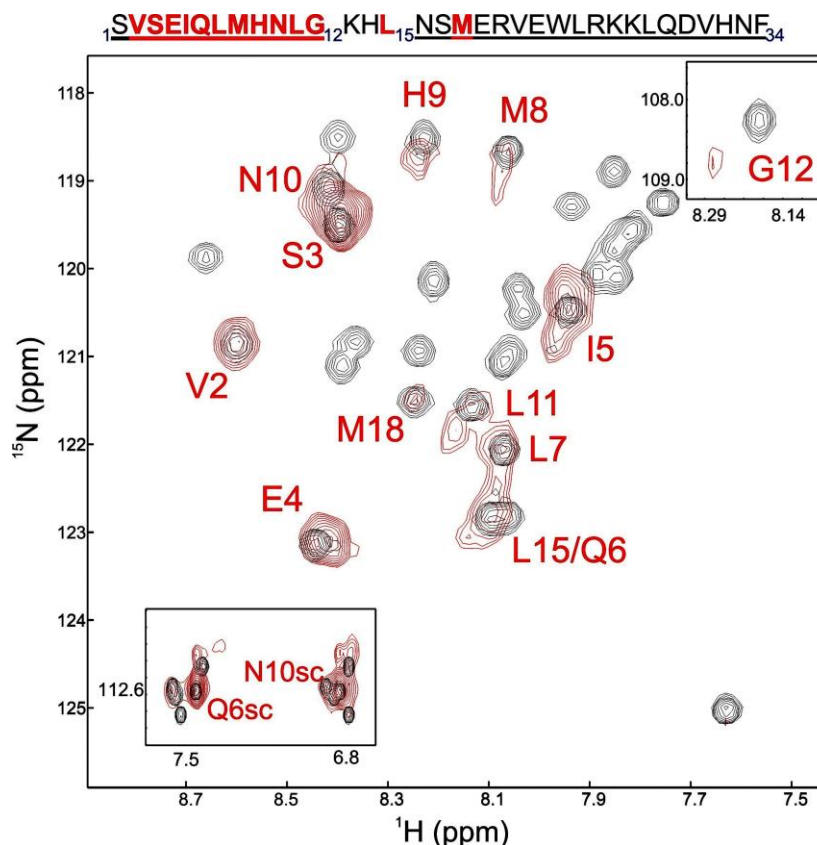


Fig. 4.12. 2D ^{15}N -HSQC spectra of free and nPTH1R bound ^{15}N -PTH (1-34). Spectra of free 0.75 mM ^{15}N -PTH (1-34) (black) and of the ^{15}N -PTH (1-34)/nPTH1R complex (red) at a ratio of 1:1.47 were recorded at 25 °C. Red letters in the PTH (1-34) sequence (top) indicate residues, which showed detectable resonance of the ^{15}N -PTH (1-34)/nPTH1R complex (Drechsler et al. 2011).

The NMR spectrum of the bound state thus indicates that the C-terminal half of PTH (1-34) binds to nPTH1R whereas the N-terminal half remains solvent exposed and flexible enough to result in observable resonances. This result is consistent with the data obtained for PTH (15-34) (see 4.4.1). The general line broadening of the latter resonances is caused by the reduced overall tumbling of the complex compared to free PTH (1-34) (Drechsler et al. 2011). This observation in solution corresponds nicely to recent

structural work, where the C-terminal fragment PTH (15-34) could be crystallized in complex with nPTH1R (Pioszak and Xu 2008). The intermediate exchange was quantified using biocore data (see 4.5.2) and the calculated value was $k_{ex} = \sim 6$ Hz, under NMR conditions.

4.6 Competition binding between PTH (15-34) and PTH (1-34) to the nPTH1R

PTH (1-34) is an agonist and PTH (15-34) is an antagonist, both bind to the nPTH1R with the K_d of $4.2 \mu\text{M}$ and $\sim 80 \mu\text{M}$, respectively, determined by ITC and SPR. NMR is a powerful technique to identify and to investigate interactions from a mixture of ligands to the protein in a competitive manner. To understand molecular level of bound

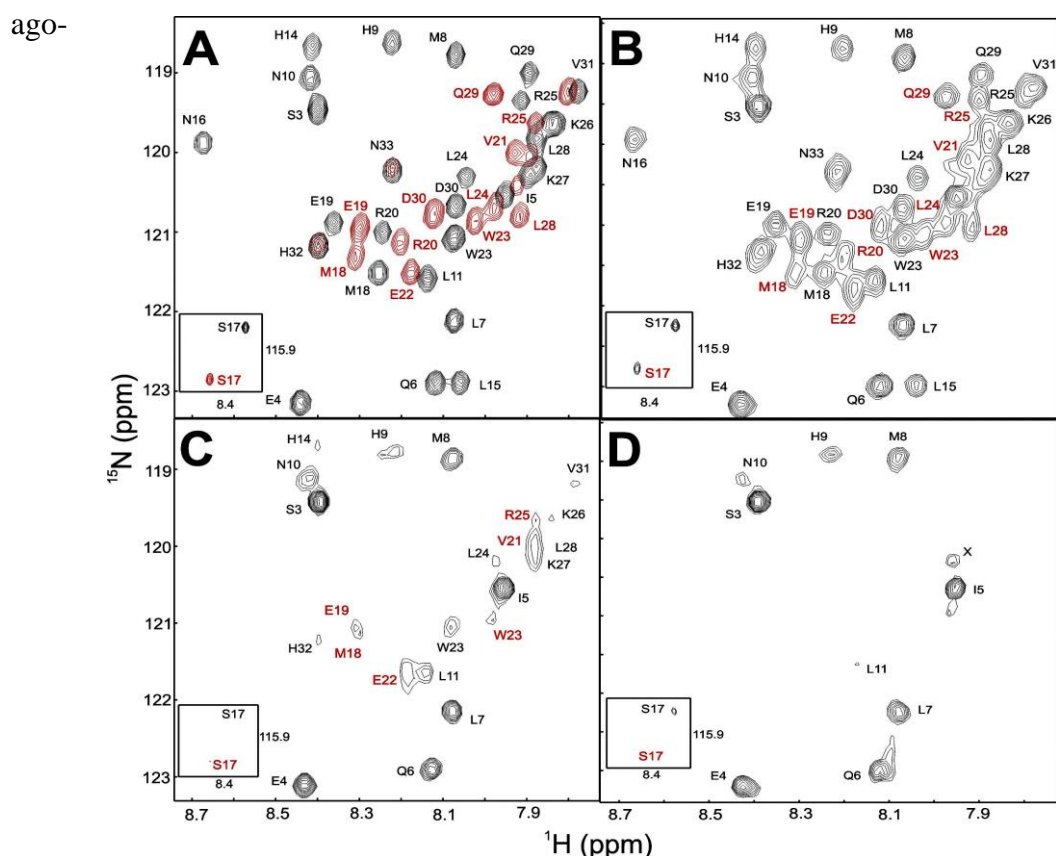


Fig. 4.13. Competitive binding of ^{15}N -PTH (15-34) and ^{15}N -PTH (1-34) to the nPTH1R monitored by NMR. A. ^{15}N -HSQC spectra of unbound ligands: ($85\mu\text{M}$) ^{15}N -PTH (15-34) in red and ($85\mu\text{M}$) ^{15}N -PTH (1-34) in black with sequential assignments. Change of HSQC spectra upon addition of ($310\mu\text{M}$) unlabeled nPTH1R: B (1:1:0.4), C (1:1:1.2) and D (1:1:2), parenthesis values correspond to the ratios of PTH (15-34) : PTH (1-34) : nPTH1R. Binding was monitored by decrease in intensity of the cross peaks. All the spectra were shown with the same signal to noise ratio.

nist/antagonist and competitive nature of both ligands to the nPTH1R, NMR ^{15}N -HSQC based competition experiments were performed. In this method, specific amino acids can be monitored from the mixture of peptides. Initially, both ^{15}N -PTH (15-34) (red in **Fig. 4.13A**) and ^{15}N -PTH (1-34) (black in **Fig. 4.13A**) were taken in an NMR tube and measured the ^{15}N -HSQC spectrum. Single letter amino acid code with residue number is shown in corresponding colors. Many of the cross peaks in the HSQC were overlaid with the same sequence specific amino acid on the other peptide, indicates both the peptides adopt the same conformation in the solution. However, S17, M18, E19, R20, L24, Q29 and D30 were distinct in both peptides and used to monitor competitive binding interaction. NMR titration studies were carried out with excess 3.7 times (1.85 times excess for each ligand) of unlabeled nPTH1R.

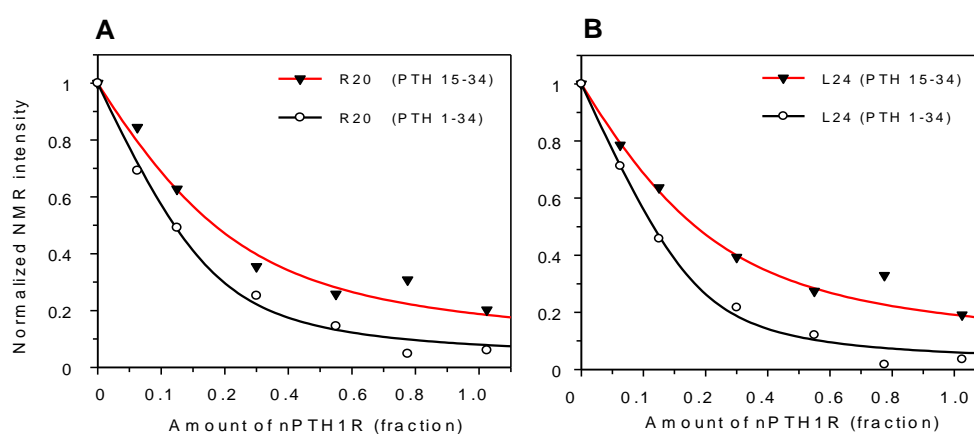


Fig. 4.14. Competitive binding curve to differentiate the binding site residues form to different PTH fragments. Residue-specific intensities of isolated peaks were picked from HSQC titration experiment and normalized. The plot shows decrease in intensity of residues R20 and L24 form both the peptides upon addition of increasing amount nPTH1R. The red (residues from PTH (15-34) and black (residues from PTH (1-34)) curves are the titration curves fitted by assuming 1:1 single site binding model using equation 3.10. The apparent K_d values given in **Table 4.4**

The addition of unlabeled nPTH1R causes decreases in intensity of cross peaks from both the peptides. This is shown in **Fig. 4.13B** and C. When the stoichiometry is 1:1:2 (ligands to the protein ratio) most of the cross peaks disappeared except residues S3 to L11 from PTH (1-34) (**Fig. 4.13D**). This implies that both PTH (15-34) and PTH (1-34) bind independently to the protein. Particularly, C-terminus of PTH (1-34) interacts to the nPTH1R. This result again proves the two-site binding model of PTH. Quantitative analysis of intensity loose of isolated cross peaks for both PTH fragments (**Fig. 4.14**) revealed that PTH (1-34) binds more strongly compared to PTH (15-34). This was further confirmed by the calculated K_d values of residues present in the binding site (R20,

L24, and D30) (Pioszak and Xu 2008). The apparent K_d values are shown in **Table 4.4**. Average fit to the tabulated residues yields K_d of 32 μM for PTH (15-34) and 9.4 μM for PTH (1-34). These values from the competitive NMR binding experiment are comparable with values obtained from ITC experiment (~ 80 μM for PTH (15-34) and 4.2 μM for PTH (1-34)). The higher affinity of PTH (1-34) is due to the extension of the binding site up to G12 (**Fig. 4.15**). The disappearance of cross peaks was due to a decrease in overall tumbling of the complex and intermediate exchange on the NMR time

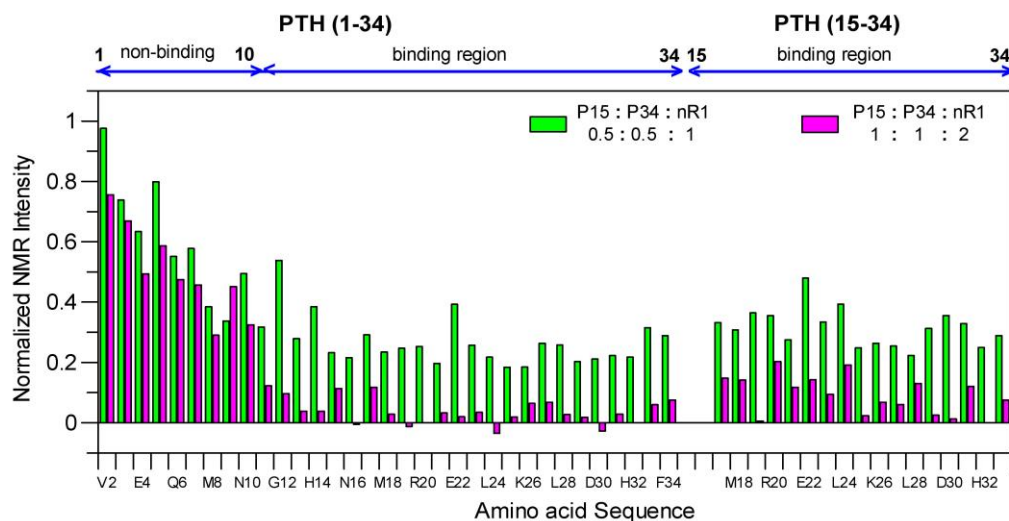


Fig. 4.15. Competitive binding characterization of ^{15}N -PTH (15-34) and ^{15}N -PTH (1-34) to the nPTH1R. Plot of normalized NMR signal intensity of half bound (in green) and bound (in fuchsia) PTH peptides. Fast decrease in intensity of PTH (1-34) indicates stronger binding than PTH (15-34) scale.

Table 4.4. The apparent K_d values calculated for sequence specific amino acid from two different peptides (PTH (15-34) and PTH (1-34)) using competitive NMR titration experiment.

Residues number	K_d for PTH (15-34) (μM)	K_d for PTH (1-34) (μM)
S17	48 \pm 14	21 \pm 4
M18	37 \pm 1	16 \pm 6
E19	2.6 \pm 1	6.6 \pm 0.4
R20	29 \pm 16	9.5 \pm 2
L24	41 \pm 20	6.9 \pm 2
D30	41 \pm 21	9.8 \pm 4
Average fit*	32 \pm 0.9	9.4 \pm 0.2

* Average fit were obtained by fitting intensities of residues S17, M18, E19, R20, L24 and D30.

R20, L24 and D30 residues were interacted to the nPTH1R, know from crystal data (PDB-3C4M)

4.7 Interaction studies of full length PTH (agonist) with nPTH1R

Parathyroid hormone is an 84 amino acid single-chain polypeptide, plays a major role in calcium metabolism by its interaction with PTH1R. Intact PTH has been licensed to treat osteoporosis and it is commercially available in Europe (Preotact®; owned by Nycomed, Denmark). This drug was approved by European medical agency in 2006 (Pietrogrande 2009), but pending for FDA approval (in phase III clinical trials). The N-terminal 34 amino acid residues are biologically active, while the role of C-terminal region of PTH (1-84) is currently unknown. However, a large portion of the C-terminus of intact PTH is highly conserved across mammalian species. This strongly suggests the possibility of additional, independent biological functions (Murray et al. 2005). Furthermore, the bound conformation of PTH (15-34) or PTH (1-34) to the nPTH1R yielded poor NMR spectra (broad peaks) caused by the intermediate exchange which hinders the access to structural details about the bound state. To elucidate the mechanism of PTH (1-84) interaction to the nPTH1R, in more detail, the role of C-terminal PTH (1-84) to the binding CD, ITC, and NMR experiments were performed. Recombinantly produced full length PTH and nPTH1R were used for these experiments.

4.7.1 PTH (1-84)/nPTH1R complex studied by CD

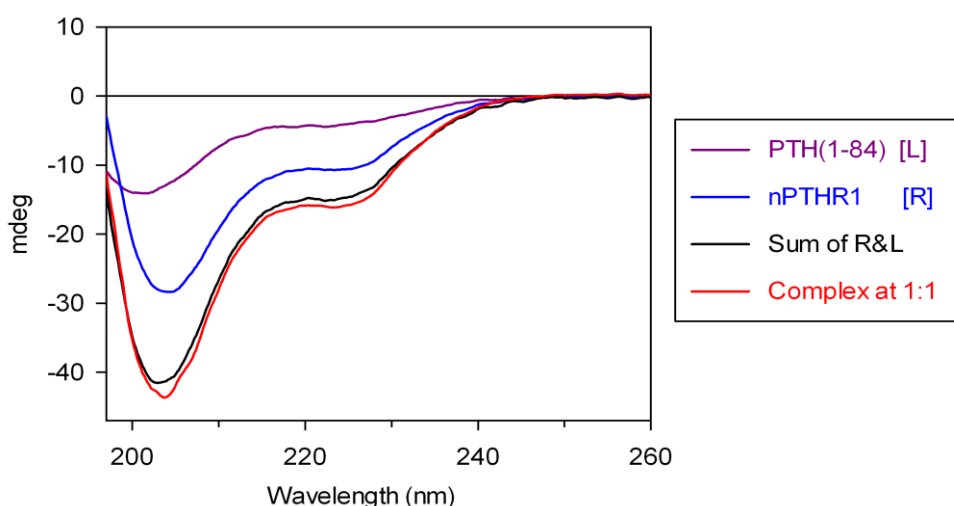


Fig. 4.16. Interaction of PTH (1-84) to the nPTH1R monitored by far-UV CD. Spectra of 10 μ M of PTH (1-84) (purple), 10 μ M nPTH1R (blue) measured separately. The complex measured with 10 μ M of ligand and 10 μ M of receptor domain (red) in 10mM sodium phosphate, 150 mM sodium sulfate, pH 6.0 at 20 °C. Theoretical spectra (black) were calculated by the addition of PTH (1-84) and nPTH1R curves.

Circular dichroism can monitor protein-protein interactions and changes in the conformation of the proteins and polypeptide chains. Far-UV CD is used mainly for studying the change in the secondary structure because the peptide bond is the principle absorbing group. CD spectra of full length PTH (purple curve in **Fig. 4.16**) and nPTH1R (blue curve in **Fig. 4.16**) showed distinct minimum at 222 nm and maxima towards higher wavelength (~195 nm) indicates the presence of small amount of α -helical structure. However, less a distinct minimum at 208 and deep minimum at 202 nm for PTH (1-84) and 205 nm for nPTH1R indicates predominantly random coil structure. This result is consistent with the NMR data obtained for ^{15}N -nPTH1R (see **Fig. 4.6A**). CD spectrum of 1:1 PTH (1-84)/nPTH1R complex (red curve in **Fig. 4.16**) only a marginal negative increase at 222 nm compared to the isolated molecules (black curve in **Fig. 4.16**). This indicates that there are no significant changes in secondary structure content upon binding and therefore the C-terminal residues of PTH (1-84) remain predominantly random coil (**Fig. 9.4**).

4.7.2 Thermodynamics of PTH (1-84)/nPTH1R binding by ITC

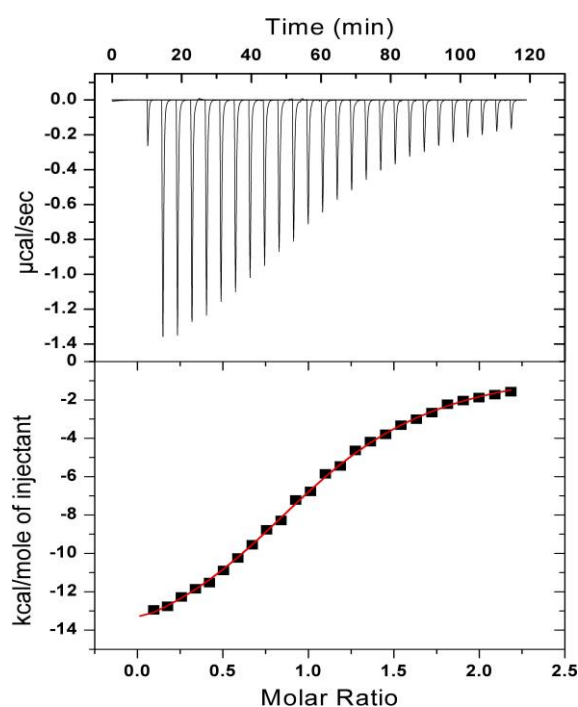


Table 4.5. Thermodynamic parameter for PTH (1-84) binding to the nPTH1R

n	1.07 ± 0.01
K_a	$1.70 \pm 0.057 \times 10^5 \text{ M}^{-1}$
ΔH	$-15.86 \pm 0.15 \text{ kcal mol}^{-1}$
ΔS	$-30.2 \text{ cal K}^{-1} \text{ mol}^{-1}$
ΔG	$-7.012 \text{ kcal mol}^{-1}$
K_d	$5.89 \pm 0.2 \times 10^{-6} \text{ M}$

Fig. 4.17. Calorimetric titration of PTH (1-84) to the nPTH1R. Upper panel: Data from titration of $320 \mu\text{M}$ PTH (1-84) ($10 \mu\text{l}$ aliquots) into a solution of $29 \mu\text{M}$ nPTH1R in 20 mM sodium phosphate buffer, 300 mM sodium sulfate, $\text{pH } 6.0$ and measured at $20 \text{ }^\circ\text{C}$. Lower panel: Plot of buffer corrected integrated enthalpies for each injection versus ligand to the nPTH1R molar ratio. The red line represents the nonlinear, least-squares best fit to the experimental data using single-site binding model. The calculated thermodynamic parameters are given on the right side Table 4.5.

ITC was used to quantify the thermodynamics parameters of binding of PTH (1-84) to the nPTH1R. A typical titration of full length PTH to the nPTH1R and integrated peak areas of each peak are shown in **Fig. 4.17**. Separate titrations were done for the heat of dilution of PTH (1-84) into the buffer and subtracted from the data. The negative trace implies the binding reaction was an exothermic reaction (upper panel). The integrated peak area was fitted to a single-site binding model assuming 1:1 stoichiometry. The fitted thermodynamic parameters were shown in **Table 4.5**. The K_d value of $5.9 \mu\text{M}$ for PTH (1-84)/nPTH1R interaction was close to the value of PTH (1-34)/nPTH1R interaction indicate that the core binding region is present at the N-terminus of the full length PTH. The negative values of apparent enthalpy and entropy indicate that the binding reaction is largely driven by favorable enthalpic forces accompanied by an unfavorable entropic penalty.

4.7.3 SPR analysis of PTH (1-84) binding to nPTH1R

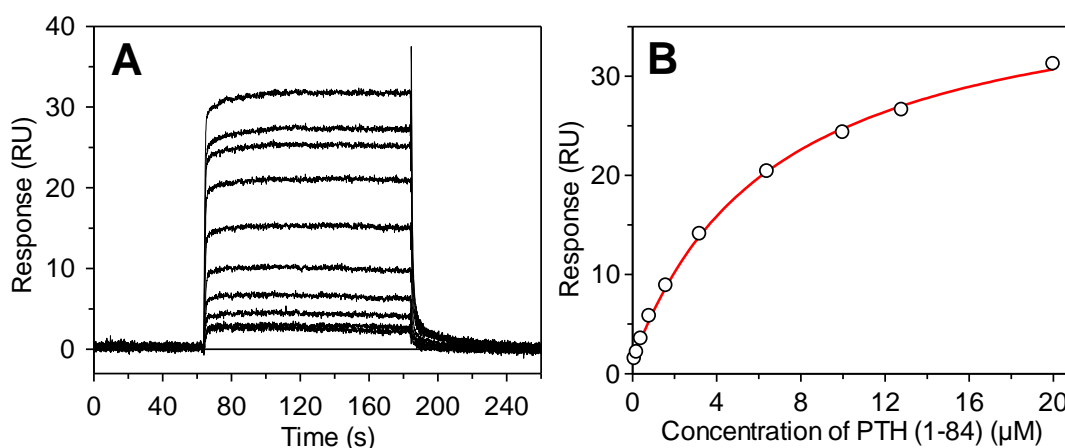


Fig. 4.18. Kinetics of PTH (1-84) binding to the nPTH1R was monitored by SPR. **A.** Biotinylated nPTH1R was immobilized on a Biocore sensor chip SA. To obtain sensorgrams, increasing concentration of (from bottom to top) 0.1, 0.2, 0.4, 0.8, 1.6, 3.2, 6.4, 10.0, 12.8, 20.0 μM PTH (1-84) was delivered to the surface. All the traces have been corrected to the buffer signal. **B.** Plateau values were plotted against the PTH (1-84) concentration. The K_d value were calculated by fitting (red line) the data (circle) to a 1:1 reversible binding model using Biocore software. The obtained kinetic and binding values were $(7.747 \pm 0.14) \times 10^4 \text{ M}^{-1}\text{s}^{-1}$ and $0.621 \pm 0.01 \text{ s}^{-1}$ and $6.77 \pm 0.5 \mu\text{M}$, k_a , k_b and K_d , respectively The experiment was performed at $20 \text{ }^\circ\text{C}$ in 50 mM sodium phosphate, 150mM NaCl, pH 7.8.

Surface plasmon resonance (SPR) was used in studying the kinetics of full length PTH-nPTH1R interaction. Biotinylated nPTH1R was immobilized on the Biocore sensor chip SA. When increasing amount of PTH (1-84) (0.1 -20 μM) was passed over on the sur-

face containing immobilized nPTH1R, an increase in the signal (RU) was observed. This was due to the fast association reaction. After reaching steady-state, the surface was washed out by glycine buffer, causing a drop in signal (**Fig. 4.18A**). Kinetic forward and reverse rate constants were obtained by fitting sensorgrams to a simple 1:1 bimolecular interaction model. The observed kinetic rate constants were $(7.747 \pm 0.14) \times 10^4 \text{ M}^{-1}\text{s}^{-1}$ and $0.621 \pm 0.01 \text{ s}^{-1}$, k_a and k_b , respectively. Compared to the kinetic values of this interaction to the PTH (1-34)-nPTH1R binding, PTH (1-84) associates 10 times faster than PTH (1-34) to the nPTH1R. Plateau values from the sensorgrams plotted against the concentration of PTH (1-84) were shown in **Fig. 4.18B**. The calculated equilibrium dissociation constant (K_d) was $6.8 \mu\text{M}$, which is in good agreement with the ITC data ($5.9 \mu\text{M}$).

4.7.4 Interaction of PTH (1-84) to the nPTH1R studied by NMR

Recombinantly produced ^{15}N or $^{13}\text{C}/^{15}\text{N}$ labeled full length PTH and unlabeled nPTH1R were used for NMR experiments. The ^{15}N -HSQC spectrum of PTH (1-84) measured with $150 \mu\text{M}$ were shown in **Fig. 4.19**. PTH (1-84) remains monomeric in solution up to $\sim 250 \mu\text{M}$. Beyond this concentration, the N-terminal peaks (V2 to A39) were disappeared from the ^{15}N -HSQC due to self-association of the peptide. Upon diluting the high concentrated sample all the peaks reappeared again in the ^{15}N -HSQC spectrum indicating that self-association is reversible.

The ^{15}N -HSQC spectrum of PTH (1-84) shows sharp peaks and limited dispersion along the ^1H axis suggesting that PTH (1-84) predominantly has a random coil structure. However, little dispersion is due to the presence of a small amount of α helical (see CD spectra of free PTH (1-84) in **Fig. 4.16**) and local amino acid sequence (Yao et al. 1997). All the backbone amide resonances in the ^{15}N -HSQC spectrum were sequentially assigned using standard triple resonance experiments (**Fig. 4.19**). A comparison of backbone chemical shifts was made between PTH (1-34) and PTH (1-84); the chemical shifts were in good agreement, except residue F34 of PTH (1-34). This confirms that the N-terminus of PTH (1-84) has a similar structure in both PTH (1-34) and full length PTH under conditions used.

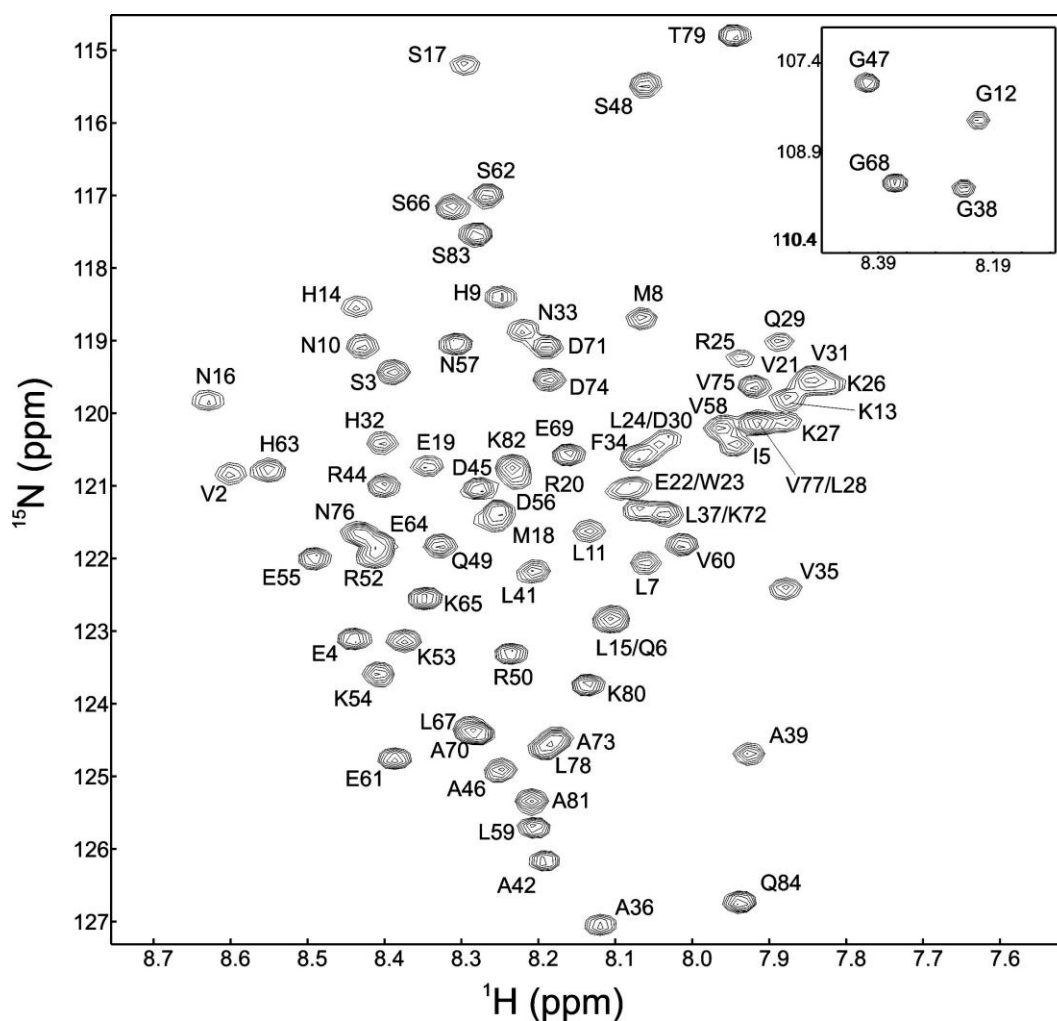


Fig. 4.19. The assigned, 2D ^{15}N -HSQC spectrum of PTH (1-84). Spectrum measured at 25 °C in 10 mM Bis-Tris, 300 mM Na_2SO_4 , 0.02% NaN_3 , 10% D_2O , and pH 5.2. Cross-peaks are labeled with residue numbers.

To gain the structural information on the nature of the physical interaction between nPTH1R and PTH (1-84), ^{15}N -HSQC titration experiment was used. Unlabeled nPTH1R (178 μM) was added to the ^{15}N -PTH (1-84) (113 μM) samples in 8 steps and the spectrum was recorded. Perturbation of the backbone chemical shift or the intensity change upon complex formation was monitored. A ^{15}N -HSQC spectrum recorded at 1:0.44 and 1:70, PTH (1-84) to the nPTH1R stoichiometric ratio are shown in **Fig. 4.20**. During the titration, significant changes were observed for amino acid residues located at the N-terminus of PTH (1-84). Some of the resonances the intensity was decreased during titration are marked in blue in **Fig. 4.20**. Further addition of a large excess of nPTH1R (2 times excess) leads to line-broadening of many amide resonances, below

the detection limit. This is possibly reaching the intermediate exchange regime in the complex state.

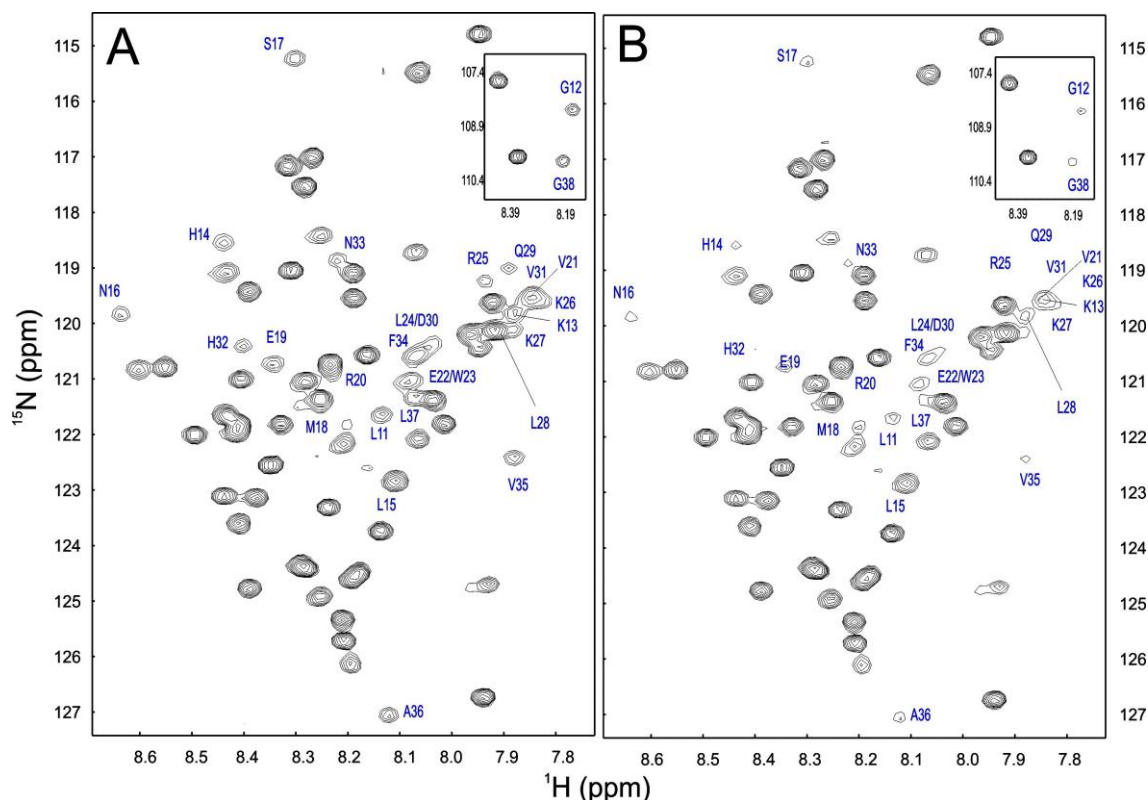


Fig. 4.20. Binding of PTH (1-84) to the nPTH1R monitored by ^{15}N -HSQC titration experiment. Spectrum recorded after addition of unlabeled nPTH1R to ^{15}N -PTH (1-84) to the stoichiometric ratio of 0.44:1 (A) and 0.7:1 (B), respectively. Back bone resonances show decreases in intensity upon complex formation were indicated in blue.

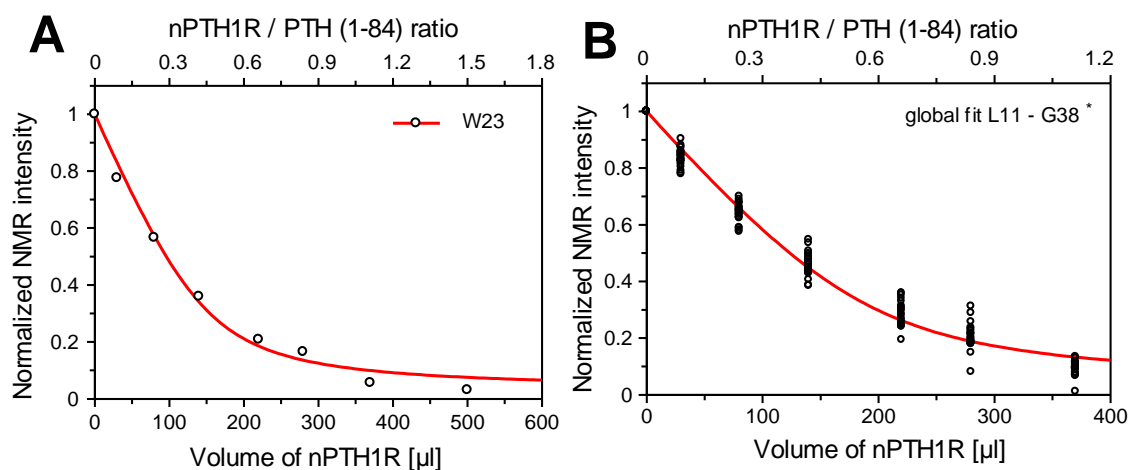


Fig. 4.21. NMR intensity plots for binding of PTH (1-84) to the nPTH1R. **A.** Upon NMR titration the intensity of the free ^{15}N -PTH (1-84) decreases due to complex formation. The normalized NMR Intensity of the W23 amide cross-peak was plotted against volume of nPTH1R/fraction of nPTH1R. **B.** The average fit was done for all residues from L11 to G38 except overlaid cross-peaks (L15, M18, R20, K26, and L28). The red line represents the best fit of a 1:1 binding model to the experimental data. The K_d of 10 μM for residue W23 and 9 μM for average fit were derived for the fit. W23 was shown to interact to the nPTH1R by X-ray crystallography (PDB code 3C4M).

The similar line-broadening effect is also noticed for PTH (15-34) and PTH (1-34). The detailed analysis of ^{15}N -HSQC titration data shows the residues that lost its intensities are from L11 to G38 (blue in **Fig. 4.22**), due to binding to the receptor in the intermediate exchange regime ($k_{\text{ex}} \sim \Delta\delta$, and k_{ex} was ~ 10 Hz calculated along with Biocore kinetics data, see section 4.7.3). Neighboring residues from the binding region show slight chemical shift perturbation; residues L7, M8, H9, N10, A42, and R44 are in fast exchange ($k_{\text{ex}} > \Delta\delta$); A39 and L41 are in slow exchange ($k_{\text{ex}} < \Delta\delta$) on the NMR time scale (green in **Fig. 4.22**). Residues not affected by the nPTH1R binding include D45 to Q84 (black in **Fig. 4.22**). The plot of normalized NMR intensity of the cross-peak against the volume of nPTH1R was used to quantify (**Fig. 4.21**) and localize the PTH (1-84) regions that are affected by receptor domain binding (**Fig. 4.23**).

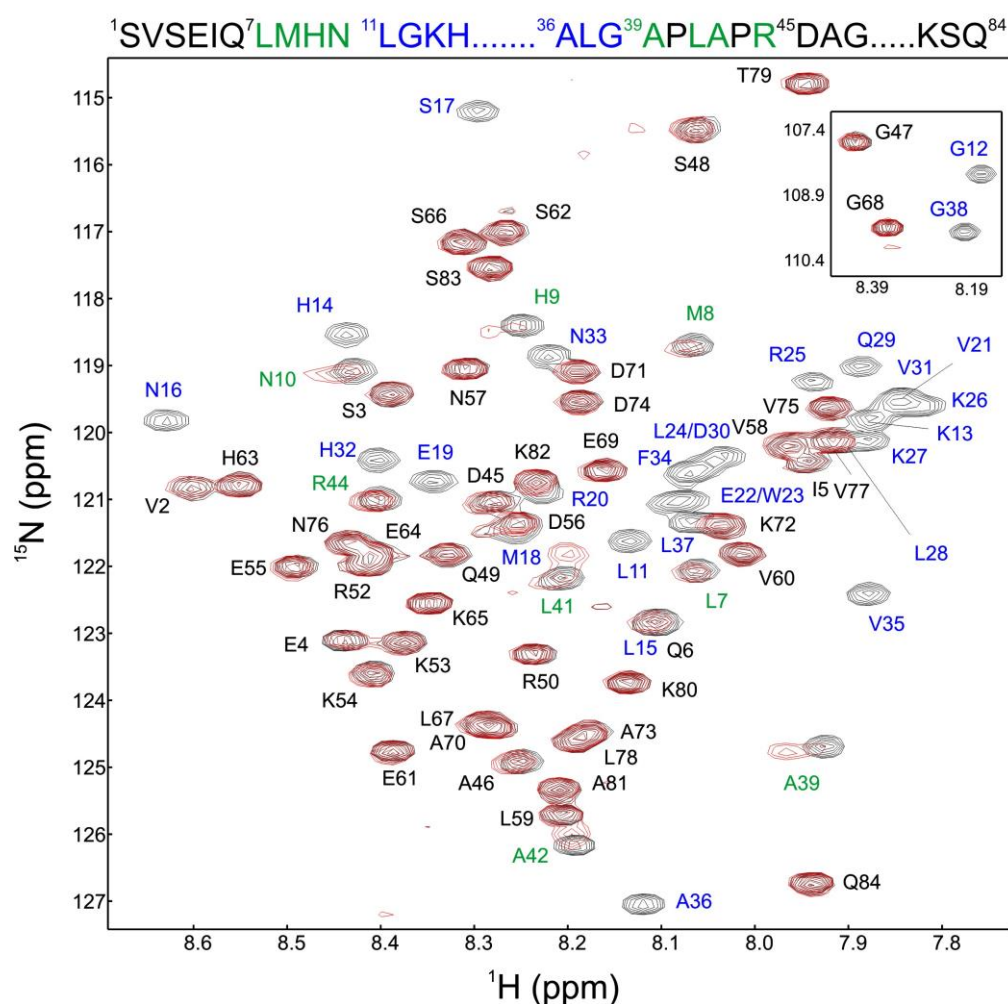


Fig. 4.22. ^{15}N -HSQC spectra of apo and halo of PTH (1-84). Overlay of 2D ^{15}N -HSQC spectra of ^{15}N -PTH (1-84) recorded in the absence (black) and presence (red) of equimolar concentrations of unlabeled nPTH1R. The amide resonances which lost their intensity were shown in blue, those affected by slight chemical shift perturbations or slight loss in intensities were labeled in green. Residues which did not show any changes are indicated in black. Same color codes are indicated in the amino acid sequence (top). Spectra were measured at 25 °C in 10 mM Bis-Tris, 300 mM Na_2SO_4 , 0.02% NaN_3 , 10% D_2O , and pH 5.2

Fitting of the data to 1:1 binding model gave K_d of $10.3 \pm 0.4 \mu\text{M}$ for residue W23. Approximately same K_d values were obtained for other binding residues while fitting to the intensity data. Average fit was done for all the residues involve in binding (L11 to G38) except overlaid cross-peaks (L11, M18, R20, K26 and L28) and K_d of $9.3 \pm 0.8 \mu\text{M}$ were obtained (**Fig. 4.21B**).

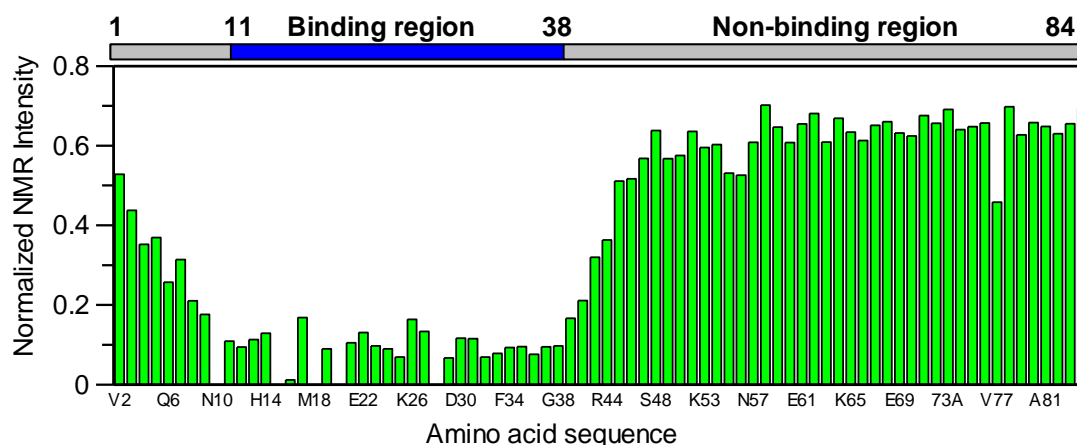


Fig. 4.23. Analysis of PTH (1-84) binding to nPTH1R from NMR intensity plot. Intensities were picked from 1:1 complex spectrum of ^{15}N -HSQC titration experiments and normalized against spectrum of free ^{15}N -PTH (1-84). Binding region (L11 to G38) was shown in blue on the amino acid sequence (top).

4.7.5 Dynamic studies of PTH (1-84)/nPTH1R complex

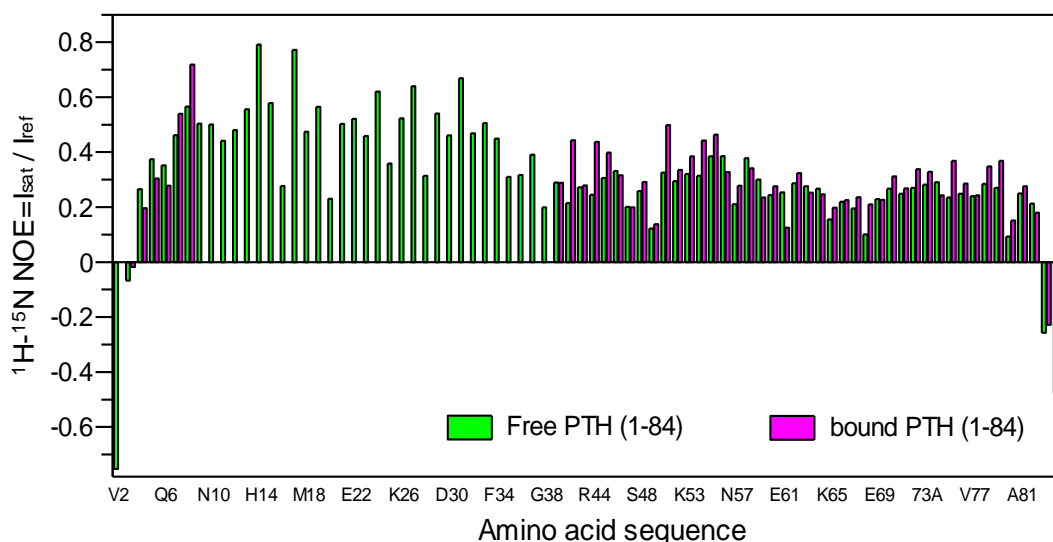


Fig. 4.24. ^1H - ^{15}N NOEs of apo and halo PTH (1-84). ^1H - ^{15}N NOEs of free (green) and unlabeled nPTH1R bound (fuchsia) ^{15}N -PTH (1-84) was plotted against amino acid sequence. The interacting residues from L11 to G38 were not shown in the plot because of broadening of the NMR signal (intermediate exchange) in the complex preventing the detection in the spectrum.

Besides the solvent effects, the negative entropy from the ITC data for binding of PTH (1-84) to the nPTH1R one could imagine that the complex corresponds to a highly compact structure (see **Fig. 4.17**). Heteronuclear NOE values are more sensitive to internal dynamics (nanoseconds to picoseconds time scale) of the peptide (Kay et al. 1989). ^1H - ^{15}N NOE experiment was performed in order to identify the effect of binding on the dynamics of the PTH (1-84). The plot of ^1H - ^{15}N NOE values of free and nPTH1R bound PTH (1-84) versus amino acid sequence is shown in **Fig. 4.24**. Both free and bound PTH (1-84) shows negative ^1H - ^{15}N NOE values for N and C terminus as expected based on high flexibility at the terminal parts. Rest of the residues is shown positive ^1H - ^{15}N NOE. C-terminal part of free and nPTH1R bound PTH (1-84) shows same ^1H - ^{15}N NOE values indicates that C-terminal part did not show any conformational change upon binding or not involve in binding. This result is well agreement with the NMR titration data (see **Fig. 4.23**). The cross-peaks that involve in binding are lost because of line-broadening of NMR signal and could not be detected in the complex spectra.

4.8 Non-specific interaction of PTH (1-84) to the membrane

The majority of drugs today on the market target membrane proteins, particularly the GPCRs. The interaction between membranes and membrane proteins are crucial for its efficacy because the receptor and ligand interaction must take place near the membrane. Many of the natural peptide agonists like PTH, secretin and vasoactive intestinal polypeptide are disorder conformations in aqueous solution and are partially helical in lipophilic solvents or in micelles (Inooka et al. 2001). This structure is believed to be active conformation of the peptide. PTH in its bioactive conformation and orientation in the membrane undergoes two-dimensional diffusion on the membrane surface that leads to specific binding to a target membrane receptor (Moroder et al. 1993). To study the non-specific interaction of PTH to the membrane several model membranes like DMPC, DMPG, POPC, POPG, brain lipids from bovine, DPC, SDS and LDAO were used. Interactions were studied by CD, ITC, solution and solid-state NMR.

4.8.1 Interaction of PTH (1-84) to the membranes studied by CD and ITC

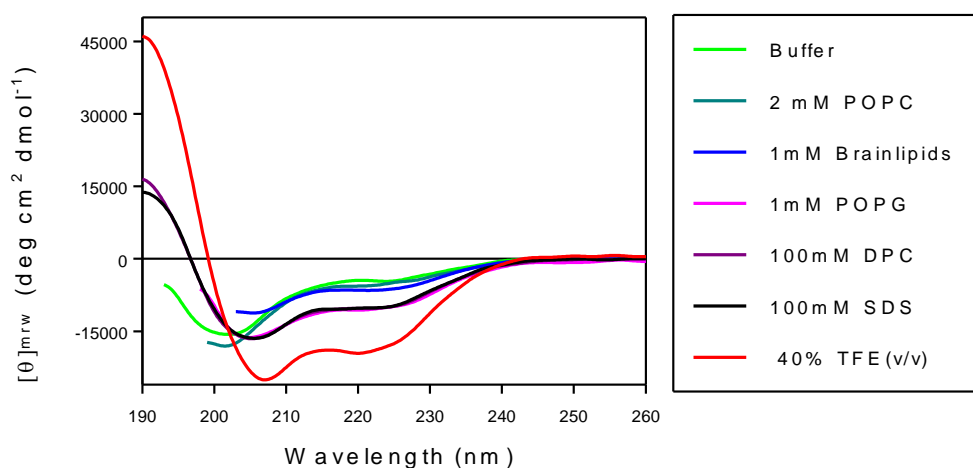


Fig. 4.25 Far UV-CD spectra for PTH (1-84) in buffer and in different membrane environments. Spectra measured with 10-20 μM of PTH (1-84) in 10 mM Sodium phosphate, 300 mM Na_2SO_4 , and pH 6.0 (green) and in different micelle and vesicles, at the concentrations indicated. 40% TFE were used as a reference.

CD spectroscopy was used to analyse the secondary structure of PTH (1-84) binding to membranes. The results were shown in **Fig. 4.25**. PTH (1-84) in buffer (green curve) displayed spectral properties that are characteristic of a partially α -helical structure. CD spectra of PTH (1-84) bound to POPC or brain lipids displayed a little change in secondary structure. Interaction of PTH (1-84) to the anionic vesicles POPG or DMPG (data not shown) or to the detergent micelles (CMC = 2mM) exhibit more α -helical structure (40-60% α -helix). The transition from disordered structure to ordered, due to binding to the membrane were seen by negative minima at 208 and 222 nm. CD spectra of PTH (1-84) in 40% TFE shown as a reference, because TEF is a strong α -helix inducer.

ITC was performed to monitor binding of PTH (1-84) to the POPC vesicles. Titration of 0.5 mM POPC to the 50 μM PTH (1-84) gave an exothermic binding isotherm (**Fig. 4.26**). Although the peptide shows binding to the vesicles, the observed heat change (upper panel) was less indicating that the binding was mainly due to hydrophobic interactions. The observed binding isotherm (lower panel) was not good enough to fit to the binding models. The control experiment showed a very small heat change and was subtracted from the protein data.

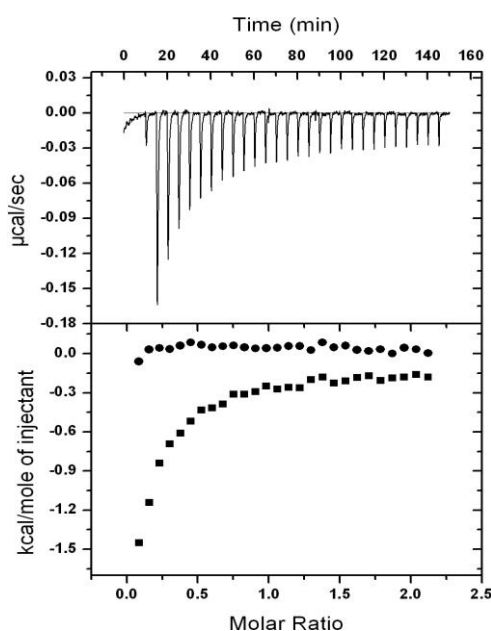


Fig. 4.26. Calorimetric titrations of PTH (1-84) to the lipid vesicles. Upper panel: data from titration of 500 μM of POPC (10 μl aliquots) vesicle into a solution of 50 μM PTH (1-84) in 20 mM Sodium phosphate, 300 mM Na_2SO_4 , and pH 6.0, measured at 25 $^\circ\text{C}$. Lower panel: plot of integrated enthalpies for each injection versus POPC to the PTH (1-84) ratio (square symbol) and buffer run (dot symbol).

4.8.2 Membrane interaction of PTH (1-84) studied by PFG-NMR

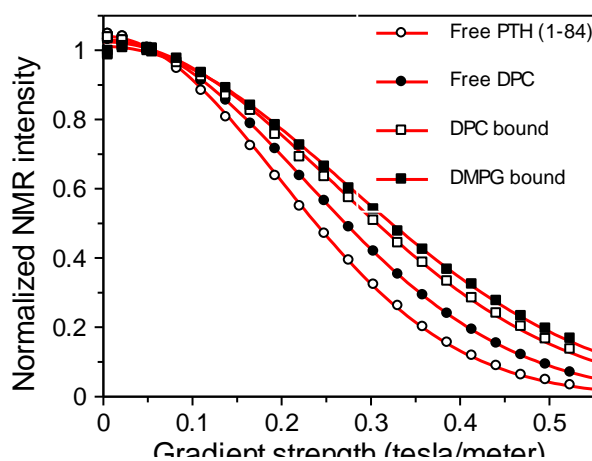


Table 4.6. Diffusion coefficients (D) of PTH (1-84) in membranes at 25 $^\circ\text{C}$

Sample	D (m^2/s) $\times 10^{-11}$
apo-PTH (1-84)	10.60 ± 0.07
apo-DPC	8.00 ± 0.01
DPC bound	6.16 ± 0.04
DMPG bound	5.56 ± 0.04

Fig. 4.27. Binding of PTH (1-84) to the micelles and vesicles were studied by PFG-NMR. Normalized peak integrals of the aliphatic resonances (0.5 and 2.5 ppm) were plotted against gradient strength. Diffusion coefficients were obtained for free and 100 mM d_{38} -DPC or 1 mM DMPG bound PTH (1-84) by fitting (red) the data (circle) to equation 3.11. Data were acquired at 25 $^\circ\text{C}$ in 20mM NaH_2PO_4 , 300mM Na_2SO_4 , 10% D_2O and pH 6.0. D values were shown on the right hand

Diffusion coefficient (D) of free PTH (1-84) and micelle (100mM d_{38} -DPC) or vesicle (1mM DMPG) bound PTH (1-84) was measured using pulse field gradient (PFG) NMR. DPC and DMPC/PG are the most studied model membrane systems. The attenuation curves are shown in the **Fig. 4.27**. The measurement (integral between 0.5 and 2.5 ppm) yield D value of $10.60 \times 10^{-11} \text{ m}^2/\text{s}$ (**Table 4.6**) for PTH (1-84) which was higher as expected for a globular 9.4 kDa molecule. For comparison to the 14.3 kDa lysozyme has the same value of ($11.0 \times 10^{-11} \text{ m}^2/\text{s}$) (Ilyina et al. 1997). This indicates again the

unstructured geometry of PTH (1-84), in good agreement with the CD and ^{15}N -HSQC data. After addition of 100mM DPC or 1mM DMPG to the PTH (1-84) the D values decreases. This was due to the formation of large complex upon membrane binding. The obtained D value for the DMPG complex nicely matches with literature value ($5.3. \times 10^{-11} \text{ m}^2/\text{s}$) (Marcotte et al. 2004). DPC alone was measured as a reference.

4.8.3 Identification of membrane binding region in PTH (1-84)

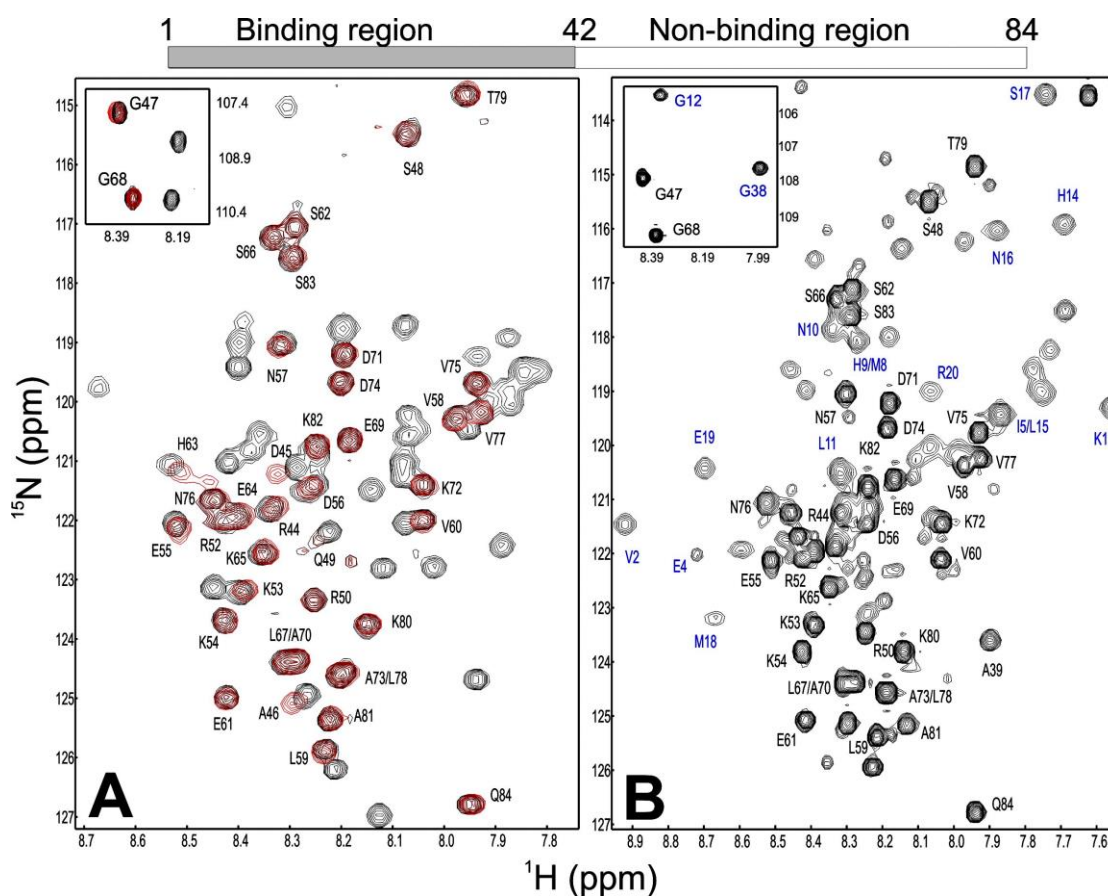


Fig. 4.28. Spectral changes in apo PTH (1-84) are induced by association with membranes. A. ^{15}N -HSQC spectra of (100 μM) ^{15}N -PTH (1-84) in the absence (black) and in the presence (red) of 2mM DMPG bicelles. The residues which are not involved in binding (42-84) are marked. **B.** ^{15}N -HSQC spectra of ^{15}N -PTH (1-84) in 100mM d_{38} -DPC. The residues marked in blue and black are binding (1-40) and non-binding (42-84) residues, respectively. About 80% of cross peaks were assigned and unassigned cross peaks are not marked.

In order to find atomic resolution information and further substantiate the CD and NMR diffusion data for the binding of PTH (1-84) to the membranes, ^{15}N -HSQC based NMR experiments were recorded. Vesicle provides a native-like a environment, in which many proteins have been found to be active (Marcotte and Auger 2005). ^{15}N -HSQC

spectra of free (black) and DMPG bound ^{15}N -PTH (1-84) (red) are shown in **Fig. 4.28A**. Upon addition of vesicle to the peptide, all N-terminal cross peaks (residues 2-42) disappeared from the spectra. This was due to the slow tumbling time of high molecular complex between N-terminus of PTH (1-84) to the vesicles. C-terminal cross peaks (residues 44-84) were visible without any change in chemical shifts or intensity. Because C-terminal residues are solvent exposed and highly dynamic to an extent that NMR could detect the cross peaks (**Fig. 4.29**). Same results were also seen for other lipids like POPG and brain lipids from bovine. However, DMPC or POPC show no change in intensity in the HSQC spectra. However, binding were seen by NMR diffusion experiments and fluorescence spectroscopy (data not shown). This indicates that PTH (1-84) interacts more strongly with anionic lipids than with zwitterionic lipids.

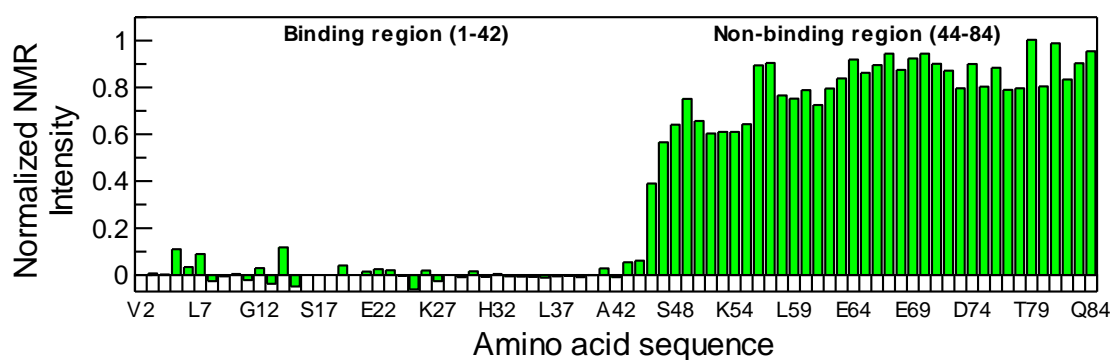


Fig. 4.29. NMR intensity plot of PTH (1-84) binding to the vesicles. Intensities were picked from ^{15}N -HSQC spectra of DMPG bound ^{15}N -PTH (1-84) and normalized against free ^{15}N -PTH (1-84) spectra.

Vesicle bound PTH (1-84) are difficult to study by solution NMR due to high rotational correlation time (for amide proton ~ 150 ns). DPC micelles are commonly used in NMR studies and they are able to maintain structure and functionality of membrane proteins (Shenkarev et al. 2002). Micelles undergo rapid reorientation in solution allowing for high resolution NMR studies. ^{15}N -HSQC spectra of d_{38} -DPC bound ^{15}N -PTH (1-84) were shown in **Fig. 4.28B**. The addition of d_{38} -DPC micelles strongly affects the backbone amide protons of N-terminus of PTH (1-84) (residues 2-40) indicating binding. However, C-terminal cross peaks (residues 41-84) were unaffected which indicates that these residues are not involved in membrane binding. Strong intensity of these cross peaks was due to the high flexibility of the solvent exposed form. During the course of titration of unlabeled DPC to the ^{15}N -PTH (1-84) undergoes slow exchange cross peak patterns. So, the cross peaks has to be reassigned. Currently, 80% of peaks were as-

signed. CD and NOE data suggest that membrane bound PTH (1-84) adopts α -helical conformation in the N-terminus of PTH (1-84).

4.9 Solid-state NMR spectroscopy for PTH-membrane interactions

Membrane interactions of peptide ligands are important for binding and activity of the GPCRs (Yamamoto et al. 2008). Solid-state NMR (SSNMR) was used as a complementary tool to the solution NMR to investigate membrane associated peptides in their native like-environment. SSNMR as an advantage that it allows studying the structure and dynamics of the peptide as well as phospholipid vesicles in their associated state (Huster et al. 2010). These studies are difficult with solution NMR due to the high molecular weight peptide-membrane complexes (fast relaxation). To obtain more information about the structure and dynamics of PTH and phospholipids interaction, ^2H and ^{13}C MAS NMR were used. Commonly used DMPC and POPC vesicles (saturated and unsaturated lipids) were used as a model membrane.

4.9.1 Structural studies of PTH-membrane interaction by ^{13}C SSNMR

Direct polarization (DP), cross-polarization (CP) and INEPT (insensitive nuclei enhanced by polarization transfer) experiments were used to investigate site-specific qualitative information about molecular dynamics of PTH bound to lipid vesicles. The direct polarization of ^{13}C experiment yields all 13-carbon signals in the molecule. While, CP yields maximal signal for rigid segments ($I_{\text{INEPT}} \approx 0$), and INEPT yields maximum signal for mobile segments ($I_{\text{CP}} \approx 0$) of the molecule (Nowacka et al. 2010). The combination of these experiments gives information about the dynamic of the molecules (Sackewitz et al. 2008). Spectra for $^{13}\text{C}/^{15}\text{N}$ -PTH (1-34)/DMPC- d_{67} (1:50 molar ratio) were shown in **Fig. 4.30A, B, and C**. SSNMR spectra show notable differences. All ^{13}C -carbon signals for $^{13}\text{C}/^{15}\text{N}$ -PTH (1-34) were seen in CP and DP (A and B) experiments including $^{13}\text{C}_\delta$ of Isoleucine-5 (PTH has only one Ile) at ~ 13 ppm. But, hardly any pep-

tide signals were detected in the INEPT experiment (C). Because binding of PTH (1-34) to the membrane leads to rigidity in the molecule and can be detected by CP and not by INEPT experiment.

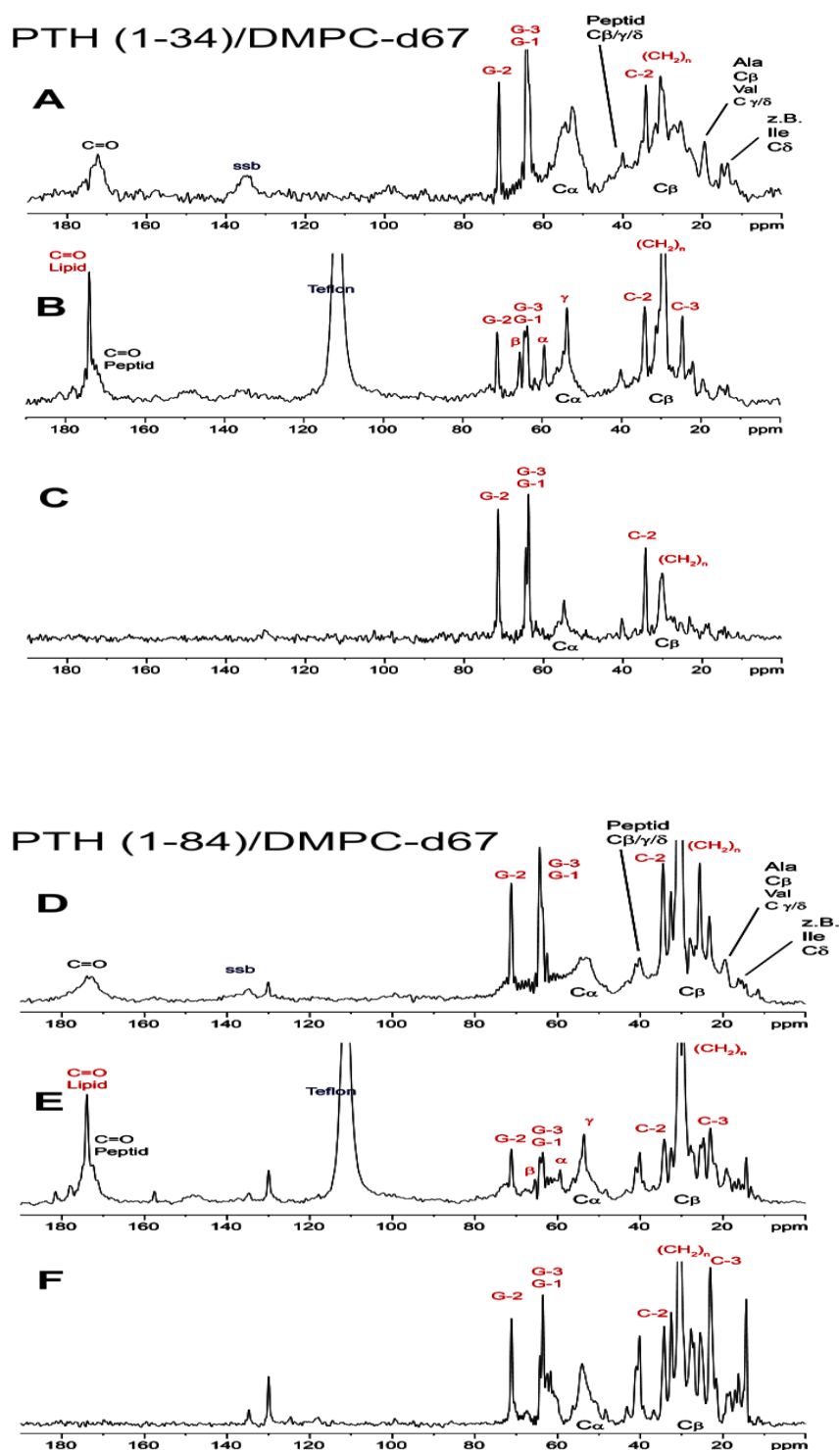


Fig. 4.30. ^{13}C MAS NMR spectra of $^{13}\text{C}/^{15}\text{N}$ PTH (1-34/84) bound to DMPC-d₆₇. A, B and C spectra were measured for $^{13}\text{C}/^{15}\text{N}$ PTH (1-34) and D, E and F measured for $^{13}\text{C}/^{15}\text{N}$ PTH (1-84). Both peptides mixed with DMPC-d₆₇ to the ratio of 1:50. Spectra were acquired with MAS rate of 7 kHz at 30 °C using CP (A and D), direct polarization (B and E) and INEPT (C and F) pulse sequences. Peptide peaks are marked in black and lipid peaks are in red. Intense signal at 110pm are from Teflon tape.

Solution NMR results revealed that residues 1-42 of PTH (1-84) interact with the membrane. To corroborate these results with solid-state NMR, same polarization experiments were performed for $^{13}\text{C}/^{15}\text{N}$ -PTH (1-84)/DMPC- d_{67} (1:50 molar ratio) sample under similar conditions. Resulting spectra were shown in **Fig. 4.30D, E and F**. The CP experiment detects rigid carbons in the segment and the DP experiment shows all carbons in the segment (D and E) indicate interaction of PTH (1-84) to lipid vesicles. Interestingly, well resolved sharp signals were observed in the INEPT spectra (F) of full length PTH compared to PTH (1-34) (no signals) (C). These sharp signals are due to the presence of unbound mobile region in the full length PTH. Excess of lipids was used to saturate all the peptides.

Overall, polarization experiments clearly indicate that the binding of PTH to the DMPC vesicles and the binding residues are from the N-terminal part of PTH (1-84). These results correlate well with the solution NMR data (section 4.8.3).

4.9.2 Dynamics of membrane upon PTH binding studied by ^2H -SSNMR

Structural details of binding of PTH to the membrane were studied by solution and solid state NMR in the previous sections. In order to investigate dynamics of the membrane upon peptide binding, ^2H NMR spectroscopy was used. PTH (1-34), the membrane binding region, and zwitterionic POPC- d_{31} membranes (ratio of 1:50) was used for these experiments. Deuterium NMR quadrupole splitting of POPC- d_{31} and POPC- d_{31} mixed with PTH (1-34) (molar ratio of 1:50) is shown in figure **Fig. 4.31A**. A typical well resolved powder pattern was obtained for pure POPC- d_{31} . Upon adding peptide to the lipids the spectrum of POPC- d_{31} changed and peaks become sharp indicating the membrane incorporation of PTH (1-34).

The order parameter (S) of the C-D bond vector was calculated (section 3.24.2) from each of the separated quadrupolar splitting data. S denotes the mobility of the system, and lower the S value higher the flexibility. Order parameter plots for POPC- d_{31} (black) alone and mixed with PTH (1-34) (red) versus the acyl chain are shown in **Fig. 4.31B**. Order parameter decreased in the presence of peptide. This shows the binding of the

peptide to the membranes and as consequence of this binding, the membrane becomes highly flexible along the carbon chain.

To corroborate the peptide induced membrane dynamics, a ^2H NMR spin-lattice relaxation (T_1) measurement was performed for the same sample. Relaxation rates R_1 , ($R_1=1/T_1$) of pure phospholipid membranes often exhibit a linear relation on the square of the order parameter (Vogel et al. 2005). Square-law plots of POPC- d_{31} in the absence and in the presence of PTH (1-34) are showed in the **Fig. 4.31C**. A linear dependence (perfect linear for saturated lipids) plot was observed for pure POPC- d_{31} which is in good agreement with the literature (Scheidt et al. 2011). For POPC- d_{31} -PTH (1-34) sample, bent shape with a sleeper slope was observed. This indicates the change in elastic property (dynamic and packing) of the membrane upon peptide binding and confirms again the order parameter data.

Order parameter and relaxation rates data indicate binding of PTH (1-34) to the lipid membrane and this event increases the dynamics of the carbohydrate chains of POPC. A molecular reason for the high mobility was difficult to find with the available date.

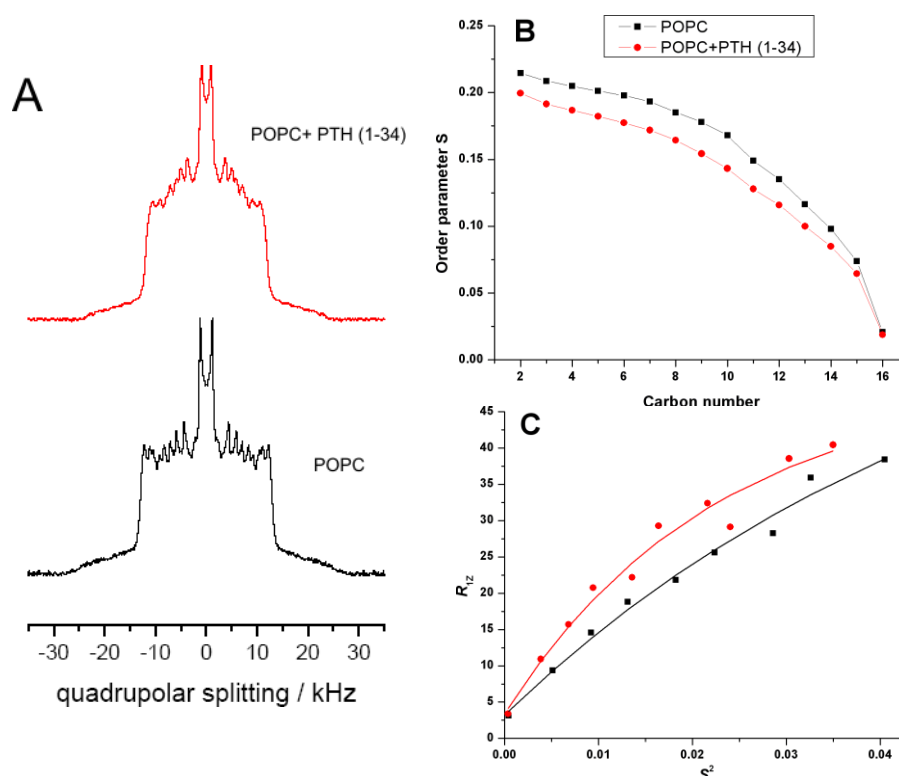


Fig. 4.31. ^2H NMR studies of PTH (1-34) binding to POPC- d_{31} membrane at 30 °C. **A.** ^2H quadrupole splitting of POPC- d_{31} in the absence (black) and in the presence (red) of PTH (1-34) at a lipid molar ratio of 1:30. **B.** The corresponding order parameter as a function of the chain segment. **C.** Plot of Zeeman order spin-lattice relaxation rates (R_1) versus the square of the order parameter.

SSNMR studies were done in collaboration with Dr. Alexander Vogel, Institute of medical physics and biophysics, University of Leipzig, Germany.

4.10 Two-step ligand transportation model for binding of PTH to the nPTH1R

A two-step ligand transportation model has been proposed for binding of peptide ligands to the GPCRs (Schwyzer 1986). According to this model, in the first step, the ligand binds nonspecifically to the cell membrane, and thereby increases the effective hormone concentration in the vicinity of the receptor. During the second step, the ligand diffuses two-dimensionally along the membrane surface to find and binds its target membrane receptor (Inooka et al. 2001). To verify this model, PTH (1-84) was pre-incubated (2-4h) with phospholipid vesicles (2.5 mM DMPC or 1 mM POPC) before start to titrate with the nPTH1R in the ITC experiments. To avoid the heat of dilution of lipids, same lipid concentrations were also taken in the nPTH1R cell solution.

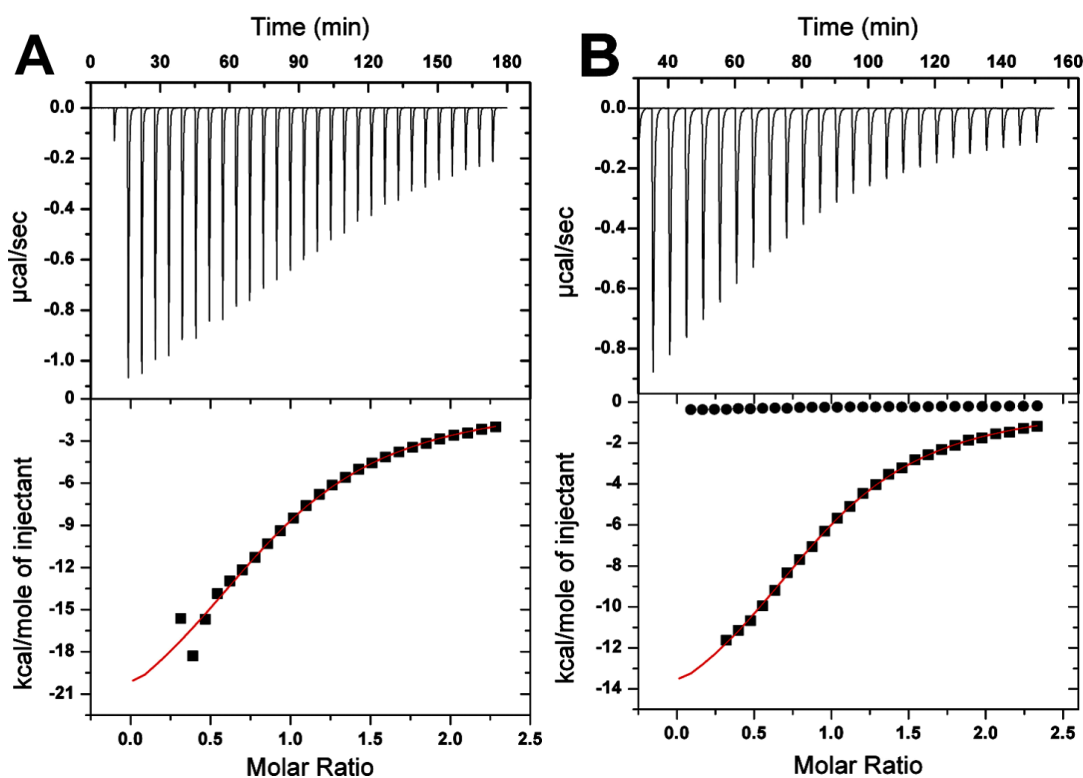


Fig. 4.32. ITC profile for the binding of PTH (1-84) to the nPTH1R in lipid environment. Upper panel: Heat flow versus time profiles from 10 μl aliquots of 285-290 μM PTH (1-84) to the 27-28 μM nPTH1R solution. Prior to the titration both cell and syringe solutions were incubated (2-4h) with 2.5 mM DMPC (A) or 1 mM POPC (B) vesicles. Samples measured in 20 mM sodium phosphate buffer, 300 mM sodium sulfate, pH 6.0 and at 20 $^{\circ}\text{C}$. Bottom panel: Plots of the heat change as function of ligand to the nPTH1R molar ratio, shown after subtraction of background heats determined in ligand to buffer experiments. The red line is the best fit to the experimental data assuming 1:1 binding model. The calculated thermodynamic parameters are given in Table 4.7.

Table 4.7. Thermodynamic parameters for binding of PTH (1-84) to the nPTH1R in lipid environments

Parameters	in DMPC ^a	in POPC ^b	in water (ref) ^c
n	0.916 ± 0.01	0.945 ± 0.01	1.07 ± 0.01
K _a (×10 ⁵ M ⁻¹)	1.22 ± 0.21	1.55 ± 0.04	1.70 ± 0.06 ⁵
ΔH (kcal mol ⁻¹)	-26.53 ± 2.43	-16.95 ± 0.22	-15.86 ± 0.15
ΔS (cal K ⁻¹ mol ⁻¹)	-67.2	-34.1	-30.2
ΔG (kcal mol ⁻¹)	-6.84	-6.96	-7.01
K _d (×10 ⁻⁶ M)	8.2 ± 1.4	6.44 ± 0.16	5.89 ± 0.2

a and b data were derived from curve fittings shown in **Fig. 4.32A&B**

c was a reference experiment measured in water, values are taken from **Table 4.5**

The injection heat signal for PTH (1-84) binding to the nPTH1R in DMPC or POPC vesicles and the integrated heat change for each injection were shown in **Fig. 4.32 A** and **B**, respectively. The corresponding binding isotherms that were best fit to the raw data with 1:1 binding site model and the obtained values are shown in **Table 4.7**. The binding of PTH (1-84) to the nPTH1R in the presence of lipid environments revealed an exothermic process similarly to the binding in the absence (see **Fig. 4.17**) of lipid vesicles. The binding process for both reactions was mainly driven by an enthalpic gain accompanied by an unfavorable entropic penalty. The binding stoichiometry of 1:1 and K_d of about 7 μM were obtained for both lipid studies. These values are in good agreement with that obtained for lipid free binding reaction (K_d of 6 μM). Similar experiments were also performed in 1mM POPG (anionic lipids) and resulted in the same thermodynamic parameters including K_d value of 4.5 μM (**Fig. 9.5**).

Although the lipids bind predominantly to the nPTHR1 binding site of PTH, the affinity to nPTHR1 is not affected; therefore, the second step of the 2-step binding model is not significantly blocked by lipid binding of PTH and the membrane functions mainly by increasing the local concentration for the membrane bound full length receptor. This membrane interaction may require for receptor subtype recognition and selection (Bader et al. 2001).

4.11 Phosphorylation of PTH (1-84)

Many proteins get modified after translation and folding are complete. Generally, these posttranslational modifications such as the addition of phosphates or carboxyl groups are reversible processes. Phosphorylation and dephosphorylation processes dynamically regulate signaling pathways either by inhibition or activation of an involving protein (Walsh et al. 2005). In early 1984 Rabbani S.A. and coworkers have shown by HPLC methods that phosphorylation of mature PTH(1-84) occurs during biosynthesis in human and bovine parathyroid glands (Rabbani et al. 1984). However, phosphorylation sites and the effect of phosphorylation on receptor activity were not investigated. In order to understand the modification of PTH (1-84) at the molecular level, crude cell lysate were prepared from Human embryonic kidney (HEK) 293 cells the phosphorylation was studied by NMR and cell-based assay (Kumar et al. 2014).

4.11.1 Phosphorylation visualized by autoradiography

To mimic *in vivo* conditions, PTH (1-84) was treated with crude cell lysate prepared from bovine parathyroid glands or HEK 293 cells. Phosphorylation of PTH (1-84) was confirmed by autoradiography for the metabolic incorporation of radiolabeled ATP (^{32}P ATP). Autoradiography gives a strong band for phosphorylated PTH (1-84) by both cell lysate shown in **Fig. 4.33**. These studies are in line with the previously reported PTH phosphorylation analyzed by HPLC (Rabbani et al. 1984).

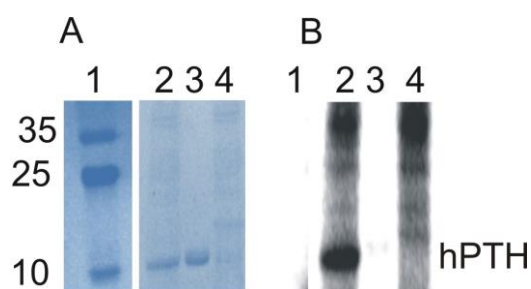


Fig. 4.33 Phosphorylation of PTH (1-84) visualized by autoradiography. Phosphorylation of PTH (1-84) by parathyroid gland extract stained by Coomassie brilliant blue (A) or autoradiography (B). Lane 1- protein molecular weight marker in kDa, lane 2- PTH (1-84) incubated with parathyroid gland extract, lane 3- PTH (1-84), and lane 4- parathyroid gland extract (Kumar et al. 2014).

4.11.2 Phosphorylation detected by mass spectrometry

After phosphorylation detected by autoradiography MALDI-TOF mass spectrometry was used to determine the number of phosphorylated sites. The experiments were carried out in a similar way with the parathyroid gland or HEK 293 cells lysate but ^{31}P ATP was used instead of a radiolabel (^{32}P -ATP). Phosphorylation of the PTH (1-84) was analyzed by MALDI-TOF tandem mass spectrometry. Control untreated PTH (1-84) resulted in a peak at 9551.2 m/z (theoretical mol weight: 9549.70 Da) corresponding to the unmodified uniformly labeled ^{15}N peptide. The ^{15}N labeling is required for subsequent NMR experiments. After 3 h of lysate treatment, a single peak corresponding to three phosphate groups attached to PTH (1-84) was observed (**Fig. 4.34**).

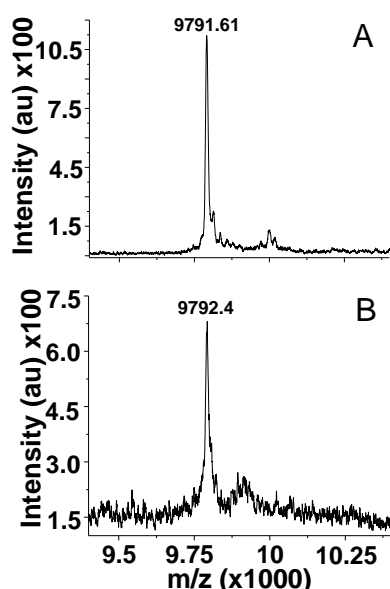


Fig. 4.34. MALDI-TOF mass spectrometric analysis of PTH (1-84) phosphorylation. PTH (1-84) was added to the lysate from (A) parathyroid gland and (B) HEK 293 cells and incubated for 3 hours (Kumar et al. 2014).

4.11.3 Identification of phosphorylation site by NMR

NMR spectroscopy is a powerful tool to identify the sites of phosphorylation and subsequent conformational rearrangements (Ito and Selenko 2010). ^{15}N labeled PTH (1-84) was incubated with HEK 293 cell lysate for 3h and then recorded ^{15}N HSQC spectra were shown in **Fig. 4.35**. Upon phosphorylation of PTH (1-84) at the serine residues, the local environment changed, making the chemical shift a sensitive tool to identify the respective serine residue (**Fig. 4.35A** and **Fig. 4.35C**).

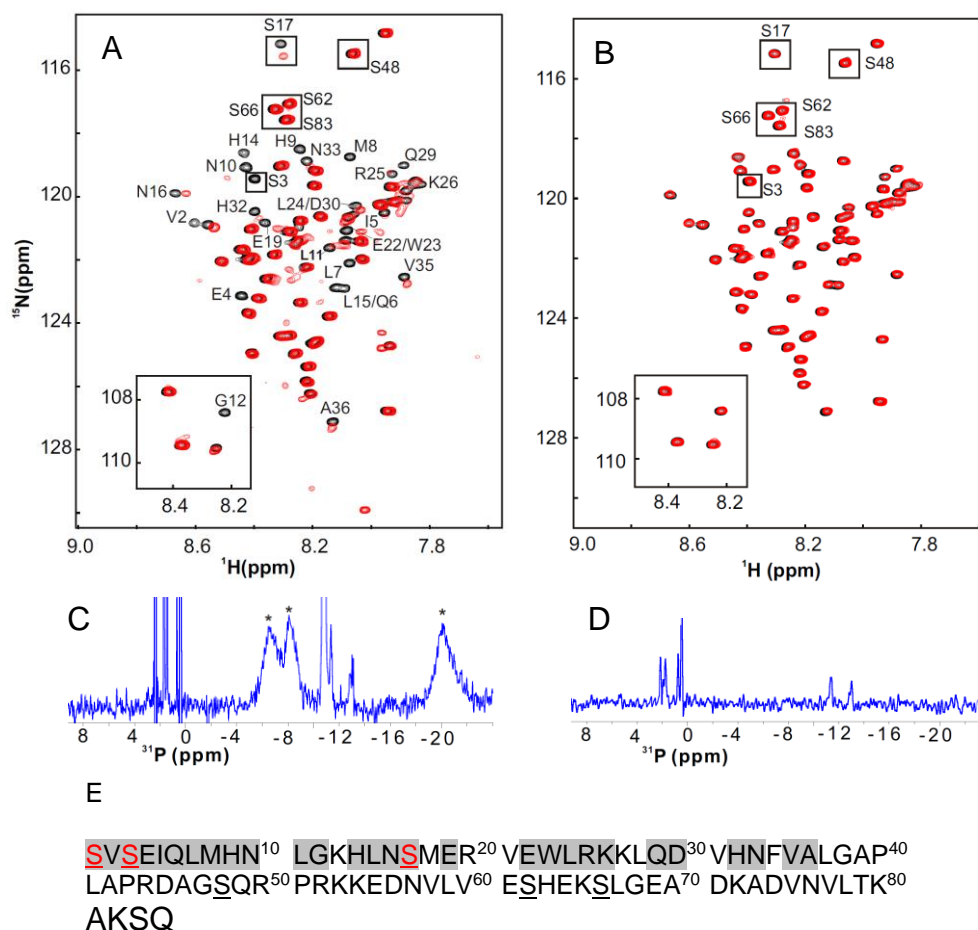


Fig. 4.35. NMR studies of phosphorylated and dephosphorylated PTH (1-84). (A) Overlaid 2D ^{15}N HSQC spectra of phosphorylated PTH (1-84) (red) and untreated peptide hormone (black). (B) Overlaid 2D ^1H - ^{15}N HSQC spectra of dephosphorylated PTH (1-84) (red) and untreated peptide hormone (black). Phosphorylation was carried out with lysate of HEK 293 cells and then the same sample was dephosphorylated by alkaline phosphatase treatment. (C) 1D ^{31}P NMR spectrum of the sample for (A), where asterisks mark ^{31}P signals arising from three phosphoserines. (D) 1D ^{31}P NMR spectrum of the sample for (B) with missing peaks of phosphoserines. Sharp peaks in the 1D ^{31}P spectrum around 0 to +4 or -10 to -14 ppm arise from the cell extract. (E) Phosphorylated serines are labeled in red on the amino acid sequence of PTH (1-84) and residues discern the phosphorylation by chemical shift changes are marked in gray (Kumar et al. 2014).

A detailed analysis of these HSQC spectra revealed that Ser3 and Ser17 specifically changed their chemical shift values, whereas Ser48, Ser62, Ser66, and Ser83 remain unchanged (Fig. 4.35A and red in Fig. 4.35E). Additionally, various neighboring residues of the N-terminal serine sense the phosphorylation by chemical shift changes (Fig. 4.35A and gray Fig. 4.35E). Whereas, the cross peak for the C-terminal serine residues or their neighbor residues did not show any chemical shift changes. Therefore, the third expected phosphoserine are assigned to Ser1, since the N-terminus typically shows no NMR cross peak in the ^{15}N -HSQC spectrum. To further confirm these NMR results, a

control experiment was carried out by treating phosphorylated PTH (1-84) with non-specific alkaline phosphatase. This dephosphorylation caused the re-appearance of all NMR cross peaks at their native chemical shift position (**Fig. 4.35B**). This also led to the disappearance of all three resonances in the 1D ^{31}P NMR spectrum corresponding to the phosphoserines (**Fig. 4.35D**). These NMR data are in full agreement with the autoradiography (**Fig. 4.33**) and mass spectrometric data (**Fig. 4.34**).

4.11.4 Effect of phosphorylation studied my cAMP activity

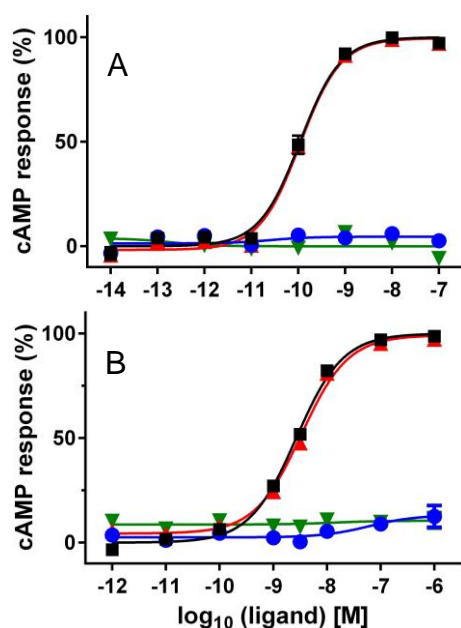


Fig. 4.36. PTH (1-84) activity of the PTH receptors. PTH (1-84) induced cAMP accumulation in HEK 293 cells stably expressing wild type receptors, (A) PTH1R and (B) PTH2R respectively. Symbols in the figures represent the mean of at least three independent experiments. Values for E_{max} were calculated as a percentage of the maximal response of hPTH(1-84). ■ – hPTH(1-84), ● – phosphorylated hPTH(1-84), ▲ – dephosphorylated hPTH(1-84), and ▼ – HEK 293 cells extract (Kumar et al. 2014).

To understand the functional effect of phosphorylated PTH (1-84), cAMP activity test was performed. The test was done by correlating the phosphorylation of PTH (1-84) with the cellular function by measuring PTH (1-84)-induced cAMP accumulation in stable HEK 293 cell lines expressing recombinant PTH1R or PTH2R (Mann et al. 2008). As a reference, the PTH (1-84) was used to mediate cAMP signaling cascade *via* PTH1R (**Fig. 4.36A**) and PTH2R (**Fig. 4.36B**). This activation led to an elevation of the cAMP level inside the cells in a concentration-dependent fashion (black in **Fig. 4.36**). Interestingly, there is a 25 fold difference in the potency of PTH (1-84) between these two receptors. PTH (1-84) displayed 9.89 ± 0.09 and 8.50 ± 0.13 pEC₅₀ values for the PTH1R and PTH2R, respectively. The same cAMP assay was performed for phosphorylated PTH (1-84). Surprisingly, the phosphorylation of PTH (1-84) almost completely ablated receptor activation (blue in **Fig. 4.36**). The same assay was performed

with the dephosphorylated form of PTH (1-84) achieved after addition of alkaline phosphatase to the phosphorylated PTH (1-84). This treatment rescued the activity of PTH (1-84) and yielded E_{\max} values, relative to hPTH(1-84), of 98.58 ± 2.24 % ($pEC_{50} - 9.97 \pm 0.08$) and 99.35 ± 2.28 % ($pEC_{50} - 8.56 \pm 0.13$) for PTH1R and PTH2R, respectively (red in **Fig. 4.36**). These results confirmed the phosphorylation-mediated inactivation of the peptide hormone. Cell lysate did not have any effect on the receptors activation (green in **Fig. 4.36**) (Kumar et al. 2014).

Autoradiography experiments were performed with the help of Dr. Lennart Eschen-Lippold, IPB at Halle. Cell-based assays were done by Dr. Amit Kumar, MLU, Halle, in collaboration with Dr. Dan Donnelly University of Leeds, UK.

4.12 Fibrillation of PTH (1-84)

PTH is secreted as 115 residues from the parathyroid glands to control calcium and phosphate level in the blood (Grauschopf et al. 2000). After proteolytic cleavage of pre and pro sequences, the mature PTH (1-84) is stored in secretory granules (Datta et al. 2007). Earlier in 1976, Kedar and coworkers showed that PTH and other peptide hormones like insulin or calcitonin form amyloids (Kedar et al. 1976). Then, in 2009 Maji and coworkers demonstrate that peptide hormones are stored as functional amyloids (Maji et al. 2009). Accumulations of amyloid fibrils can also cause diseases such as Alzheimer's, Parkinson's, Huntington's or diabetes (Datta et al. 2007).

4.12.1 PTH (1-84) fibril formation

Fibril formation of PTH (1-84) was tested at three different pH values (3.0, 7.4, 9.0) and two different temperature (37 °C and 65 °C). Formation of fibril could be observed in 50 mM borate buffer, pH 9.0 at a concentration of 10 mg/ml, incubation at 65 °C (**Fig. 4.37**) within 1 hour.

The time-dependent aggregation of PTH (1-84) was monitored by the fluorescent dye thioflavin T (ThT). Binding of ThT to aggregated amyloid species leads to a several-fold increase in its fluorescence intensity at 480 nm (LeVine 1993). ThT is thermally

unstable at 65 °C, so a standard ThT assay could not be performed. Therefore, 16 individual samples of the same concentrations were incubated in parallel and then measured one by one between 0 and 20 min. ThT shows only a small fluorescence signal for monomeric PTH (1-84) at 0 min. Next sample at 1 min, the fluorescence intensity increased significantly up to 12 fold (**Fig. 4.37A**). The increased fluorescence indicates that the peptide hormone forms higher aggregated/fibrils species with a time course typical for amyloid fibril formation of other archetypical peptides. Surprisingly, the ThT kinetics for PTH (1-84) was found to be very fast and completed within five minutes of incubation under the mentioned conditions.

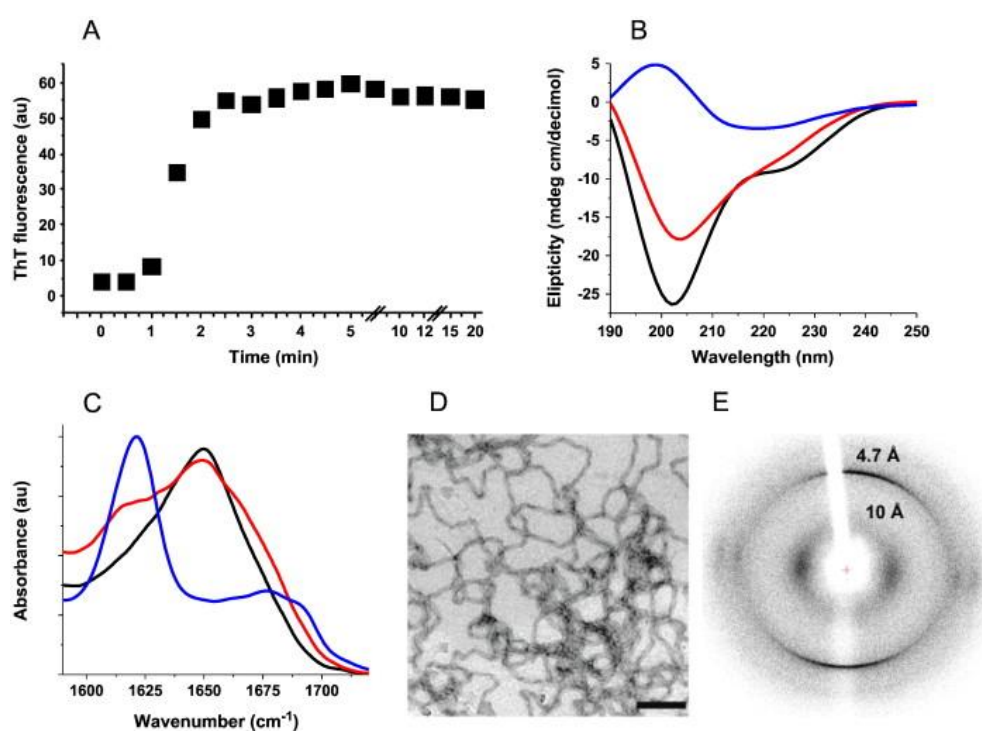


Fig. 4.37. Characterization of PTH (1-84) fibrils. (A) Thioflavin T binding kinetics. (B) Secondary structural analysis upon fibril formation monitored by far-UV CD spectroscopy. (C) ATR-FTIR spectroscopy analysis of fibril formation. Only the amide I spectral regions are plotted. (D) Transmission electron micrograph of PTH (1-84) fibrils. Scale bar: 200 nm. (E) X-ray diffraction pattern of the PTH fibrils. Colors in (B) and (C): black – PTH (1-84) monomers, red – PTH (1-84) fibrils, blue - A β (1–40) amyloid fibrils as a comparison (Gopalswamy et al. 2015).

4.12.2 Structural characterization of PTH fibrils

The CD spectrum shows negative ellipticity around 222 nm corresponding to the α -helical contribution and a large negative ellipticity around 200 nm indicative of an intrinsically disordered section (**Fig. 4.37B**). Fibril formation is accompanied by the for-

mation of a β -sheet-rich secondary structure regardless of the structure of the native protein (Marshall and Serpell 2009). The CD spectrum of PTH (1-84) fibrils shows a loss in negative ellipticity at 222 nm (red in **Fig. 4.37B**) compared to the monomeric PTH (1-84) (black in **Fig. 4.37**) which indicates the β -sheet formation. Furthermore, the CD spectrum of fibrils of the Alzheimer's A β (1-40) peptide (blue in **Fig. 4.37B**) shows that PTH (1-84) still contains significant contributions from random coil structures (ellipticity around 200 nm) indicating that only parts of the 84 residues end up in the cross- β structure.

To study further about the secondary structures upon fibril formation ATR-FTIR spectroscopy were used. The amide I spectral region between 1600 and 1700 cm^{-1} is informative about the stretching mode vibrations of the backbone carbonyl groups and is affected by the secondary structure of the polypeptide chain (Hiramatsu and Kitagawa 2005). IR spectrum of PTH (1-84) showed amide I vibrations occur at 1650 cm^{-1} (black in **Fig. 4.37C**) and an extra shoulder at 1615 cm^{-1} (red in **Fig. 4.37C**) suggests the presence of random coil-like structure and amyloid-like elements of β -sheet structure respectively (Zandomeneghi et al. 2004). Yet, the amplitude of 1615 cm^{-1} band for PTH (1-84) fibril was far less pronounced than the large peak seen at this position in the spectrum of Alzheimer's A β (1-40) peptide fibrils (blue in **Fig. 4.37C**). This observation is consistent with the CD data which suggested that only a parts of the PTH (1-84) are involved in the formation of the fibril β -sheet structure.

TEM analysis was carried out for PTH (1-84) to see if fibrils were formed under different experimental conditions (section 4.12.1). The screening of various conditions showed that filamentous morphologies of PTH (1-84) were found within one hour when the peptide was incubated at pH 9.0 and 65 °C (**Fig. 4.37D**). These fibrils had a length of up to several micrometers and possessed an unbranched curvilinear morphology. Fibril diameters ranged between 10-20 nm.

In order to identify the fibril architecture, X-ray diffraction patterns were analysed. The X-ray diffractogram is shown in **Fig. 4.37E**. The obtained pattern is defined by meridional reflections at 4.7 Å which correspond to inter β -strand spacing and an equatorial

reflection at 10 Å corresponding to the distance between stacked β sheets. The obtained data is in good agreement with the cross- β structure of other amyloid fibrils (Greenwald and Riek 2010).

4.12.3 Identification of the fibril core

Computer-based *in silico* predictions like PASTA (Trovato et al. 2007) and Waltz (Reumers et al. 2009) indicate that the region of residues S1-M10 and predominantly D30-G40 of PTH(1-84) are prone to aggregation (**Fig. 4.38**). Resistance to proteolytic cleavage is another defining characteristic for the presence of amyloid fibrils (Hartley et al. 2008).

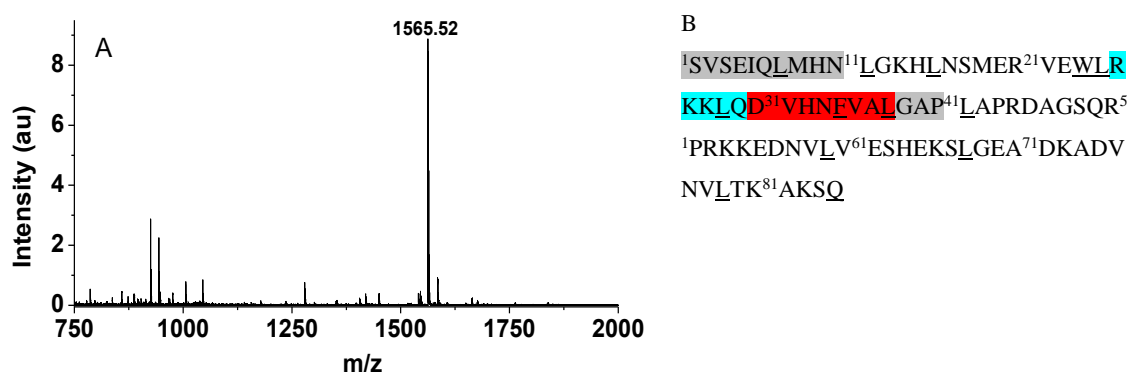


Fig. 4.38. Identification of the fibril core of PTH (1-84) by limited proteolysis. (A) MALDI-TOF analyses of PTH (1-84) fibrils digested with chymotrypsin after 2 h of incubation. (B) Amyloid regions are highlighted on the primary sequence: in silico predicted regions by Waltz and PASTA were shown in gray, the fibril core identified by MALDI-TOF and ESI-MS-MS were shown in cyan and red indicates the common region identified by mass spectrometry and in silico program. According to proteolytic cleavage protection, underlined are the possible cleavage sites for chymotrypsin (Gopalswamy et al. 2015).

Upon fibril formation, certain residues are well protected against protease cleavage which helps to identify the fibril core. Accordingly, PTH (1-84) monomers and fibrils were subjected to limited proteolysis by chymotrypsin. It is known that the enzyme cleaves predominantly at aromatic residues and it has a reduced propensity to cleave at leucine and methionine ((Appel 1986)). Proteolysis was carried out over 0-22 hours and samples were collected at the different time. These samples were analyzed by MALDI-TOF mass spectrometry. The spectrum indicated a dominant peak at $m/z = 1565.52$ Da, and this peak consistently appeared upon longer incubation times of 22 h (**Fig. 4.38A**). This $m/z = 1565.52$ Da corresponds to region 25R – 37L (theoretical wt: 1567.8 Da) suggested by the computer based online program (ProteinProspector). On the other

hand, monomers of PTH (1-84) did not result in any protected specific cleavage patterns and the corresponding peaks were absent in the spectrum.

To confirm the fibril core identified by MALDI-TOF, the most abundant mono MH^+ peak ($m/z = 1565.52$ Da) was further subjected to fragment base ESI-MS-MS. The analysis of ESI-MS-MS revealed that the fibril core formation is 25R – 37L. Although the identified sequence consists of two cleavage sites for chymotrypsin, L28 and F23 (**Fig. 4.38B**) the corresponding cleaved product could not be detected by MALDI-TOF or ESI-MS-MS, thus, confirming the protection against chymotrypsin. These data correlated well with the *in silico* prediction, where the involvement of the same residues ~30-40 was predicted to form the fibril core. However, as revealed by the MS data, the first 10 residues of PTH (1-84) were not protected against digestion.

4.12.4 Inhibition of PTH (1-84) fibril formation by EGCG

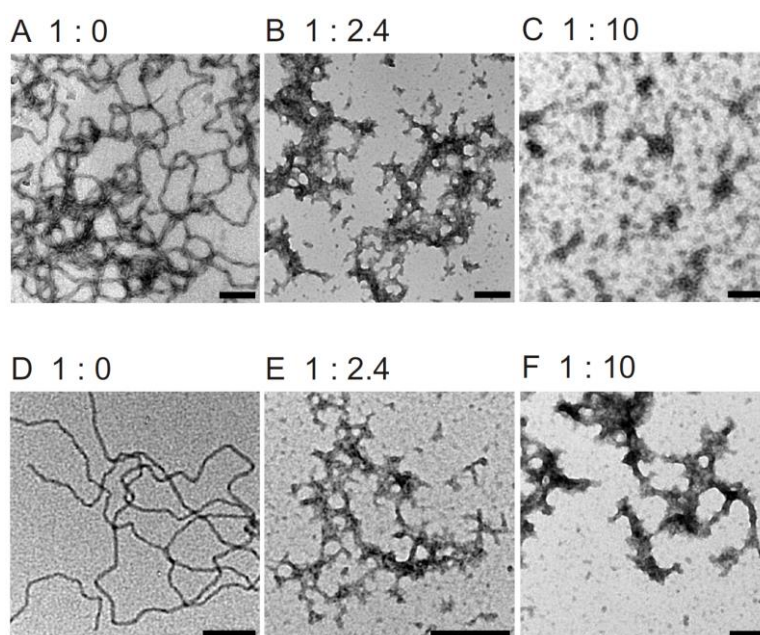


Fig. 4.39. Electron micrographs of EGCG-treated PTH (1-84) fibrils. EGCG and PTH (1-84) was co-incubated at the indicated PTH (1-84):EGCG ratio and EM micrographs were taken after 1h (upper panel) and 48 h (lower panel). The scale bars represent 200 nm (Gopalswamy et al. 2015).

The polyphenol (-)-epi-gallocatechine gallate (EGCG) is a very effective amyloid inhibitor suppressing or modulating the amyloid formation of different polypeptides including α -synuclein, the Alzheimer's peptide $A\beta$ (Ehrnhoefer et al. 2008; Meng et al. 2010; Huang et al. 2012). Here EGCG was used to investigate the inhibition of PTH (1-84)

fibril growth. PTH (1-84) and EGCG was incubated at a molar ratio of 1:2.4 or 1:10 for a period of 48 h at 65 °C. Aliquots were taken at various time points for both with and without EGCG and examined by EM. PTH (1-84) incubated with EGCG at 1:2.4 or 1:10 molar ratio completely inhibited the fibril growth and led to the formation of amorphous protein aggregates at all analyzed times (**Fig. 4.39**). About 30 nm sizes of small spherical particles were observed at a mixing ratio of 1:10 after 1 h of co-incubation (**Fig. 4.39C**). The formed species at both ratios are distinctly different from mature fibrils, which were only detected in the samples without EGCG (**Fig. 4.39A** and **Fig. 4.39D**). Similar effects were reported for α -synuclein or A β when treated with EGCG (Bieschke et al. 2010).

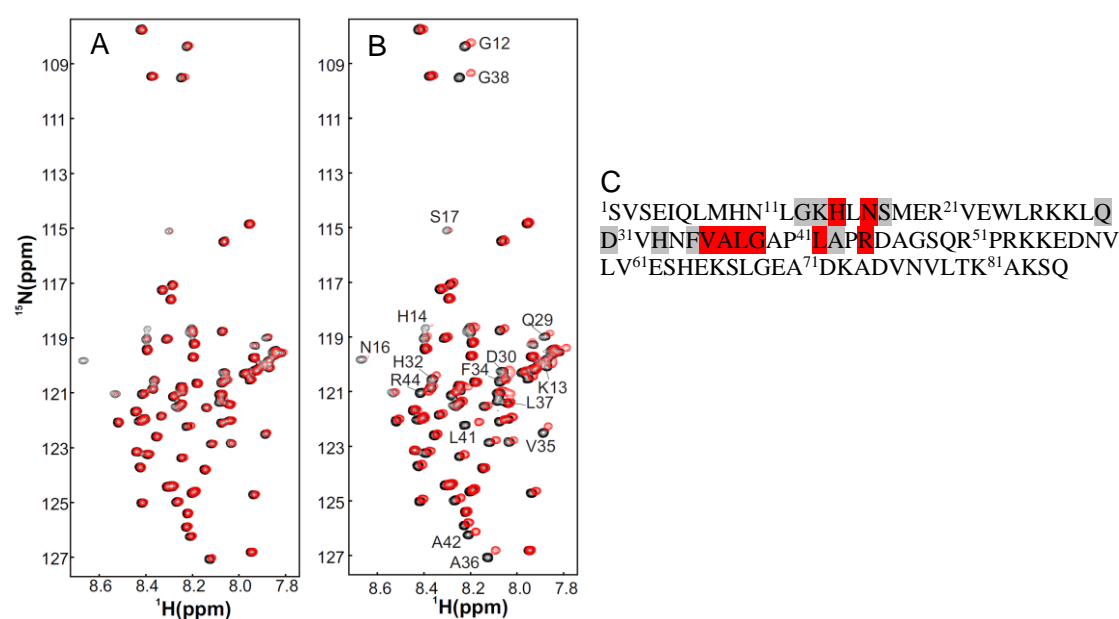


Fig. 4.40. NMR analysis of hPTH(1-84)-EGCG interaction. Overlay of the ¹⁵N-HSQC spectra of free ¹⁵N-hPTH(1-84) (black) and in complex with EGCG (red) at a 1:1 ratio (**A**) and a 1:5 ratio (**B**). (**C**) Residues are marked on the PTH(1-84) primary sequence in grey with moderate chemical shift changes and in red with significant changes upon EGCG interactions (Gopalswamy et al. 2015).

To reveal residue resolution of this inhibition, NMR spectroscopy was employed using the backbone N-H resonance assignments of PTH (1-84) (section 4.7.4). ¹⁵N-PTH (1-84) was titrated with increasing concentration of EGCG and analyzed by 2D ¹⁵N-HSQC spectra (**Fig. 4.40**). As the concentrations of EGCG increased, the intensity and chemical shift changes of resonances of those residues involved in the binding of EGCG to the PTH (1-84). In the 2D spectra, only marginal chemical shift changes were observed at a 1:1 (protein: EGCG) ratio. When the molar ratio was increased above 1:3, significant changes were observed. The majority of residues which are located in the fibril

core as predicted by the *in silico* tools and mass spectrometry data also show significant chemical shift changes in the NMR titration experiment (**Fig. 4.40C**) and thus binding of EGCG to these residues inhibits fibril growth.

ThT kinetics and limited proteolysis experiments were performed together with Dr. Amit Kumar, MLU, Halle.

5 Discussion

The parathyroid hormone (PTH) is the main endocrine factor acting in bone and kidney to regulate blood calcium and phosphate level. This linear peptide of 84 amino acids acts by binding to its PTH 1 receptor (PTH1R). The first objective of this work is to study the interaction of PTH to the extracellular domain of PTH1R (nPTH1R) and the second is to unravel the two-step binding model of this interaction at an atomic level. Furthermore, the regulation of the PTH receptor by phosphorylated PTH should be investigated and the final goals of this thesis are structural investigations of PTH fibrils (functional amyloid).

5.1 Binding mechanism of PTH to the nPTH1R

The two-step binding model of PTH towards its receptor is difficult to investigate under *in vivo* conditions. Therefore it is essential to recombinantly produce the various involved proteins in a large quantity for *in vitro* studies by using *E. coli* as a host system. Several peptides *viz.* PTH (1-84), PTH (1-34), PTH (15-34), and nPTH1R were produced with high yields. SUMO fusion is an efficient system to produce the protein and/or peptides in the bacterial cytosol as soluble fraction. Also, small peptides are difficult to express in bacterial systems. Therefore all constructs of PTH were expressed in *E. coli* BL21 codonPlus-RIL strain as SUMO fusion protein. The PTH could be cleaved from the SUMO using the Ulp1 SUMO protease which is specific for this task. The cleaved peptides hormones were efficiently purified using the Ni-affinity chromatography followed by gel filtration chromatography. One exception to this is nPTH1R which could not be expressed as a soluble protein because it tends to form inclusion bodies inside bacteria. Therefore it was purified from these inclusion bodies under denaturation conditions using Ni-affinity and gel filtration chromatography after renaturation.

It was intriguing to find out whether nPTH1R exists as monomers or dimers in solution. Previous studies have shown that the nPTH1R exist as monomer (Grauschopf et al. 2000) or dimer (Pioszak et al. 2010) state in solution. Therefore pulse field gradient

(PFG) NMR diffusion measurements were performed (see 3.23.3). The experimental results are in well agreement with a monomeric state according to the observed diffusion constant ($D = 1.13 \pm 0.01 \times 10^{-10} \text{ m}^2/\text{s}$) and effective hydrodynamic radii ($R_h = 20.34 \pm 0.18 \text{ \AA}$) and the predicted hydrodynamic radii 21.7 \AA .

In parallel, it is also necessary to confirm that the recombinant PTH is a functional agonist. As mentioned earlier parathyroid hormone is secreted as a 84 residues peptide in humans, however, its first 34 residues are sufficient for receptor activation. There are two principal signal transduction pathways activated by the G protein-coupled receptors: the cAMP signal pathway and the phosphatidylinositol signal pathway (Gilman 1987). The parathyroid hormone is involved in the cAMP pathway for its biological regulation. The recombinantly produced peptide hormones are able to activate the receptor which was manifested by the cAMP accumulation inside the HEK 293 cells (**Fig. 4.36**). Thus these studies clearly suggest that the recombinant peptide hormones, as well as the receptor, are in their functional state.

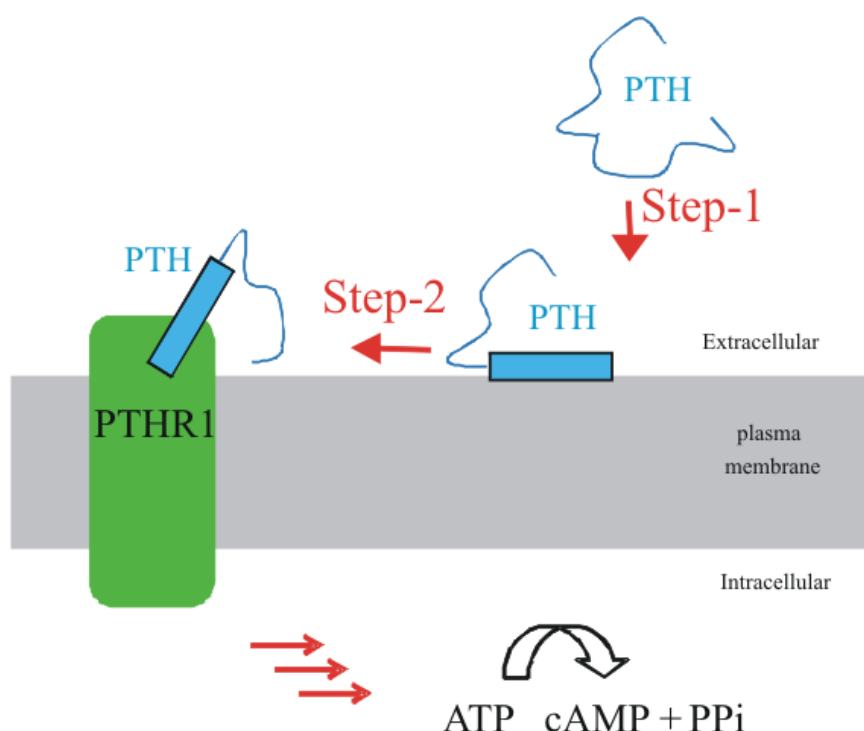


Fig. 5.1. Two-step model of membrane mediated peptide-receptor interactions. Step-1: The electrostatic and hydrophobic interaction of flexible, amphipathic peptide PTH with lipid membranes. The N-terminal part of PTH interacts to the membrane and the C-terminal segments remain in the aqueous head group region. **Step-2:** The two-dimensional diffusion of PTH on the membrane surface leads to specific binding to the PTH1 receptor. These processes finally stimulate cAMP

The basic signal transduction starts when the peptide hormone binds to the extracellular domain of the receptor. A two-step binding model (**Fig. 5.1**) was proposed for the PTH and its receptor interaction based upon mutational manipulations and photochemical cross-linking studies (Castro et al. 2005; Gensure et al. 2005). This model proposed that the hormone first binds to the membrane followed by interaction with the extracellular domains as the second step (Sargent and Schwyzer 1986; Pellegrini et al. 1998; Inooka et al. 2001). However, the molecular basis of their interaction and exact binding model remained elusive. The first discussion sections herein cover the hormone interaction with lipid membrane while second sections will cover the interaction of peptide hormones with the receptor.

5.1.1 PTH interaction to the membrane

Concerning the interaction of PTH with the membrane, a non-specific interaction is expected between the peptide hormone and the membrane, and full length agonist (PTH (1-84)) was chosen for this study. Some lipids such as POPC or brain lipids induce little structural change while anionic vesicles for example formed by POPG or DMPG or detergent micelles induce some α -helical structure. As expected, hydrophobic interactions were observed by the ITC when PTH (1-84) to the POPC vesicles. This was confirmed by pulse field gradient (PFG) NMR showing a diffusion constant of $10.60 \times 10^{-11} \text{ m}^2/\text{s}$ for free PTH(1-84) and a lower value when bounding to DPC and DMPC. Furthermore, resonances corresponding to residues 2 – 42 disappeared from ^{15}N -HSQC spectra when POPG, brain lipids or DMPG vesicles were titrated to ^{15}N -PTH (1-84) while the C-terminal residues were not affected. This is due to the slow tumbling of the high molecular weight complex between PTH (1-84) and the vesicles. The C-terminal residues (43-84) which are not interacting to the vesicles were exposed to the solvent and flexible enough to be detected by NMR. These solution NMR data further supported by the amphipathic helical properties of PTH (1-43) (**Fig. 5.2**) predicted by the Heliquet software (Gautier et al. 2008). The hydrophobic face of the helix binds to the acyl chains and the polar residues interact with the lipid polar heads and solvents. The large size of vesicle-PTH (1-84) complex makes it difficult to determine the structure of membrane bound PTH. Therefore, membrane mimetic, DPC micelles were used, which

also maintain the structure and functionality of proteins and peptides (Shenkarev et al. 2002). The d_{38} -DPC bound PTH (1-84) showed the same results and the chemical shift of region 2-40 were the most affected upon interaction. Additionally, CD and NOE data suggest that parts of membrane bound PTH (1-84) adopt an α -helical conformation. Thus these studies confirm that the parathyroid hormone indeed interacts with the membrane probably before approaching towards the receptor.

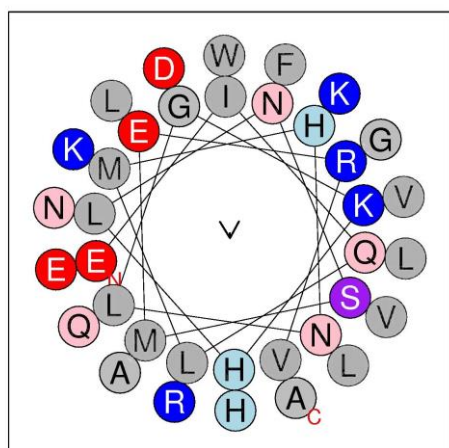


Fig. 5.2. Helical wheel diagram of PTH. PTH (4-39) Color codes are: Hydrophobic residues (gray), charged residues (blue and red), polar residues (pink, purple and light blue).

PTH (4-39): EIQLMHN LGKHLNSMER
VEWLRKKLQD VHNFVALGA

Although solution NMR studies have provided enough evidence of the two steps binding model it is quite difficult to study the peptides in the membrane due to the large size of the complex. Therefore solid state NMR was employed for further clarifications. The signals for $^{13}\text{C}/^{15}\text{N}$ -PTH (1-34) bound to DMPC- d_{67} were only seen in the CP and DP experiments while they were not detectable in the INEPT experiments. This clearly indicated the binding and slow tumbling of PTH (1-34) when bound to the membranes. Same studies with PTH (1-84) showed very sharp signals in the INEPT experiment arising from the mobile region in the full length PTH not inserted into the membrane. In the deuterium NMR spectrum, a typical well resolved powder pattern was obtained for pure POPC- d_{31} , which got significantly perturbed upon adding PTH (1-34) and the peaks became sharp. Additionally, the order parameter decreased in presence of the peptide. This clearly indicates that the membrane incorporation of PTH (1-34) and the binding of the peptide to the membranes, and concomitant changes in the membrane flexibility along the carbon chain. Often, relaxation rates R_1 of pure phospholipid membranes exhibit a linear relation to the square of the order parameter. Therefore, a linear dependence plot was observed for pure POPC- d_{31} , while a bent shape with a steeper slope was

observed when bounding to the PTH (1-34). This is attributed to the change in an elastic property of the membrane upon peptide binding. Although, these results indicted the binding of PTH (1-34) to the lipid membrane and this event makes the membranes very flexible and dynamic, yet it is difficult to explain the high mobility with the available data. Similar effects have been noticed for DMPC/Ras-peptide complex and it was explained that the hydrocarbon chains of ras occupy a greater conformational space than the DMPC hydrocarbon chains (Vogel et al. 2005). Nevertheless, results correlate well with the solution NMR data where residues 1-40 were involved in membrane interactions.

5.1.2 PTH binding to the nPTH1R

In order to understand at the molecular level the PTH-nPTH1R interaction and nPTH1R recognition of other ligands in solution, first thermodynamic parameters were obtained by ITC and SPR. Both the techniques provide the ligand binds to the nPTH1R with lower micromolar affinity and forms a 1:1 complex. The process was found to be driven in an enthalpic and entropic compensative manner. Although a nanomolar affinity of PTH (1-84) to its receptor ($K_d=50$ nM) was found under the *in vivo* conditions (Castro et al. 2005) such a high affinity was not obtain from the present *in vitro* experiments. High affinity was not expected as the studies were performed for the extracellular domains only. The other interacting sites are present at the TM domain (TM3, TM5, and Thr427 at TM6) and extracellular loops (Met425 at loop 3 and Leu261 at loop 1) which were identified from cross-linking studies (Gensure et al. 2005). CD spectroscopy shows an increase in the ellipticity upon interaction when compared to the isolated peptides. These changes could be attributed towards the conformational change upon binding and formation of ordered secondary structure in the complex. To understand the interaction at an atomic level in solution, ^{15}N -nPTH1R sample was prepared (section 3.9). In a titration experiment, significant chemical shift perturbation was absorbed at <1:2 molar ratio of receptor domain to agonist (^{15}N -nPTH1R: unlabeled PTH (1-84)). A typical behavior of binding was observed where some cross peaks first disappeared and appeared at different chemical shifts or new cross peaks emerged. This is indicating that intermolecular interactions are in the slow exchange regime ($k_{ex}<\Delta\delta$) on the NMR

chemical shift time scale. Interestingly, bound nPTH1R is to some extent more structured than the unbound form, attributed to the relatively large area of dispersed NMR cross peaks in the bound state. Previous studies have shown similar results for the other members of class B GPCR family receptor *viz.*, ECD of corticotrophin-releasing factor 1 receptor, which is also largely unstructured (Grace et al. 2010). These studies clearly suggested the interaction of PTH (1-84) with the nPTH1R.

A residue level information of nPTH1R could not be obtained due to the heavy overlap of backbone cross peaks. But the same is possible for the binding partner PTH (1-84). PTH show very well resolved cross peaks due to the alpha helical structural elements present from 1-38 residues. The titration experiments show perturbations of the backbone chemical shift and signal intensity changes upon complex formation. Only N-terminal residues from L11 to G38 of PTH (1-84) are involved in the interaction with nPTH1R. Few neighboring residues also showed minor changes in their NMR properties as expected. The C-terminal part however, is not involved in the nPTH1R interactions, remained solvent exposed and showed unchanged NMR resonances. The NMR titration also revealed a lower micro molar binding affinity. Dynamic studies also support the titration data. Here, the C-terminal part of free and nPTH1R bound PTH (1-84) shows the same ^1H - ^{15}N NOE values.

The N-terminal cross-peaks reporting bindings show line-broadening and could not be detected in the complex spectra. The exchange rate (k_{ex}) of ~ 10 Hz between free and bound conformation of PTH (1-84) can be calculated from the kinetic forward (k_{a}) and reverse (k_{b}) reaction from SPR data (section 4.7.3). This exchange rate exactly falls into the intermediate exchange regime in the simulated exchange curves (**Fig. 3.3**) which explain the disappearance of the cross peaks. Thus these results clearly demonstrate that only the N-terminal part of PTH (1-84) is important for extracellular domain binding and residues $\sim 11 - 38$ are involved in this interaction.

This observation was further strengthened by choosing the truncated peptides *viz.*, PTH (1-34) and PTH (15-34). The backbone chemical shifts comparison between the PTH (1-34) and PTH (1-84) are in well agreement confirming that the N-terminus of PTH

has a similar structure in both PTH (1-34) and full length PTH(1-84) under our experimental conditions. PTH (1-34) showed the similar micromolar affinity and stoichiometry with nPTH1R as observed for PTH (1-84). The exothermic nature which is accompanied by a loss of entropic energy has revealed that the system becomes more ordered upon complex formation. Even though the K_d is similar for both PTH (1-84) and PTH (1-34) the kinetic rate constants are different. The k_a rate for PTH (1-84) is 10 times faster and k_{off} rate is 2 times slower compared to PTH (1-34). This kinetic data state that the additional Val35, Ala36, and Leu37 residues contribute to the specificity and stability of the complex and support the NMR data.

The binding affinity towards nPTH1R was 10 - 15 times lower for PTH (15-34) compared to PTH (1-84) or PTH (1-34). In an NMR titration of ^{15}N -PTH (1-34) with unlabeled nPTH1R, half of the resonances of C-terminus (Glu19 to Phe34) got broadened beyond detection limits possibly because of reaching the intermediate exchange regime in the bound state, while Val2-Gly12, Leu15, and Met18 show detectable resonances in the bound state. This clearly suggested that the only ~15 – 34 residues are crucial for interaction with the receptor. This could be further strengthened by taking the PTH (15 – 34) where most of the cross peaks disappeared upon complex formation with nPTH1R. Residues of N or C terminus *viz.*, S17, N33, F34 and side chains NHs were still visible but with slightly different chemical shifts indicating even these involved in interactions. The drop in affinity for PTH (15-34) is expected due to the short length and lacking of accessory neighbor residues (extension of the binding site up to G12). In each reported structure, the ligand occupies the same binding groove of its ECD of the receptors (Parthier et al. 2009; Culhane et al. 2015). One exception is the PACAP ligand, which occupies another binding groove than the common binding mode in the solution NMR structure of PACAP (6-36) in complex with ECD-PAC1R (Sun et al. 2007). So, to investigate whether nPTH1R has a second binding site, a competitive experiment was performed between the ^{15}N -PTH (1-34) and ^{15}N -PTH (15-34). The intensity of the peptides NMR resonances decreased while adding unlabeled nPTH1R (**Fig. 4.13**) and the apparent K_d was calculated assuming a single fit 1:1 binding model. The binding affinities were nearly same as when the peptide-nPTH1R was studied alone. When there is a second binding site we would expect higher K_d for one of the ligand,

which is not the case. Also, this experiment demonstrated that only the middle residues i.e., ~12 – 34 are involved in the interactions.

So far we have seen that the PTH interacts with its receptor as well as to the membrane which confirms the two-step binding model. In a two-step binding model the PTH binds to the membrane on the cell surface and further diffuse towards its receptor thereby increasing the effective concentration (**Fig. 5.1**). Further proof came by the ITC titration experiments in the membrane environment (DMPC or POPC). Here pre-bound PTH (1-84) to membranes showed still interactions to the nPTH1R. The interaction behavior was similar to the ITC study in the membrane free environment in terms of stoichiometry and dissociation constant. These observations suggested that the lipid environment does not prevent the binding and has no effect on receptor recognition. The membrane is required to keep PTH in a bioactive conformation and to avoid entropic penalties so that the rate of receptor recognition and selection is efficient (Sargent and Schwyzer 1986; Schwyzer 1986).

5.2 Structural and functional studies of PTH phosphorylation

Protein phosphorylation is one of the major post-translational modifications in signal transduction. Phosphorylation plays a pivotal role in many cellular processes including cell growth, membrane transport, division, organelle trafficking and muscle contraction. Kinases have to select their potential substrates from among the 700,000 possible phosphorylation sites that might encounter (Ubersax and Ferrell 2007). Phosphorylation of PTH (1-84) has been reported in early 1984 (Rabbani et al. 1984). However, the specific phosphorylation sites and their functional implications were not known.

To experimentally probe the role of modified PTH, HEK 293 cell lysates were used to phosphorylate PTH (1-84). A strong band was detected by autoradiography confirming the phosphorylation of PTH (1-84) and these results nicely correlate with the previously published data (Rabbani et al. 1984). Furthermore, an increased in molecular weight of 240 Da for lysate treated PTH (1-84) from the MALDI-TOF experiments demonstrates

triple phosphorylation. Mass data was further confirmed by three broad peaks at ^{31}P -NMR. It has been shown in the literature that the ^{31}P -NMR signal is broader for phosphorylated proteins and sharp signals for small molecules (Rao et al. 1979).

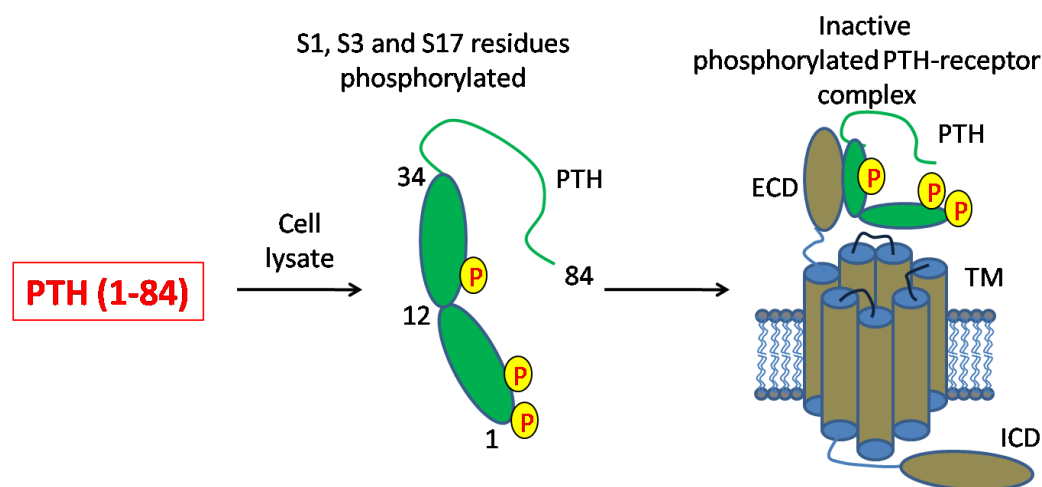


Fig. 5.3. Phosphorylation mediated inactivation of PTH receptor. PTH (1-84) is triple phosphorylated (S1, S3, and S17 residues) by incubating with HEK 293 cell lysates. The phosphorylated PTH (1-84) fails to activate the receptor.

Although Rabbani and coworker discussed phosphorylation of PTH, they fail to identify the exact position of phosphorylation in the polypeptide sequence (Rabbani et al. 1984). The site-specific phosphorylation was identified by ^{15}N -HSQC experiments. HSQC data revealed Ser3, Ser 17 and the residues which are in close proximity to these two serines by their chemical shift perturbation. Ser48, Ser62, Ser66, Ser83 and other C-terminal residues remain unchanged (**Fig. 4.35A**). The third has been phosphoserine assigned to Ser1 since it is not visible in the ^{15}N -HSQC spectra. Similar experiments were previously shown for phosphorylation of viral SV40 large T antigen studied with *Xenopus laevis* egg extract (Selenko et al. 2008) and transcription factors such as *c-myc* studied with HeLa cell lysate (Liokatis et al. 2010). Note, that the phosphate group could be eliminated from PTH (1-84) while incubating with alkaline phosphatase, which confirms mass data and autoradiography.

N-terminally modified and truncated PTH was found in blood. It has been reported that the modified PTH was oversecreted in patients with severe primary hyperparathyroidism or with parathyroid carcinoma and it was suggested that a residue Ser17 may be phosphorylated (Arakawa et al. 2006; Rubin et al. 2007). But the specific role of phos-

phorylated PTH remained unclear. Therefore a cAMP assay was performed for phosphorylated and unphosphorylated PTH (1-84). The results of this assay (**Fig. 4.36**) indicate that the PTH (1-84) activates both PTH1R and PTH2R with similar pEC₅₀ values, which is in good agreement with the previously published results (Lim et al. 2004; Gensure et al. 2005). Interestingly, the phosphorylation of PTH (1-84) almost completely ablated receptor activation for both receptors and dephosphorylated form of PTH (1-84) rescued the activity of PTH (1-84) more than 99%. These results confirmed the phosphorylation-mediated inactivation of the peptide hormone. The complete loss of activity is probably due to the strong negative repulsion and bulky size of the phosphate groups (mainly 1 and 3 residues) which may not allow interacting to the transmembrane domain (**Fig. 5.3**). Furthermore, it has been shown that the α helical conformation between residues 3 and 10 is important for activating the receptors (Lim et al 2004). Phosphorylated PTH (1-84) can still bind to the PTH1R ECD domain (Kumar et al. 2014). Therefore, we propose that PTH phosphorylation blocks PTH 1 and 2 receptor activation at the TM domain. The next challenging task would be the identification of the specific kinase that acts on PTH.

5.3 Systematic study of PTH fibril

Amyloid fibrils are formed by proteins that escape the folding pathway towards native folding. Such amyloid deposits are quite commonly seen in neurodegenerative diseases (Fandrich et al. 2011). On the other hand, proteins/peptides of secretory pathways can be deposited in densely packed membrane coated granules referred to as functional amyloids (Maji et al. 2009). Although functional amyloids are distinctly different from the disease-causing amyloids, they exhibited the same basic architecture of cross- β -sheet-rich conformations (Maji et al. 2009). In early 1976, the formation of fibrils from PTH (1-84) was reported, however, without a detailed molecular characterization (Kedar et al. 1976; Maji et al. 2009). The obtained results for PTH (1-84) fibrils (section 4.12) reveals a conformational transition from a disordered protein containing partial sections of α helical to a cross β motif forming fibrils by intermolecular interactions.

In a systematic screening of fibril forming *in vitro* conditions, it was found that high pH and temperature are suitable condition for amyloid formation. The fibril growth experiments showed fast kinetics and fibril formation accomplished within the first five minutes after a short lag phase (**Fig. 4.37A**). Similar to other amyloid forming peptides (Hamley 2012), we expect a nucleation process of higher oligomers during this lag phase before ThT binding associates can form. The addition of EGCG disturbs the fibrillation kinetics (**Fig. 4.39**) by binding already to the monomers as monitored by NMR (**Fig. 4.40**). Mature fibrils were found in an unbranched, curvilinear morphology of several micrometers length and 10-20 nm of diameters (**Fig. 4.37D**). Such a morphology has been observed for other amyloidogenic peptides including A β and α -synuclein (Hamley 2012) and other peptide hormones (Maji et al. 2009). PTH (1-84) contains an α -helical secondary structure at the N-terminus (Marx et al. 2000; Pioszak and Xu 2008), while fibril formation showed the characteristics of a β -sheet conformation. The presence of cross- β structure was observed in the CD spectrum and confirmed by the meridional and equatorial reflections in the X-ray diffraction data (**Fig. 4.37B** and **E**). Often, fibrils show β -sheet rich structures regardless of the secondary structure composition of the native peptide/protein structure (Marshall and Serpell 2009).

Aggregated or fibrillar PTH (1-84) might correspond to a storage form of the hormone, which implies that monomers can dissociate from the associated forms. For somatostatin-14 and corticotropin-releasing factor for example dissociation from the fibrillar storage form in secretory granules into monomers has been reported (Maji et al. 2009). The PTH fibrils release 10% of monomer over 24 hours, which supports the possible storage form in the granules (Gopalswamy et al. 2015).

Amyloid prediction programs PASTA and Waltz predicted the region of residues 30-40 prone for amyloid formation and some tendency for residues 1-10 (**Fig. 4.38B**). The mass spectrometry analysis identified that 13 residues (25R-37L) are involved in the fibril core formation. Because, this sequence is well protected against chymotrypsin digestion, even though it was having two cleavage sites (L28 and F34) within the sequence (**Fig. 4.38A**). So, only 13 out of 84 residues are part of the PTH fibril which form β -sheet structures as confirmed by CD or FT-IR spectroscopy and a comparison

with the spectra of A β (1-40) fibrils helped to identify the corresponding spectral features (**Fig. 4.37B** and **Fig. 4.38A**). Similar cases have been reported in the literature where only a part of the amino acids is in the fibril core. Orb2 is a functional amyloid that plays a key role in *Drosophila* memory formation. The first 22 amino acids are in the fibril core even though the full length protein is comprises over 500 residues (Cervantes et al. 2016). Another example is N-terminal PABPN1 (nuclear polyalanine binding protein) comprising of 125 amino acids, however fibrils are formed by the first 10 amino acids (Rohrberg et al. 2008).

EGCG is known to inhibit amyloid fibril formation (Ehrnhoefer et al. 2008; Meng et al. 2010) and indeed the growth of PTH (1-84) fibrils was inhibited by this small chemical compound. NMR analysis of monomeric PTH titrated to EGCG shows that the majority of changes in chemical shifts were observed particularly for those residues which end up in the core of mature fibrils (**Fig. 4.40**). This indicates that EGCG masks the aggregation prone sections of PTH (1-84) and thus stops the fibril formation at least for 48 hours. Similar results have been previously reported for human calcitonin which also belongs to the same class of GPCR family, where EGCG interact with the aromatic rings of EGCG and the side chains of aromatic and hydrophobic residues (Y12, F16, F22, and A31) (Huang et al. 2012). Another study on SEVI amyloid precursor peptide PAP(248-286) fibrils, which enhance the HIV infectivity has shown that EGCG inhibited the SEVI formation by interacting at two regions (K251–R257 and N269–I277) of primarily charged residues, particularly lysine (Popovych et al. 2012). For PTH (1-84) we found that EGCG primarily interacts with aromatic residues (H14, H32, F34) and hydrophobic sections (F34, V35, A36, L37, L42, A43) flanked by negatively charged K13 and R44. These interactions probably mask the hydrophobic patches in the PTH monomers and inhibit the self-association.

6 Conclusion

The thesis involved the various aspects of parathyroid hormone including receptor and membrane interaction for two-step binding model, phosphorylation and amyloid formation (**Fig. 7.1**). This has been concluded in three different sections

PTH binds to its receptor in order to regulate the blood Ca^{2+} level. A detailed and structural analysis of the binding mode of the PTH to its receptor is not clear. In the section 4.1-4.10 and 5.1 were presented the straight forward answer to the two-step binding model at a molecular level. Here, three different PTH fragments, namely PTH (15-34) (antagonist), PTH (1-34) (agonist) and full length PTH (agonist) were used for the agonist and antagonist interaction studies. CD and NMR data showed the presence of an α -helix in the N-terminal part of PTH (1-84), whereas the C-terminal part is largely unstructured. The PTH-receptor interactions are in a low micromolar range determined by ITC, SPR, and NMR. The core binding residues are Leu15 to Phe34 and boundaries starts from Leu11 and goes up to G38. The C-terminal part of PTH is not involved in binding. PTH binding to the membrane adopts a bioactive α -helical conformation. From the NMR data, it became obvious that the first N-terminal 40 amino acids are interacting with the membrane and the same residues also interact to the receptor, which supports the two-step binding model. Dynamic studies from solid-state NMR showed that the PTH-membrane complex is flexible which may facilitate mobility towards receptor binding. Overall, the first step involved the membrane interaction on the cell surface followed by the receptor recognition and binding in the second step. We anticipate that other peptide hormones might follow the same molecular mechanism of GPCR activation. The role of the C-terminal residues still remained to be discovered.

The parathyroid hormone regulates the blood Ca^{2+} level by binding and activation of the corresponding GPCR. Early 1984 studies suggested that PTH is posttranslationally phosphorylated in the parathyroid glands and also a modified form of it was found in blood circulation (Rabbani et al. 1984). It has been reported that the patients with severe primary hyperparathyroidism or with parathyroid carcinoma overproduce the N-terminal truncated fragments that was distinct from the PTH (1-84) and those fragments

are suggested to be a post-translational modification in the region 12-18 of PTH molecule (Arakawa et al. 2006; Rubin et al. 2007). PTH Despite these findings, the functional significance of this process is not well characterized. In chapters 4.11 and 5.2 of this thesis, we elucidated the detailed molecular and structural characterization of the post-translational event. The mass spectrometric analysis revealed that PTH gets phosphorylated to three sites. The NMR spectroscopy assigned the modified sites to the serine residues at the N-terminus of the hormone. Furthermore, NMR showed that the three phosphate groups remotely disturb the α -helical propensity up to Ala36, while the serines from the C-terminus of PTH remained unmodified. The N-terminus of the peptide hormone is important for receptor recognition and activation. Intriguingly, intracellular cAMP accumulation assays elucidated that the phosphorylation ablated the PTH-mediated signaling. This highlights the biological significance of this phosphorylation. These studies thus shed light on functional implications of phosphorylation at native PTH as an additional level of regulation.

Misfolded proteins often resulted in the formation of amyloid deposits in various tissues. In contrast, one of the fundamental mechanisms of storing secretory proteins and peptides are in the form of membrane coated granules as functional amyloids. In sections 4.12 and 5.3 of this thesis, a detailed characterization of in vitro generated amyloid fibrils from human parathyroid hormone PTH (1–84) is described. Formation of amyloid fibrils followed a fast kinetic and then slowly dissociate again into functional monomers. Such a slow regulation may require maintaining functional PTH molecules in the blood. Several endocrine hormones like GLP, VIP, CRF, and Galanin follow the same storage and highly regulated releasing mechanism (Maji et al. 2009). In abnormal conditions such as diet, stress or age, the functional amyloids may cause diseases, but this remains to be determined. Under the pathological conditions, EGCG can be used as a potential drug against amyloids.

7 Summary

The thesis addressed various mechanistic aspects of the human parathyroid hormone including the two-step binding model, phosphorylation, and functional amyloid formation. This has been summarised in different sections.

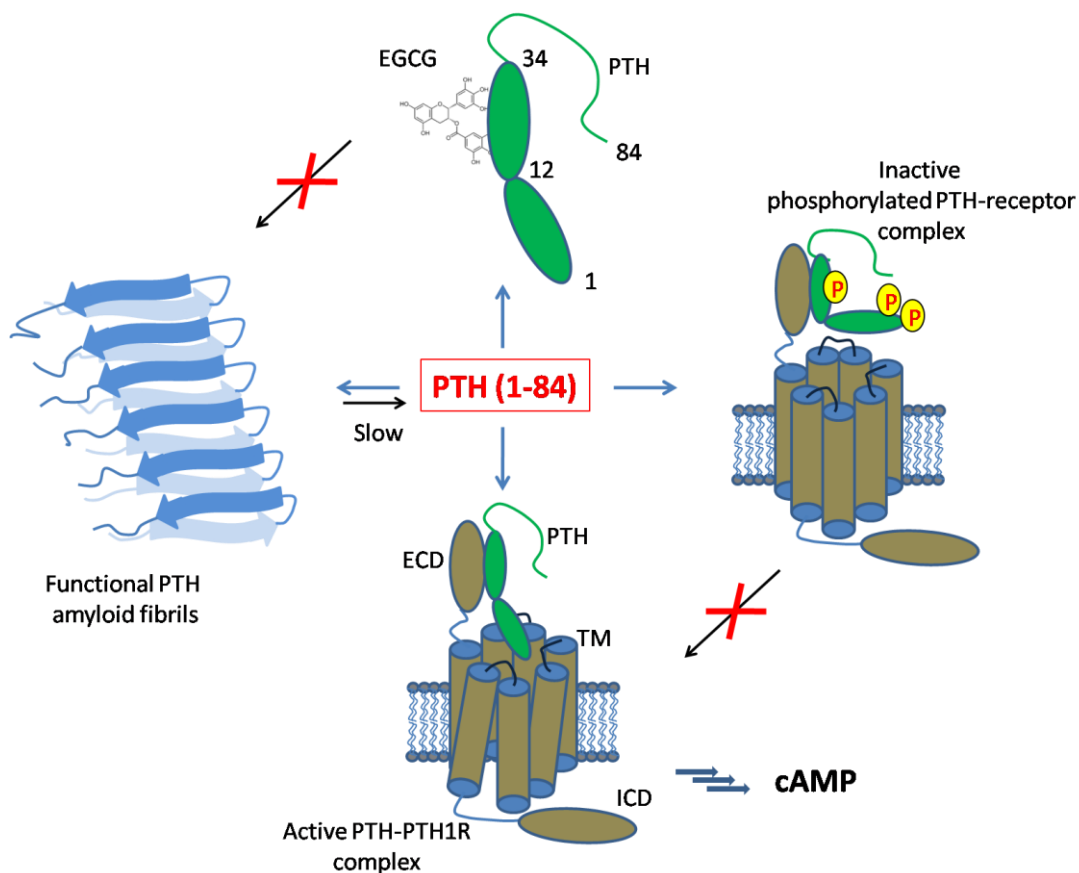


Fig. 7.1. PTH and its action to the PTH1 receptor.

PTH binds to its receptor in order to regulate the blood Ca^{2+} level. A detailed and structural analysis of the binding mode of PTH to its receptor remained elusive. A straight forward answer to the two-step binding model could be given at a molecular level. The first step involves the membrane interaction on the cell surface followed by the receptor recognition and binding in the second step. Often, in diseases such as hyperparathyroidism, it is necessary to control the function of PTH. We anticipate that the present studies might be helpful in order to develop drug molecules blocking either the membrane binding step or the receptor activation step. Additionally, for many of the GPCR agonists,

their molecular mechanism of binding to their receptor is unclear. Therefore, the present studies might be helpful in better understanding the mechanism of action of other GPCR agonists. The present studies showed that the N-terminus residues 1-38 of PTH (1-84) are involved in receptor binding and activation but the role of the C-terminal residues still remained to be explored.

The parathyroid hormone regulates the blood Ca^{2+} level *via* GPCR binding and subsequent activation of cAMP mediated intracellular signaling cascades. Early 1984 studies suggested that PTH is posttranslationally modified in the parathyroid glands and also this modified form of it was found in blood circulation. Despite this observation, the functional significance of this process was not well characterized. In chapter 4.11 and 5.2, the molecular and structural details of this important event were elucidated. Present studies revealed PTH undergoes three sites of phosphorylation at the N-terminus of the hormone disrupting the α -helical propensity up to Ala36. This event ablated the PTH-mediated cAMP signaling. The studies thus uncovered the important finding that the function of PTH can be controlled by phosphorylation. In the cancer patients, this post-translationally modified form may increase up to 40 – 60 % of whole PTH. Thus, if we develop a diagnostic kit for the detection of phosphorylated PTH, it might help in early detection of cancer based on the PTH level. Additionally, this studies may shed a light on functional implications of phosphorylation at native PTH as an additional level of regulation to the current ‘PTH and its regulation’ paradigm.

In section 4.12 and 5.3, a detailed characterization is presented for in vitro generated amyloid fibrils from PTH (1–84). Formation of amyloid fibrils followed a fast kinetic. Fully mature fibrils could be obtained after a short lag phase within five minutes. These fibrils showed the characteristic of a repeating cross- β structure and exhibited curvilinear and long structures and residues 25R–37L from the cross- β core structure of the fibrils. One of the fundamental mechanisms of storing secretory proteins and peptides are in the form of membrane coated granules as functional amyloids. These are released once the physiological level of hormone drops down or it is required as a trigger of biochemical reactions. On the other hand, most of the diseases related to the secreted proteins are caused by the accumulation of misfolded proteins often resulted in the for-

mation of amyloid and the progressive degeneration of the associated tissues. Early studies indicated the formation of amyloid deposits under pathological conditions of parathyroid glands. In the present studies, we have demonstrated the formation of PTH amyloids as well as their slow dissociation upon dilution. However, it is yet to be physiologically discovered that whether amyloid deposits are functional or these form due to some pathological condition such as cancer.

8 Zusammenfassung

Diese Arbeit befasst sich mit verschiedenen mechanistischen Aspekten des menschlichen Parathormons (PTH) einschließlich des zweistufigen Bindungsmodells, der Phosphorylierung und der funktionellen Amyloidbildung. Dies wurde in verschiedenen Abschnitten zusammengefasst.

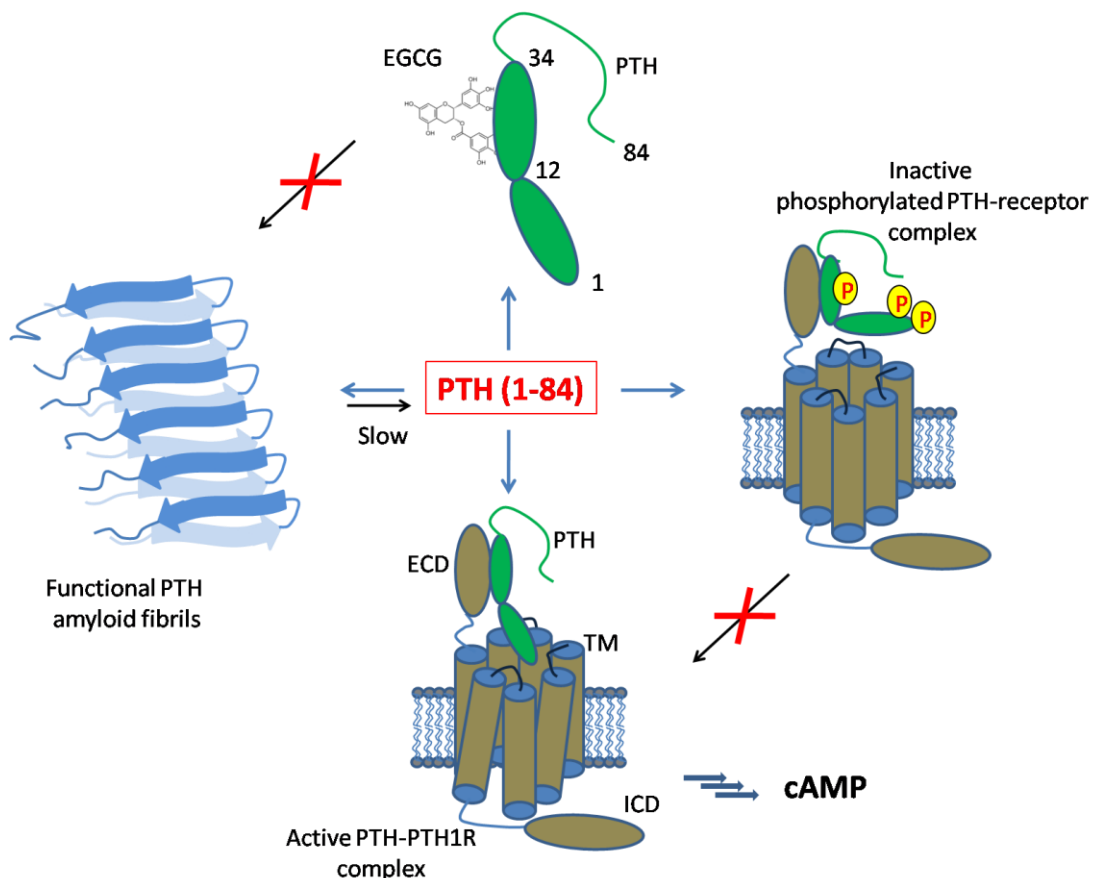


Fig. 8.1. PTH and its action to the PTH1 receptor

PTH bindet an seinen Rezeptor, um den Ca^{2+} - und Phosphat-Spiegel im Blut zu regulieren. Eine detaillierte strukturelle Analyse der Bindungsweise von PTH an seinen Rezeptor ist bislang noch nicht beschrieben. Eine geradlinige Antwort auf das zweistufige Bindungsmodell könnte auf molekularer Ebene gegeben werden. Der erste Schritt beinhaltet die Membraninteraktion auf der Zelloberfläche, gefolgt von der Rezeptorerkennung und Bindung im zweiten Schritt.

Bei Krankheiten wie zum Beispiel Hyperparathyreoidismus ist es notwendig, die Funktion von PTH zu kontrollieren. Die vorliegenden Ergebnisse könnten hilfreich sein, um Wirkstoffmoleküle zu entwickeln, die entweder den Membranbindungsschritt oder den Rezeptoraktivierungsschritt blockieren. Zusätzlich ist der molekulare Mechanismus der Bindung an ihren Rezeptor für viele der GPCR-Agonisten unklar. Daher könnten die vorliegenden Studien hilfreich sein, um den Wirkmechanismus anderer GPCR-Agonisten besser zu verstehen. Die vorliegenden Untersuchungen zeigten, dass die N-terminalen Reste 1-38 von PTH(1-84) an der Rezeptorbindung und -aktivierung beteiligt sind, aber die Rolle der C-terminalen Reste noch weiter untersucht werden müssen.

Das Parathormon reguliert den Ca^{2+} Spiegel im Blut über die Bindung an ihre G-Protein gekoppelten Rezeptoren 1 und 2 und die anschließende Aktivierung von cAMP-vermittelten intrazellulären Signalkaskaden. Frühe Studien aus dem Jahre 1984 deuteten darauf hin, dass PTH in den Nebenschilddrüsen posttranslational modifiziert wird und dass auch diese modifizierte Form im Blutkreislauf gefunden wird. Trotz dieser Beobachtung war die funktionale Bedeutung dieses Prozesses nicht gut charakterisiert. Die molekularen und strukturellen Details dieses wichtigen Ereignisses konnten aufgeklärt werden. Gegenwärtige Studien zeigten, dass PTH an drei Stellen des N-Terminus einer Phosphorylierung unterliegt, was die α -helikale Vorzugskonformation bis zu Ala36 unterbricht. Dieses Ereignis blockiert die PTH-vermittelte cAMP-Aktivierung. Das zeigt, dass die Funktion von PTH durch Phosphorylierung kontrolliert werden kann. Bei Krebspatienten kann diese posttranslational modifizierte Form bis zu 40 - 60% des gesamten PTHs betragen. Wenn also ein diagnostisches Kit für den Nachweis von phosphoryliertem PTH entwickeln werden könnte, könnte es bei der Früherkennung von Krebs auf der Grundlage des PTH-Niveaus helfen. Darüber hinaus

können diese Studien die funktionellen Implikationen der Phosphorylierung des nativen PTHs -als eine zusätzliche Regulationsebene zum aktuellen Paradigma von PTH und dessen Regulation- aufklären.

In einem weiteren Teil der Arbeit wird eine detaillierte Charakterisierung für *in vitro* erzeugte Amyloidfibrillen aus PTH(1-84) vorgestellt. Die Bildung von Amyloidfibrillen folgt einer überraschend schnellen Kinetik. Vollständig gereifte Fibrillen konnten nach einer kurzen Latenzphase innerhalb von fünf Minuten erhalten werden. Diese leicht gekrümmten Fibrillen zeigen eine sich wiederholende *cross-β* Struktur, wobei die Reste 25R - 37L die Kernstruktur der Fibrillen bilden. Einer der grundlegenden Mechanismen sekretorischer Proteine und Peptide ist ihre Speicherung in mit einer Membran umgebenen Granula in Form von funktionellen Amyloiden. Diese werden freigegeben, sobald das physiologische Niveau des Hormons abfällt oder es als Auslöser biochemischer Reaktionen erforderlich ist. Auf der anderen Seite werden die meisten Krankheiten, die mit sekretierten Proteinen zusammenhängen, durch Anhäufung von fehlgefalteten Proteinen verursacht und resultieren oftmals in der Bildung von Amyloid und der fortschreitenden Degeneration des assoziierten Gewebes. Frühe Studien wiesen auf die Bildung von Amyloidablagerungen unter pathologischen Zuständen der Nebenschilddrüsen hin. In den vorliegenden Studien haben wir die Bildung von PTH-Amyloiden sowie deren langsame Dissoziation bei Verdünnung nachgewiesen. Allerdings bleibt es noch physiologisch zu klären, ob Amyloidablagerungen funktionell sind oder ob diese aufgrund eines pathologischen Zustands wie Krebs entstehen.

9 Appendix

9.1 CSI for PTH (15-34)

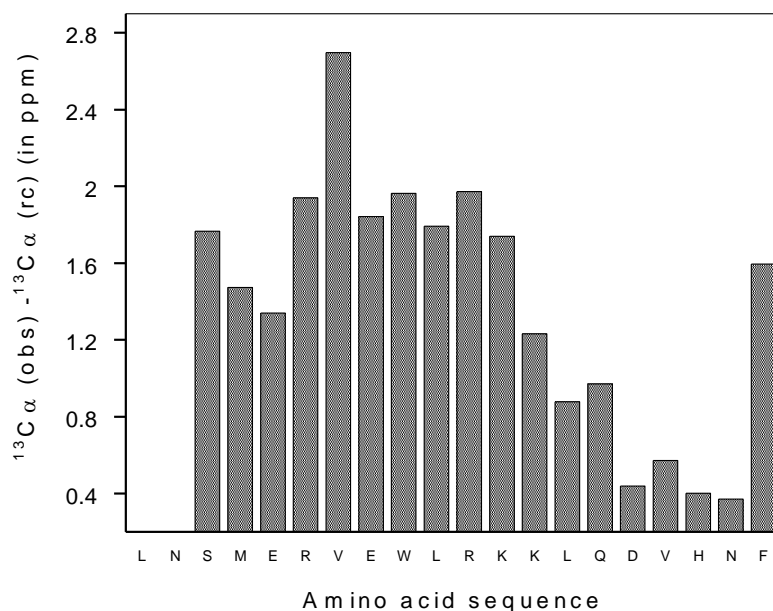


Fig. 9.1. The plot of secondary structure indices calculated for PTH (15-34). Chemical shift differences are calculated by subtracting the observed chemical shift from its random coil value. Positive chemical shift difference values correspond to an α helix.

The chemical shift index (CSI) was used to predict the secondary structure. This is a correlation between the deviations of $^{13}\text{C}\alpha$ chemical shift from their random coil values with the secondary structure of the protein (Wishart et al. 1995). Upfield shifted indicates in the figure (CSI fig) shows existence of α helix in the peptide

9.2 Interaction of PTH (15-34) to the nPTH1R studied by SPR

Surface Plasmon resonance (SPR) experiment was carried out to study the interaction of PTH (15-34) to the nPTH1R. The nPTH1R was biotinylated and immobilized on the surface of the biocore sensor chip. Increasing concentration of PTH (1-34) was passed over on the sensor chip and the signal response was recorded. Steady-state values were

obtained from the plateau of sensorgrams and plotted against the concentration of PTH (15-34). The data points were fitted to the single site binding model (**Fig. 9.2**), yielding a K_d value of $61 \pm 12 \mu\text{M}$, which in good agreement with the ITC data ($80 \pm 12 \mu\text{M}$)

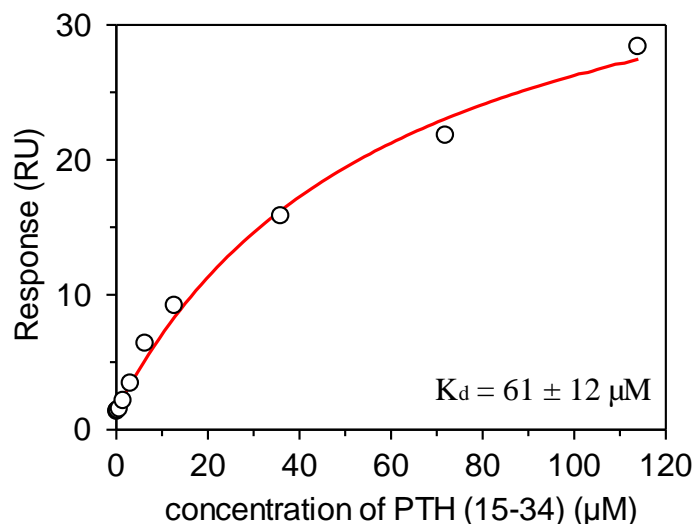


Fig. 9.2. Determination of dissociation constant for PTH (15-34)-nPTH1R complex studied by SPR. A. Biotinylated nPTH1R was immobilized on the Biocore sensor chip SA and serial injections of PTH (15-34) at a concentration of 0.2, 0.4, 0.8, 1.6, 3.2, 6.4, 12.8, 36, 72, 114 μM on the sensor chip. Steady-state value of the sensorgrams were taken (circle) and plotted against concentration of PTH (15-34). The experimental data are fitted (red) globally to a 1:1 single site binding model. The obtained K_d value was $61 \pm 12 \mu\text{M}$. Experiment was performed at 20°C

9.3 CD spectra and Heteronuclear NOE for PTH (1-34)

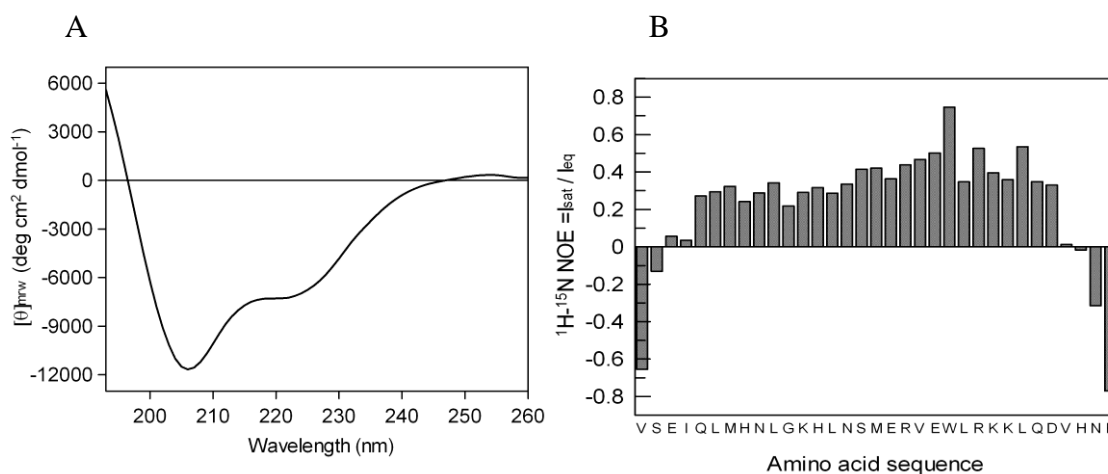


Fig. 9.3 Far-UV CD spectrum and heteronuclear NOE of PTH (1-34). A. CD spectrum of PTH (1-34) measured with $11 \mu\text{M}$ in 10mM sodium phosphate, 150 mM sodium sulfate, pH 6.0 at 20°C . B. Heteronuclear NOE correlation map of PTH (1-34) measured in NMR buffer at 25°C

Far-UV CD spectra of PTH (1-34) (**Fig. 9.3A**) exhibited a peak maximum at 193 nm and two troughs at 206 nm (not at 208 nm, due to the unstructured content) and 222 nm, which is characteristic of a peptide containing α helical with a considerable percentage of random coil structural elements. The heteronuclear NOE correlation map (average value of 0.33) shows that the peptide is highly flexible (**Fig. 9.3B**).

9.4 CSI for full length PTH (1-84)

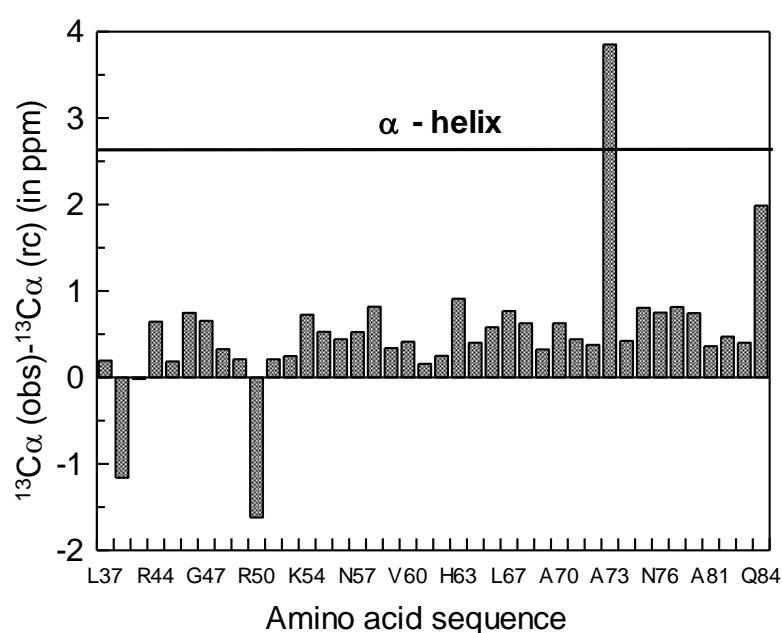


Fig. 9.4 Chemical shift perturbations of $^{13}\text{C}\alpha$ resonances of PTH (1-84). Residues from L37 to Q84 were plotted, rest of the amino acids not seen in the spectra due to low sample concentration. Chemical shift difference are calculated by subtracting the observed chemical shift from its random coil value. Horizontal line at 2.6 ppm represents chemical shift index expected for regular α helix. Slight positive chemical shift difference values correspond to presence of residual α helix structure under these conditions

Chemical shift index were calculated for full length PTH using method described by Wishart and co-workers (Wishart et al. 1995). The plot of chemical shift perturbation for every residues from R44 to Q84 versus amino acid sequence were shown in **Fig. 9.4**. $^{13}\text{C}\alpha$ resonance for residues from V2 to 42A were not assign due to poor signal to noise ratio in the 3D experiments. In general, CSI for $^{13}\text{C}\alpha$ resonance are about 2.6 ppm for regular proteins (Qian Yi, JMB 2000. 299, 1341-51). However, PTH (1-84) shows con-

siderable downfield shift compared to the random coil values suggesting that there is some residual helical content in the C-terminus of PTH (1-84) under NMR conditions.

9.5 Binding of PTH (1-84) to the nPTH1R in the presence of POPG vesicle

Binding reaction of PTH (1-84) to the nPTH1R was studied in the presence of 1 mM POPG vesicle (anionic lipid). The reaction was exothermic and the calculated thermodynamic parameters nicely match between POPC and DMPC binding reaction except for stoichiometry. This may be due to partial inactive nPTH1R caused by negatively charged lipid vesicle

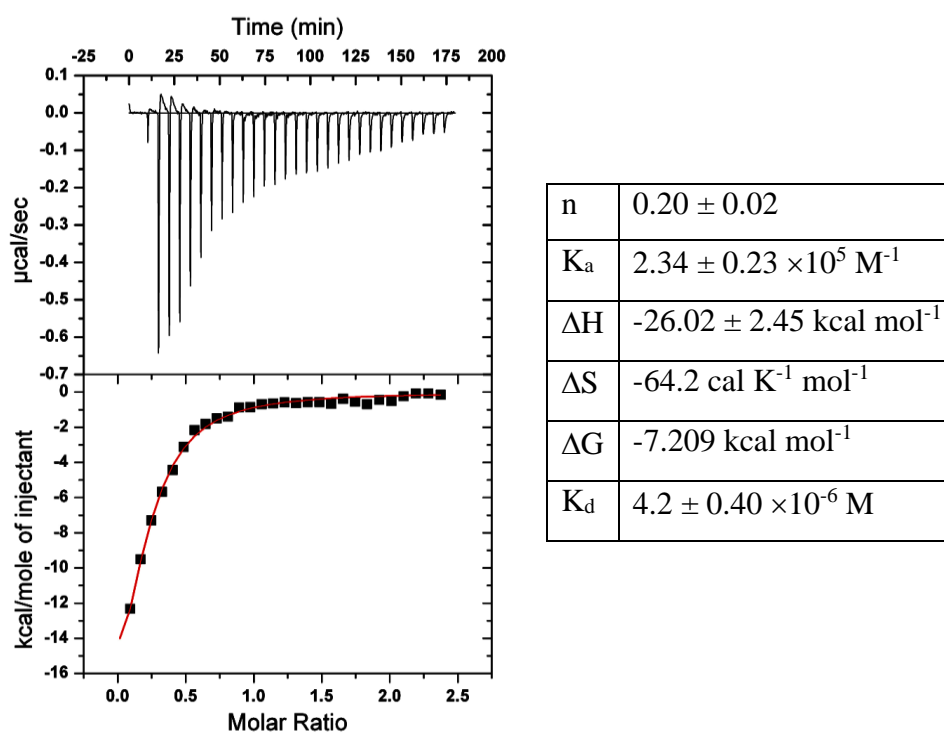


Fig. 9.5 ITC profile for the binding of PTH (1-84) to the nPTH1R in lipid environment.

Upper panel: Heat flow versus time profiles from 10 μl aliquots of containing 280 μM PTH (1-84) on to the 26 μM nPTH1R solution. Prior to the titration both cell and syringe solutions were incubated (2-4h) with 1 mM POPG vesicles. Samples measured in 20 mM sodium phosphate buffer, 300 mM sodium sulfate, pH 6.0 and at 20 $^\circ\text{C}$. Bottom panel: Plots of the heat change as function of ligand to the nPTH1R molar ratio, shown after subtraction of background heats determined in ligand to buffer experiments. The red line is the best fit to the experimental data assuming 1:1 binding model. The calculated thermodynamic parameters are given in the following table.

10 Abbreviation

ΔG	Change in free energy
ΔH	Change in enthalpy
ΔS	Change in Entropy
cAMP	Cyclic denosine monophosphate
CD	Circular dichroism
CP	Cross polarization
CSP	Chemical shift perturbation
CTD	C-terminal domain
D	Diffusion coefficient
DMPC	1 2-dimyristoyl-sn-glycero-3-phosphocholine
DMPG	1 2-dimyristoyl-sn-glycero-3-phosphoglycerol
DP	Direct polarization
DPC	dodecylphosphocholine
ECD	Extracellular domain
EDTA	Ethylenediaminetetraacetic acid
EGCG	Epigallocatechin-3-gallate
FTIR	Fourier transform infrared spectroscopy
GPCR	G-protein coupled receptor
hNOE	Heteronuclear overhauser effect
HSQC	Heteronuclear single quantum coherence
IB	Inclusion bodies
INEPT	Insensitive nuclei enhanced by polarization transfer
IPTG	Isopropylthiogalactoside
ITC	Isothermal titration calorimetry
k_a	Rate of forward reaction
K_a	Equilibrium association constant
k_b	Rate of reverse reaction
K_d	equilibrium dissociation constant
NMR	Nuclear magnetic resonance
nPTH1R	N-terminal domain of PTH1R
NTD	N-terminal domain
PFG	Pulsed field gradient
POPC	1-Palmitoyl-2-oleoyl-sn-glycero-3-phosphocholine
POPG	1-palmitoyl-2-oleoyl-sn-glycero-3-phosphoglycerol
PTH	Parathyroid hormone
PTH1R	Parathyroid hormone 1 receptor
PTH2R	Parathyroid hormone 2 receptor
PTHrP	Parathyroid hormone related peptide
SPR	Surface plasmon resonance
SSNMR	Solid state NMR
SUMO	Small ubiquitin-like modifier
TIP	tuberoinfundibular peptide
Xray	X ray diffraction

11 Bibliography

- Ahn, T. G., S. E. Antonarakis, et al. (1986). "Familial Isolated Hypoparathyroidism - a Molecular Genetic-Analysis of 8 Families with 23 Affected Persons." Medicine **65**(2): 73-81.
- Appel, W. (1986). "Chymotrypsin: molecular and catalytic properties." Clin Biochem **19**(6): 317-22.
- Arakawa, T., P. D'Amour, et al. (2006). "Overproduction and secretion of a novel amino-terminal form of parathyroid hormone from a severe type of parathyroid hyperplasia in uremia." Clinical Journal of the American Society of Nephrology **1**(3): 525-531.
- Bader, R., A. Bettio, et al. (2001). "Structure and dynamics of micelle-bound neuropeptide Y: Comparison with unligated NPY and implications for receptor selection." Journal of Molecular Biology **305**(2): 307-329.
- Bai, Y. W., J. S. Milne, et al. (1993). "Primary Structure Effects on Peptide Group Hydrogen-Exchange." Proteins-Structure Function and Genetics **17**(1): 75-86.
- Bai, Y. W., J. S. Milne, et al. (1994). "Protein Stability Parameters Measured by Hydrogen-Exchange." Proteins-Structure Function and Genetics **20**(1): 4-14.
- Balbach, J. (2000). "Compaction during protein folding studied by real-time NMR diffusion experiments." Journal of the American Chemical Society **122**(24): 5887-5888.
- Barden, J. A., R. M. Cuthbertson, et al. (1997). "Solution structure of parathyroid hormone related protein (residues 1-34) containing an Ala substituted for an Ile in position 15 (PTHrP[Ala(15)]-(1-34))." Journal of Biological Chemistry **272**(47): 29572-29578.
- Bennett, A. E., C. M. Rienstra, et al. (1995). "Heteronuclear Decoupling in Rotating Solids." Journal of Chemical Physics **103**(16): 6951-6958.
- Berger, S. and S. Braun (2004). "200 and More NMR Experiments : A Practical Course." **3th edition**: Wiley-VCH.
- Bhattacharya, S., Z. P. Dai, et al. (2010). "A Conformational Switch in the Scaffolding Protein NHERF1 Controls Autoinhibition and Complex Formation." Journal of Biological Chemistry **285**(13): 9981-9994.
- Bieschke, J., J. Russ, et al. (2010). "EGCG remodels mature alpha-synuclein and amyloid-beta fibrils and reduces cellular toxicity." Proc Natl Acad Sci U S A **107**(17): 7710-5.
- Boothby, W. M. (1921). "The parathyroid glands: a review of th literature." Endocrinology **5**(4): 403-440.
- Bosse-Doenecke, E., U. Weininger, et al. (2008). "High yield production of recombinant native and modified peptides exemplified by ligands for G-protein coupled receptors." Protein Expr Purif **58**(1): 114-121.
- Bridges, T. M. and C. W. Lindsley (2008). "G-protein-coupled receptors: From classical modes of modulation to allosteric mechanisms." Acs Chemical Biology **3**(9): 530-541.
- Burtis, W. J. (1992). "Parathyroid Hormone-Related Protein - Structure, Function, and Measurement." Clinical Chemistry **38**(11): 2171-2183.
- Castro, M., V. O. Nikolaev, et al. (2005). "Turn-on switch in parathyroid hormone receptor by a two-step parathyroid hormone binding mechanism." Proceedings of

- the National Academy of Sciences of the United States of America **102**(44): 16084-16089.
- Cavanagh, J., W. J. Frairbrother, et al. (2007). "Protein NMR Spectroscopy." **2th edition**: Academic Press.
- Cervantes, S. A., T. H. Bajakian, et al. (2016). "Identification and Structural Characterization of the N-terminal Amyloid Core of Orb2 isoform A." Scientific Reports **6**: 38265.
- Cherezov, V., D. M. Rosenbaum, et al. (2007). "High-resolution crystal structure of an engineered human beta2-adrenergic G protein-coupled receptor." Science **318**(5854): 1258-65.
- Christopeit, T., P. Hortschansky, et al. (2005). "Mutagenic analysis of the nucleation propensity of oxidized Alzheimer's beta-amyloid peptide." Protein Sci **14**(8): 2125-31.
- Clore, G. M. and A. M. Gronenborn (1991). "Structures of larger proteins in solution: three- and four-dimensional heteronuclear NMR spectroscopy." Science **252**(5011): 1390-1399.
- Collip, J. B. (1925). "The extraction of parathyroid hormone which will prevent or control parathyroid tetany and which regulates the level of blood calcium." Journal of Biological Chemistry **63**(2): 395-438.
- Culhane, K. J., Y. T. Liu, et al. (2015). "Transmembrane signal transduction by peptide hormones via family B G protein-coupled receptors." Frontiers in Pharmacology **6**.
- Datta, R., A. Waheed, et al. (2007). "Signal sequence mutation in autosomal dominant form of hypoparathyroidism induces apoptosis that is corrected by a chemical chaperone." Proc Natl Acad Sci U S A **104**(50): 19989-94.
- Davis, J. H., K. R. Jeffrey, et al. (1976). "Quadrupolar Echo Deuteron Magnetic-Resonance Spectroscopy in Ordered Hydrocarbon Chains." Chemical Physics Letters **42**(2): 390-394.
- De Amici, M., C. Dallanoce, et al. (2010). "Allosteric Ligands for G Protein-Coupled Receptors: A Novel Strategy with Attractive Therapeutic Opportunities." Medicinal Research Reviews **30**(3): 463-549.
- Delaglio, F., S. Grzesiek, et al. (1995). "Nmrpipe - a Multidimensional Spectral Processing System Based on Unix Pipes." Journal of Biomolecular Nmr **6**(3): 277-293.
- Desbuquois, B. (1974). "Interaction of Vasoactive Intestinal Polypeptide and Secretin with Liver-Cell Membranes." European Journal of Biochemistry **46**(3): 439-450.
- Drechsler, N., J. Frobel, et al. (2011). "Binding specificity of the ectodomain of the parathyroid hormone receptor." Biophysical Chemistry **154**(2-3): 66-72.
- Ehrnhoefer, D. E., J. Bieschke, et al. (2008). "EGCG redirects amyloidogenic polypeptides into unstructured, off-pathway oligomers." Nat Struct Mol Biol **15**(6): 558-66.
- Evans, J. (1995). "Biomolecular NMR Spectroscopy." Oxford University Press.
- Ezer, U. (2014). "G-Protein Coupled Receptor (GPCR) Targeting: Technologies and Global Markets." Global Markets: A BCC Research Report **BIO136A**: Aug 26.
- Fandrich, M., M. Schmidt, et al. (2011). "Recent progress in understanding Alzheimer's beta-amyloid structures." Trends Biochem Sci **36**(6): 338-45.

- Feeney, J., J. G. Batchelor, et al. (1979). "Effects of Intermediate Exchange Processes on the Estimation of Equilibrium-Constants by Nmr." Journal of Magnetic Resonance **33**(3): 519-529.
- Feng, W., R. Tejero, et al. (1998). "Solution NMR structure and backbone dynamics of the major cold-shock protein (CspA) from Escherichia coli: evidence for conformational dynamics in the single-stranded RNA-binding site." Biochemistry **37**(31): 10881-10896.
- Gardella, T. J. and H. Juppner (2001). "Molecular properties of the PTH/PTHrP receptor." Trends in Endocrinology and Metabolism **12**(5): 210-217.
- Gardella, T. J., M. D. Luck, et al. (1996). "Inverse agonism of amino-terminally truncated parathyroid hormone (PTH) and PTH-related peptide (PTHrP) analogs revealed with constitutively active mutant PTH/PTHrP receptors." Endocrinology **137**(9): 3936-3941.
- Gautier, A., H. R. Mott, et al. (2010). "Structure determination of the seven-helix transmembrane receptor sensory rhodopsin II by solution NMR spectroscopy." Nat Struct Mol Biol **17**(6): 768-74.
- Gautier, R., D. Douguet, et al. (2008). "HELIQUEST: a web server to screen sequences with specific alpha-helical properties." Bioinformatics **24**(18): 2101-2102.
- Gemmecker, G., W. Jahnke, et al. (1993). "Measurement of Fast Proton-Exchange Rates in Isotopically Labeled Compounds." Journal of the American Chemical Society **115**(24): 11620-11621.
- Gensure, R. C., T. J. Gardella, et al. (2005). "Parathyroid hormone and parathyroid hormone-related peptide, and their receptors." Biochem Biophys Res Commun **328**(3): 666-78.
- Gether, U. (2000). "Uncovering molecular mechanisms involved in activation of G protein-coupled receptors." Endocrine Reviews **21**(1): 90-113.
- Gill, S. C. and P. H. von Hippel (1989). "Calculation of protein extinction coefficients from amino acid sequence data." Anal Biochem **182**(2): 319-326.
- Gilman, A. G. (1987). "G-Proteins - Transducers of Receptor-Generated Signals." Annual Review of Biochemistry **56**: 615-649.
- Goold, C. P., T. B. Usdin, et al. (2001). "Regions in rat and human parathyroid hormone (PTH) 2 receptors controlling receptor interaction with PTH and with antagonist ligands." Journal of Pharmacology and Experimental Therapeutics **299**(2): 678-690.
- Gopalswamy, M., A. Kumar, et al. (2015). "Structural characterization of amyloid fibrils from the human parathyroid hormone." Biochimica Et Biophysica Acta-Proteins and Proteomics **1854**(4): 249-257.
- Grace, C. R. R., M. H. Perrin, et al. (2004). "NMR structure and peptide hormone binding site of the first extracellular domain of a type B1 G protein-coupled receptor." Proceedings of the National Academy of Sciences of the United States of America **101**(35): 12836-12841.
- Grace, C. R. R., M. H. Perrin, et al. (2007). "Structure of the N-terminal domain of a type B1 G protein-coupled receptor in complex with a peptide ligand." Proceedings of the National Academy of Sciences of the United States of America **104**(12): 4858-4863.
- Grace, C. R. R., M. H. Perrin, et al. (2010). "NMR Structure of the First Extracellular Domain of Corticotropin-releasing Factor Receptor 1 (ECD1-CRF-R1) Com-

- plexed with a High Affinity Agonist." Journal of Biological Chemistry **285**(49): 38580-38589.
- Grauschopf, U. (2000a). "Strukturelle und funktionelle Untersuchungen am humanen Parathormon-Rezeptor." Doctoral Dissertation, Martin-Luther univeristy, Halle, Germany.
- Grauschopf, U., H. Lilie, et al. (2000). "The N-terminal fragment of human parathyroid hormone receptor 1 constitutes a hormone binding domain and reveals a distinct disulfide pattern." Biochemistry **39**(30): 8878-8887.
- Greenwald, J. and R. Riek (2010). "Biology of amyloid: structure, function, and regulation." Structure **18**(10): 1244-60.
- Gross, J. D., P. R. Costa, et al. (1995). "Multidimensional Nmr in Lipid Systems - Coherence Transfer through J-Couplings under Mas." Journal of Magnetic Resonance Series B **106**(2): 187-190.
- Grzesiek, S. and A. Bax (1992). "Correlating Backbone Amide and Side-Chain Resonances in Larger Proteins by Multiple Relayed Triple Resonance Nmr." Journal of the American Chemical Society **114**(16): 6291-6293.
- Grzesiek, S. and A. Bax (1993a). "The Importance of Not Saturating H₂O in Protein Nmr - Application to Sensitivity Enhancement and Noe Measurements." Journal of the American Chemical Society **115**(26): 12593-12594.
- Grzesiek, S. and A. Bax (1993c). "The importance of not saturating water in protein NMR. Application to sensitivity enhancement and NOE measurements." Journal of the American Chemical Society **115**: 12593-12594.
- Grzesiek, S., S. J. Stahl, et al. (1996). "The CD4 determinant for downregulation by HIV-1 Nef directly binds to Nef. Mapping of the Nef binding surface by NMR." Biochemistry **35**(32): 10256-10261.
- Guerreiro, P. M., A. V. M. Canario, et al. (2010). "Piscine PTHrP regulation of calcium and phosphate transport in winter flounder renal proximal tubule primary cultures." American Journal of Physiology-Regulatory Integrative and Comparative Physiology **299**(2): R603-R611.
- Hamley, I. W. (2012). "The amyloid beta peptide: a chemist's perspective. Role in Alzheimer's and fibrillization." Chem Rev **112**(10): 5147-92.
- Hammes, G. G. (2007). "Physical chemistry for the biological sciences." Methods Biochem Anal **50**: 3-345.
- Hartley, D. M., C. Zhao, et al. (2008). "Transglutaminase induces protofibril-like amyloid beta-protein assemblies that are protease-resistant and inhibit long-term potentiation." J Biol Chem **283**(24): 16790-800.
- Haupt, C., I. Morgado, et al. (2011). "Amyloid fibril recognition with the conformational B10 antibody fragment depends on electrostatic interactions." J Mol Biol **405**(2): 341-8.
- Hennig, J. (2010). "Strukturelle Untersuchungen an den extrazellulären Ligandenbindenden Domänen der Parathormon Rezeptoren 1 und 2 sowie der L-Glutamin:GlykosylParomamine-3"-Aminotransferase TobS2." Doctoral Dissertation, Martin-Luther univeristy, Halle, Germany.
- Henze, M. (2016). "Die humanen Parathormon-Rezeptoren 1 und 2 : heterologe Expression und Charakterisierung von Peptidliganden und ihrer extrazellulären Bindungsdomänen." PhD Thesis: 66.
- Hiller, S., R. G. Garces, et al. (2008). "Solution structure of the integral human membrane protein VDAC-1 in detergent micelles." Science **321**(5893): 1206-1210.

- Hiramatsu, H. and T. Kitagawa (2005). "FT-IR approaches on amyloid fibril structure." *Biochim Biophys Acta* **1753**(1): 100-7.
- Hoare, S. R. J., D. A. Rubin, et al. (2000). "Evaluating the ligand specificity of zebrafish parathyroid hormone (PTH) receptors: Comparison of PTH, PTH-related protein, and tuberoinfundibular peptide of 39 residues." *Endocrinology* **141**(9): 3080-3086.
- Hoare, S. R. J. and T. B. Usdin (2000). "Tuberoinfundibular peptide (7-39) [TIP(7-39)], a novel, selective, high-affinity antagonist for the parathyroid hormone-1 receptor with no detectable agonist activity." *Journal of Pharmacology and Experimental Therapeutics* **295**(2): 761-770.
- Hollenstein, K., C. de Graaf, et al. (2014). "Insights into the structure of class B GPCRs." *Trends in Pharmacological Sciences* **35**(1): 12-22.
- Hope, M. J., M. B. Bally, et al. (1985). "Production of Large Unilamellar Vesicles by a Rapid Extrusion Procedure - Characterization of Size Distribution, Trapped Volume and Ability to Maintain a Membrane-Potential." *Biochimica Et Biophysica Acta* **812**(1): 55-65.
- Huang, J., S. Chen, et al. (2013). "Crystal structure of oligomeric beta1-adrenergic G protein-coupled receptors in ligand-free basal state." *Nat Struct Mol Biol* **20**(4): 419-25.
- Huang, R., S. Vivekanandan, et al. (2012). "NMR characterization of monomeric and oligomeric conformations of human calcitonin and its interaction with EGCG." *J Mol Biol* **416**(1): 108-20.
- Huster, D., K. Arnold, et al. (1998). "Influence of docosahexaenoic acid and cholesterol on lateral lipid organization in phospholipid mixtures." *Biochemistry* **37**(49): 17299-17308.
- Huster, D., S. Theisgen, et al. (2010). "A solid-state NMR study of the structure and dynamics of the myristoylated N-terminus of the guanylate cyclase-activating protein-2." *Biochimica Et Biophysica Acta-Biomembranes* **1798**(2): 266-274.
- Ilyina, E., V. Roongta, et al. (1997). "A pulsed-field gradient NMR study of bovine pancreatic trypsin inhibitor self-association." *Biochemistry* **36**(11): 3383-3388.
- Inooka, H., T. Ohtaki, et al. (2001). "Conformation of a peptide ligand bound to its G-protein coupled receptor." *Nature Structural Biology* **8**(2): 161-165.
- Isogai, S., X. Deupi, et al. (2016). "Backbone NMR reveals allosteric signal transduction networks in the beta(1)-adrenergic receptor." *Nature* **530**(7589): 237.
- Ito, Y. and P. Selenko (2010). "Cellular structural biology." *Curr Opin Struct Biol* **20**(5): 640-8.
- Jeener, J., B. H. Meier, et al. (1979). "Investigation of Exchange Processes by 2-Dimensional Nmr-Spectroscopy." *Journal of Chemical Physics* **71**(11): 4546-4553.
- Jianyi Yang and Y. Zhang (2014). "GPCRSD: a database for experimentally solved GPCR structures." <http://zhanglab.ccmb.med.umich.edu/GPCRSD/> Feb 27.
- Jin, L., S. L. Briggs, et al. (2000). "Crystal structure of human parathyroid hormone 1-34 at 0.9-A resolution." *J Biol Chem* **275**(35): 27238-44.
- Johnson, B. A. and R. A. Blevins (1994). "Nmr View - a Computer-Program for the Visualization and Analysis of Nmr Data." *Journal of Biomolecular Nmr* **4**(5): 603-614.

- Kaplan, J. I. (1980). "Nmr Line-Shape in the Regime Where the Chemical-Exchange Time Gamma-E Approaches the Motional Correlation Time Gamma-C." Physical Review A **22**(3): 1022-1024.
- Kay, L. E., M. Ikura, et al. (1990). "3-Dimensional Triple-Resonance Nmr-Spectroscopy of Isotopically Enriched Proteins." Journal of Magnetic Resonance **89**(3): 496-514.
- Kay, L. E., D. A. Torchia, et al. (1989). "Backbone dynamics of proteins as studied by ¹⁵N inverse detected heteronuclear NMR spectroscopy: application to staphylococcal nuclease." Biochemistry **28**(23): 8972-8979.
- Kedar, I., M. Ravid, et al. (1976). "In vitro synthesis of "amyloid" fibrils from insulin, calcitonin and parathormone." Isr J Med Sci **12**(10): 1137-40.
- Kempf, G. J., J. P. Loria, et al. (2004). "Measurement of Intermediate Exchange Phenomena." Methods in Molecular Biology : Book- Protein NMR Techniques **278**: 185-231.
- Kim, E. S. and G. M. Keating (2015). "Recombinant Human Parathyroid Hormone (1-84): A Review in Hypoparathyroidism." Drugs **75**(11): 1293-1303.
- Koide, S., W. Jahnke, et al. (1995). "Measurement of Intrinsic Exchange-Rates of Amide Protons in a N-15-Labeled Peptide." Journal of Biomolecular Nmr **6**(3): 306-312.
- Kolakowski, L. F. (1994). "Gcrdb - a G-Protein-Coupled Receptor Database." Receptors & Channels **2**(1): 1-7.
- Kumar, A., M. Gopalswamy, et al. (2014). "N-Terminal Phosphorylation of Parathyroid Hormone (PTH) Abolishes Its Receptor Activity." Acs Chemical Biology **9**(11): 2465-2470.
- Kumar, S., A. Pioszak, et al. (2011). "Crystal Structure of the PAC1R Extracellular Domain Unifies a Consensus Fold for Hormone Recognition by Class B G-Protein Coupled Receptors." Plos One **6**(5).
- Kuwasako, K., K. Kitamura, et al. (2009). "Flow cytometric analysis of the calcitonin receptor-like receptor domains responsible for cell-surface translocation of receptor activity-modifying proteins." Biochemical and Biophysical Research Communications **384**(2): 249-254.
- Kuziemko, G. M., M. Stroh, et al. (1996). "Cholera toxin binding affinity and specificity for gangliosides determined by surface plasmon resonance." Biochemistry **35**(20): 6375-6384.
- Lehmann, A., K. Boblewski, et al. (2009). "Hypertensive activity of synthesized PTH(25-34) and Ac-PTH(25-30)-NH₂ in rats." Peptides **30**(2): 378-384.
- LeVine, H., 3rd (1993). "Thioflavine T interaction with synthetic Alzheimer's disease beta-amyloid peptides: detection of amyloid aggregation in solution." Protein Sci **2**(3): 404-10.
- Lewis, E. A. and K. P. Murphy (2005). "Isothermal titration calorimetry." Methods Mol Biol **305**: 1-16.
- Lilie, H., E. Schwarz, et al. (1998). "Advances in refolding of proteins produced in E. coli." Curr Opin Biotechnol **9**(5): 497-501.
- Lim, S. K., E. J. Lee, et al. (2004). "The 10th and 11th residues of short length N-terminal PTH(1-12) analogue are important for its optimum potency." J Pept Res **64**(1): 25-32.

- Liokatis, S., A. Dose, et al. (2010). "Simultaneous Detection of Protein Phosphorylation and Acetylation by High-Resolution NMR Spectroscopy." Journal of the American Chemical Society **132**(42): 14704-14705.
- Lodish, H., A. Berk, et al. (2000). "Molecular and cell biology." **4th edition**: W. H. Freeman and Company. New York.
- Maji, S. K., M. H. Perrin, et al. (2009). "Functional amyloids as natural storage of peptide hormones in pituitary secretory granules." Science **325**(5938): 328-32.
- Mann, R., M. J. Wigglesworth, et al. (2008). "Ligand-receptor interactions at the parathyroid hormone receptors: Subtype binding selectivity is mediated via an interaction between residue 23 on the ligand and residue 41 on the receptor." Molecular Pharmacology **74**(3): 605-613.
- Mann, R., M. J. Wigglesworth, et al. (2008). "Ligand-receptor interactions at the parathyroid hormone receptors: subtype binding selectivity is mediated via an interaction between residue 23 on the ligand and residue 41 on the receptor." Mol Pharmacol **74**(3): 605-13.
- Marblestone, J. G., S. C. Edavettal, et al. (2006). "Comparison of SUMO fusion technology with traditional gene fusion systems: Enhanced expression and solubility with SUMO." Protein Science **15**(1): 182-189.
- Marcotte, I. and M. Auger (2005). "Bicelles as model membranes for solid- and solution-state NMR studies of membrane peptides and proteins." Concepts in Magnetic Resonance Part A **24A**(1): 17-37.
- Marcotte, I., F. Separovic, et al. (2004). "A multidimensional H-1 NMR investigation of the conformation of methionine-enkephalin in fast-tumbling bicelles." Biophysical Journal **86**(3): 1587-1600.
- Marion, D., M. Ikura, et al. (1989). "Rapid Recording of 2d Nmr-Spectra without Phase Cycling - Application to the Study of Hydrogen-Exchange in Proteins." Journal of Magnetic Resonance **85**(2): 393-399.
- Marshall, K. E. and L. C. Serpell (2009). "Structural integrity of beta-sheet assembly." Biochem Soc Trans **37**(Pt 4): 671-6.
- Marx, S. J. (2000). "Hyperparathyroid and hypoparathyroid disorders." N Engl J Med **343**(25): 1863-75.
- Marx, U. C., K. Adermann, et al. (2000). "Solution structures of human parathyroid hormone fragments hPTH(1-34) and hPTH(1-39) and bovine parathyroid hormone fragment bPTH(1-37)." Biochemical and Biophysical Research Communications **267**(1): 213-220.
- Mason, A. J., J. J. Lopez, et al. (2005). "A spectroscopic study of the membrane interaction of tuberoinsfundibular peptide of 39 residues (TIP39)." Biochimica Et Biophysica Acta-Biomembranes **1714**(1): 1-10.
- Mattson, M. P., D. S. Gary, et al. (2001). "Perturbed endoplasmic reticulum function, synaptic apoptosis and the pathogenesis of Alzheimer's disease." Neuronal Signal Transduction and Alzheimer's Disease(67): 151-162.
- Mccabe, M. A. and S. R. Wassall (1995). "Fast-Fourier-Transform Depaking." Journal of Magnetic Resonance Series B **106**(1): 80-82.
- McConnell, H. M. (1958). "Reaction Rates by Nuclear Magnetic Resonance." Journal of Chemical Physics **28**(3): 430-431.
- Meng, F., A. Abedini, et al. (2010). "The flavanol (-)-epigallocatechin 3-gallate inhibits amyloid formation by islet amyloid polypeptide, disaggregates amyloid fibrils,

- and protects cultured cells against IAPP-induced toxicity." *Biochemistry* **49**(37): 8127-33.
- Mills, F. D., V. C. Antharam, et al. (2008). "The helical structure of surfactant peptide KL4 when bound to POPC: POPG lipid vesicles." *Biochemistry* **47**(32): 8292-8300.
- Monaghan, P., I. Woznica, et al. (2007). "Recombinant expression and purification of the N-terminal extracellular domain of the parathyroid hormone receptor." *Protein Expression and Purification* **54**(1): 87-93.
- Morcombe, C. R. and K. W. Zilm (2003). "Chemical shift referencing in MAS solid state NMR." *Journal of Magnetic Resonance* **162**(2): 479-486.
- Mori, S., C. Abeygunawardana, et al. (1997). "NMR study of rapidly exchanging backbone amide protons in staphylococcal nuclease and the correlation with structural and dynamic properties." *Journal of the American Chemical Society* **119**(29): 6844-6852.
- Mori, S., C. Abeygunawardana, et al. (1995). "Improved sensitivity of HSQC spectra of exchanging protons at short interscan delays using a new fast HSQC (FHSQC) detection scheme that avoids water saturation." *J Magn Reson B* **108**(1): 94-98.
- Moroder, L., R. Romano, et al. (1993). "New Evidence for a Membrane-Bound Pathway in Hormone-Receptor Binding." *Biochemistry* **32**(49): 13551-13559.
- Morris, G. A. and R. Freeman (1979). "Enhancement of Nuclear Magnetic-Resonance Signals by Polarization Transfer." *Journal of the American Chemical Society* **101**(3): 760-762.
- Mossessova, E. and C. D. Lima (2000). "Ulp1-SUMO crystal structure and genetic analysis reveal conserved interactions and a regulatory element essential for cell growth in yeast." *Mol Cell* **5**(5): 865-876.
- Murray, T. M., L. G. Rao, et al. (2005). "Parathyroid hormone secretion and action: Evidence for discrete receptors for the carboxyl-terminal region and related biological actions of carboxyl-terminal ligands." *Endocrine Reviews* **26**(1): 78-113.
- Naud, J., T. D. Nolin, et al. (2012). "Current Understanding of Drug Disposition in Kidney Disease." *Journal of Clinical Pharmacology* **52**: 10s-22s.
- Nowacka, A., P. C. Mohr, et al. (2010). "Polarization Transfer Solid-State NMR for Studying Surfactant Phase Behavior." *Langmuir* **26**(22): 16848-16856.
- Oldenburg, K. R., R. F. Eppard, et al. (1996). "Conformational studies on analogs of recombinant parathyroid hormone and their interactions with phospholipids." *Journal of Biological Chemistry* **271**(29): 17582-17591.
- Onyuksel, H., H. Ikezaki, et al. (1999). "A novel formulation of VIP in sterically stabilized micelles amplifies vasodilation in vivo." *Pharmaceutical Research* **16**(1): 155-160.
- Ott, C. M. and V. R. Lingappa (2002). "Integral membrane protein biosynthesis: why topology is hard to predict." *Journal of Cell Science* **115**(10): 2003-2009.
- Pal, K., K. Swaminathan, et al. (2010). "Structural Basis for Hormone Recognition by the Human CRFR2 alpha G Protein-coupled Receptor." *Journal of Biological Chemistry* **285**(51): 40351-40361.
- Palczewski, K., T. Kumasaka, et al. (2000). "Crystal structure of rhodopsin: A G protein-coupled receptor." *Science* **289**(5480): 739-45.
- Park, S. H., B. B. Das, et al. (2012). "Structure of the chemokine receptor CXCR1 in phospholipid bilayers." *Nature* **491**(7426): 779-83.

- Parthier, C., S. Reedtz-Runge, et al. (2009). "Passing the baton in class B GPCRs: peptide hormone activation via helix induction?" Trends in Biochemical Sciences **34**(6): 303-310.
- Pellegrini, M., A. Bisello, et al. (1998). "Binding domain of human parathyroid hormone receptor: From conformation to function." Biochemistry **37**(37): 12737-12743.
- Pellegrini, M., A. Bisello, et al. (1998a). "Binding domain of human parathyroid hormone receptor: From conformation to function." Biochemistry **37**(37): 12737-12743.
- Pellegrini, M., M. Royo, et al. (1998). "Addressing the tertiary structure of human parathyroid hormone-(1-34)." Journal of Biological Chemistry **273**(17): 10420-10427.
- Perozzo, R., G. Folkers, et al. (2004). "Thermodynamics of protein-ligand interactions: history, presence, and future aspects." J Recept Signal Transduct Res **24**(1-2): 1-52.
- Pervushin, K., R. Riek, et al. (1997). "Attenuated T-2 relaxation by mutual cancellation of dipole-dipole coupling and chemical shift anisotropy indicates an avenue to NMR structures of very large biological macromolecules in solution." Proceedings of the National Academy of Sciences of the United States of America **94**(23): 12366-12371.
- Pierce, M. M., C. S. Raman, et al. (1999). "Isothermal titration calorimetry of protein-protein interactions." Methods **19**(2): 213-221.
- Pietrogrande, L. (2009). "Update on the efficacy, safety, and adherence to treatment of full length parathyroid hormone, PTH (1-84), in the treatment of postmenopausal osteoporosis." Int J Womens Health **1**: 193-203.
- Pietrogrande, L. (2010). "Update on the efficacy, safety, and adherence to treatment of full length parathyroid hormone, PTH (1-84), in the treatment of postmenopausal osteoporosis." Int J Womens Health **1**: 193-203.
- Pioszak, A. A., K. G. Harikumar, et al. (2010). "Dimeric Arrangement of the Parathyroid Hormone Receptor and a Structural Mechanism for Ligand-induced Dissociation." Journal of Biological Chemistry **285**(16): 12435-12444.
- Pioszak, A. A., N. R. Parker, et al. (2009). "Structural Basis for Parathyroid Hormone-related Protein Binding to the Parathyroid Hormone Receptor and Design of Conformation-selective Peptides." Journal of Biological Chemistry **284**(41): 28382-28391.
- Pioszak, A. A. and H. E. Xu (2008). "Molecular recognition of parathyroid hormone by its G protein-coupled receptor." Proceedings of the National Academy of Sciences of the United States of America **105**(13): 5034-5039.
- Piotto, M., V. Saudek, et al. (1992). "Gradient-tailored excitation for single-quantum NMR spectroscopy of aqueous solutions." J Biomol NMR **2**(6): 661-665.
- Piscitelli, P., G. Iolascon, et al. (2008). "Osteoporosis and cardiovascular diseases' cosegregation: epidemiological features." Clin Cases Miner Bone Metab **5**(1): 14-8.
- Popovych, N., J. R. Brender, et al. (2012). "Site specific interaction of the polyphenol EGCG with the SEVI amyloid precursor peptide PAP(248-286)." J Phys Chem B **116**(11): 3650-8.

- Potter, H., L. Weir, et al. (1984). "Enhancer-dependent expression of human kappa immunoglobulin genes introduced into mouse pre-B lymphocytes by electroporation." *Proc Natl Acad Sci U S A* **81**(22): 7161-5.
- Price, W. S., H. Ide, et al. (1999). "Self-diffusion of supercooled water to 238 K using PGSE NMR diffusion measurements." *Journal of Physical Chemistry A* **103**(4): 448-450.
- Rabbani, S. A., R. Kremer, et al. (1984). "Phosphorylation of parathyroid hormone by human and bovine parathyroid glands." *J Biol Chem* **259**(5): 2949-55.
- Rang, H. P. (2006). "The receptor concept: pharmacology's big idea." *Br J Pharmacol* **147 Suppl 1**: S9-16.
- Rao, B. D. N., F. J. Kayne, et al. (1979). "P-31 Nmr-Studies of Enzyme-Bound Substrates of Rabbit Muscle Pyruvate-Kinase - Equilibrium-Constants, Exchange-Rates, and Nmr Parameters." *Journal of Biological Chemistry* **254**(8): 2689-2696.
- Rasmussen, S. G., H. J. Choi, et al. (2011). "Structure of a nanobody-stabilized active state of the beta(2) adrenoceptor." *Nature* **469**(7329): 175-80.
- Rasmussen, S. G., H. J. Choi, et al. (2007). "Crystal structure of the human beta2 adrenergic G-protein-coupled receptor." *Nature* **450**(7168): 383-7.
- Reumers, J., J. Schymkowitz, et al. (2009). "Using structural bioinformatics to investigate the impact of non synonymous SNPs and disease mutations: scope and limitations." *BMC Bioinformatics* **10 Suppl 8**: S9.
- Rohrberg, J., R. Sachs, et al. (2008). "Monitoring fibril formation of the N-terminal domain of PABPN1 carrying an alanine repeat by tryptophan fluorescence and real-time NMR." *Febs Letters* **582**(11): 1587-1592.
- Rubin, M. R., S. J. Silverberg, et al. (2007). "An N-terminal molecular form of parathyroid hormone (PTH) distinct from hPTH(1-84) is overproduced in parathyroid carcinoma." *Clinical Chemistry* **53**(8): 1470-1476.
- Ruiz-Gomez, G., J. D. Tyndall, et al. (2010). "Update 1 of: Over one hundred peptide-activated G protein-coupled receptors recognize ligands with turn structure." *Chem Rev* **110**(4): PR1-41.
- Runge, S., H. Thogersen, et al. (2008). "Crystal structure of the ligand-bound glucagon-like peptide-1 receptor extracellular domain." *Journal of Biological Chemistry* **283**(17): 11340-11347.
- Sackewitz, M., H. A. Scheidt, et al. (2008). "Structural and dynamical characterization of fibrils from a disease-associated alanine expansion domain using proteolysis and solid-state NMR spectroscopy." *Journal of the American Chemical Society* **130**(23): 7172-7173.
- Salim, N. N. and A. L. Feig (2009). "Isothermal titration calorimetry of RNA." *Methods* **47**(3): 198-205.
- Salzmann, M., K. Pervushin, et al. (1998). "TROSY in triple-resonance experiments: New perspectives for sequential NMR assignment of large proteins." *Proceedings of the National Academy of Sciences of the United States of America* **95**(23): 13585-13590.
- Sarell, C. J., L. A. Woods, et al. (2013). "Expanding the repertoire of amyloid polymorphs by co-polymerization of related protein precursors." *J Biol Chem* **288**(10): 7327-37.

- Sargent, D. F. and R. Schwyzer (1986). "Membrane Lipid Phase as Catalyst for Peptide Receptor Interactions." Proceedings of the National Academy of Sciences of the United States of America **83**(16): 5774-5778.
- Schagger, H. (2006). "Tricine-SDS-PAGE." Nat Protoc **1**(1): 16-22.
- Schagger, H. and G. von Jagow (1987). "Tricine-sodium dodecyl sulfate-polyacrylamide gel electrophoresis for the separation of proteins in the range from 1 to 100 kDa." Anal Biochem **166**(2): 368-379.
- Scheidt, H. A., A. Sickert, et al. (2011). "The interaction of lipid modified pseudopeptides with lipid membranes." Organic & Biomolecular Chemistry **9**(20): 6998-7006.
- Schleucher, J., M. Sattler, et al. (1993). "Coherence Selection by Gradients without Signal Attenuation - Application to the 3-Dimensional Hnco Experiment." Angewandte Chemie-International Edition in English **32**(10): 1489-1491.
- Schleucher, J., M. Schwendinger, et al. (1994). "A General Enhancement Scheme in Heteronuclear Multidimensional Nmr Employing Pulsed-Field Gradients." Journal of Biomolecular Nmr **4**(2): 301-306.
- Schmid, F. X. (1997). "Optical spectroscopy to characterize protein conformation and conformational changes, in." Protein Structure: A Practical Approach: (Greighton, T.E., Ed.) Oxford University Press, Oxford, U.K.
- Schwyzler, R. (1986). "Molecular Mechanism of Opioid Receptor Selection." Biochemistry **25**(20): 6335-6342.
- Scian, M., M. Marin, et al. (2006). "Backbone dynamics of human parathyroid hormone (1-34): flexibility of the central region under different environmental conditions." Biopolymers **84**(2): 147-160.
- Scian, M., M. Marin, et al. (2006). "Backbone dynamics of human parathyroid hormone (1-34): Flexibility of the central region under different environmental conditions." Biopolymers **84**(2): 147-160.
- Selenko, P., D. P. Frueh, et al. (2008). "In situ observation of protein phosphorylation by high-resolution NMR spectroscopy." Nature Structural & Molecular Biology **15**(3): 321-329.
- Shenkarev, Z. O., T. A. Balashova, et al. (2002). "Spatial structure of zervamicin IIB bound to DPC micelles: Implications for voltage-gating." Biophysical Journal **82**(2): 762-771.
- Singer, S. J. and G. L. Nicolson (1972). "Fluid Mosaic Model of Structure of Cell-Membranes." Science **175**(4023): 720-731.
- Siu, F. Y., M. He, et al. (2013). "Structure of the human glucagon class B G-protein-coupled receptor." Nature **499**(7459): 444-9.
- Spiegel, R. (2003). "Phychopharmacology: An Introduction." **4th edition**: John Wiley & Sons Ltd, England.
- States, D. J., R. A. Haberkorn, et al. (1982). "A Two-Dimensional Nuclear Overhauser Experiment with Pure Absorption Phase in 4 Quadrants." Journal of Magnetic Resonance **48**(2): 286-292.
- Sun, C. H., D. Y. Song, et al. (2007). "Solution structure and mutational analysis of pituitary adenylate cyclase-activating polypeptide binding to the extracellular domain of PAC1-Rs." Proceedings of the National Academy of Sciences of the United States of America **104**(19): 7875-7880.
- Tesmer, J. J. (2010). "The quest to understand heterotrimeric G protein signaling." Nat Struct Mol Biol **17**(6): 650-2.

- Trovato, A., F. Seno, et al. (2007). "The PASTA server for protein aggregation prediction." *Protein Eng Des Sel* **20**(10): 521-3.
- Ubersax, J. A. and J. E. Ferrell, Jr. (2007). "Mechanisms of specificity in protein phosphorylation." *Nat Rev Mol Cell Biol* **8**(7): 530-41.
- Vogel, A., C. P. Katzka, et al. (2005). "Lipid modifications of a Ras peptide exhibit altered packing and mobility versus host membrane as detected by 2H solid-state NMR." *Journal of the American Chemical Society* **127**(35): 12263-12272.
- Vuister, G. W. and A. Bax (1992). "Resolution Enhancement and Spectral Editing of Uniformly C-13-Enriched Proteins by Homonuclear Broad-Band C-13 Decoupling." *Journal of Magnetic Resonance* **98**(2): 428-435.
- Walsh, C. T., S. Garneau-Tsodikova, et al. (2005). "Protein posttranslational modifications: the chemistry of proteome diversifications." *Angew Chem Int Ed Engl* **44**(45): 7342-72.
- Weininger, U. (2009). "Strukturelle Charakterisierung von Proteinfaltungsintermediaten mit NMR-Spektroskopie." Doctoral Dissertation, Martin-Luther univeristy, Halle, Germany.
- Wennerström, H. (1972). "Nuclear Magnetic-Relaxation Induced by Chemical Exchange." *Molecular Physics* **24**(1): 69-80.
- Wilkins, D. K., S. B. Grimshaw, et al. (1999). "Hydrodynamic radii of native and denatured proteins measured by pulse field gradient NMR techniques." *Biochemistry* **38**(50): 16424-31.
- Wishart, D. S., C. G. Bigam, et al. (1995). "H-1, C-13 and N-15 Random Coil Nmr Chemical-Shifts of the Common Amino-Acids .1. Investigations of Nearest-Neighbor Effects." *Journal of Biomolecular Nmr* **5**(1): 67-81.
- Yamamoto, T., P. Nair, et al. (2008). "The Importance of Micelle-Bound States for the Bioactivities of Bifunctional Peptide Derivatives for delta/mu Opioid Receptor Agonists and Neurokinin 1 Receptor Antagonists." *Journal of Medicinal Chemistry* **51**(20): 6334-6347.
- Yang, J. T., C. S. Wu, et al. (1986). "Calculation of protein conformation from circular dichroism." *Methods Enzymol* **130**: 208-269.
- Yao, S., A. G. Fane, et al. (1997). "An investigation of the fluidity of concentration polarisation layers in crossflow membrane filtration of an oil-water emulsion using chemical shift selective flow imaging." *Magnetic Resonance Imaging* **15**(2): 235-242.
- Yasothan, U. and S. Kar (2008). "Osteoporosis: Overview and pipeline." *Nature Reviews Drug Discovery* **7**(9): 725-726.
- Zandomenighi, G., M. R. Krebs, et al. (2004). "FTIR reveals structural differences between native beta-sheet proteins and amyloid fibrils." *Protein Sci* **13**(12): 3314-21.

12 Resume

Mohanraj Gopalswamy

📍 Enzianstraße 7, 85748 Garching bei München

📞 (+49) 17662319896 📠 (+49) 89-28913284

✉️ mohanraj.gopalswamy@tum.de
mohanraj.gopalswamy@physik.uni-halle.de

📅 **Date of birth** 19.03.1981 | **Nationality** Indian

Work experience

05.2013 – 06.2016

Research assistant

Prof. Dr. Michael Sattler, Technical University of Munich, München (Germany)

06.2006 – 04.2013

Research assistant

Prof. Dr. Jochen Balbach, Martin Luther Universität Halle-Wittenberg, Halle/Saale (Germany)

09.2004 – 05.2006

Project assistant - National NMR Centre

Prof. Dr. KV. Ramanathan, Indian Institute of Science, Bangalore (India)

02.2004 – 08.2004

Trainee scientist, Chemoinformatics

Jubilant Biosys Limited, Bangalore (India)

Education qualification

06.2006 –

Ph.D.

Institute for Physics, Martin Luther University of Halle-Wittenberg, Halle/Saale (Germany)

06.2001 – 04.2003

Master of science - Chemistry

University of Madras, Chennai (India)

06.1997 – 04.2001

Bachelor of science- Chemistry

University of Madras, Chennai (India)

01.06.2015–05.06.2015

EMBO practical course

Modern biophysical methods for protein-ligand interactions, Oulu (Finland)

13 Publications

- Dhurvas Chandrasekaran Dinesh, Michael Kovermann, **Mohanraj Gopalswamy**, Antje Hellmuth, Luz Irina A. Calderón Villalobos, Hauke Lilie, Jochen Balbach, Steffen Abel. “Solution structure of the PsIAA4 oligomerization domain reveals interaction modes for transcription factors in early auxin response”. Under second revision. *PNAS*. **2015**, *1122(19)*, 6230-5.
- **Mohanraj Gopalswamy***, Amit Kumar*, Juliane Adler, Monika Baumann, Mathias Henze, Senthil T. Kumar, Marcus Fändrich, Holger A. Scheidt, Daniel Huster, Jochen Balbach. “Structural characterization of amyloid fibrils from the human parathyroid hormone”. *Biochim Biophys Acta*. **2015**, *1854*, 249, 249-57. (*equal contributions)
- Amit Kumar, **Mohanraj Gopalswamy**, Clare Wishhart, Mathias Henze, Lennart Eschen-Lippoid, Dan Donnelly, Jochen Balbach. “N-terminal phosphorylation of parathyroid hormone (PTH) abolishes its receptor activity”. *ACS Chemical Biology*. **2014**, *9(11)*, 2465-70.
- Nils Drechsler, Julia Fröbel, Günther Jahreis, **Mohanraj Gopalswamy**, Jochen Balbach, Eva Bosse-Doenecke, Rainer Rudolph. “Binding specificity of the ectodomain of the parathyroid hormone receptor”. *Biophysical Chemistry*. **2011**, *154(2-3)*, 66-72.
- Eva Bosse-Doenecke, Ulrich Weininger, **Mohanraj Gopalswamy**, Jochen Balbach, Sanne Møller Knudsen, Rainer Rudolph. “High yield production of recombinant native and modified peptides exemplified by ligands for G-protein coupled receptors”. *Protein Expression and Purification*, **2008**, *58(1)*, 114–121.
- Amit Kumar, **Mohanraj Gopalswamy**, Annika Wolf, Mechthild Hatzfeld, Jochen Balbach. “Phosphorylation-induced local unfolding controls p19^{INK4d} during the human cell cycle”. *PNAS under review*.
- **Mohanraj Gopalswamy**, Mathias Henze, Eva Bosse-Doenecke, Rainer Rudolph, Jochen Balbach. “Structural insight into two step binding model: PTH and PTH1 receptor”. *Manuscript in preparation*.
- Qi Zhang, **Mohanraj Gopalswamy**, Jochen Balbach, Rainer Rudolph, Sven Pfeifer. “Selection of an artificial binding protein against the ectodomain PTH1 receptor”. *Manuscript in preparation*.

Publications not related to the thesis

- Sivaraman Subramaniam, Axel Erler, Jun Fu, Andrea Kranz, Jing Tang, **Mohanraj Gopalswamy**, Saminathan Ramakrishnan, Adrian Keller, Guido Grundmeier, Daniel Muller, Michael Sattler, and Adrian Stewart. “DNA annealing by Red β is insufficient for homologous recombination and the additional requirements involve intra- and inter-molecular interactions”. *Sci Rep.* **2016**, Oct 6, 6:34525.
 - Leonidas Emmanouilidis, **Mohanraj Gopalswamy**, Daniel M. Passon, Matthias Wilmanns, Michael Sattler. “Structural biology of the import pathways of peroxisomal matrix proteins”. *Biochim Biophys Acta.* **2016**, 1863 (5), 804-813
 - Thenmozhi G, Jayakumar D, **Mohanraj Gopalswamy**, Jaya Santhi R. “Synthesis, characterization and biological applications of conducting poly (*p*-amino phenol) and its nano compound” *Der Pharma Chemica*, **2011** , 3(4), 116-126.
 - **Mohanraj Gopalswamy**, Chen Zheng, Peijian Zou, Iris Antes, Michael Sattler. “Structural insights into the peroxisomal import receptor complex: Pex5 and Pex14”. *Manuscript in preparation*. We will submit it to JBC.
-

Awards

- **Selected for EMBO-course 2015**: “Modern biophysical methods for protein-ligand interactions”. June 1-5, 2015, Oulu finland.
 - **Best Poster and Award 2011** : 2nd International Meeting (DFG Graduiertenkolleg 1026)
“GPCR receptor interaction of the human Parathyroid hormone”
Mohanraj Gopalswamy, Rainer Rudolph, Jochen Balbach
March 3-5, 2011, Conformational Transitions in Macromolecular Interactions, Halle (Saale), Germany.
 - **Invited speaker 2011**: BIT’s 9th Annual Congress of International Drug Discovery Science and Technology. Session 11-2: “Rapid Production and Formulation Process of Biopharmaceuticals”
-

14 Declaration (Erklärung)

I declare that I have carried out this thesis by myself and have not used external help except where explicitly indicated. This thesis was not submitted to any other university. I did not make any earlier attempt to submit this work as a doctoral thesis.

Hiermit erkläre ich, diese Arbeit selbstständig und ohne fremde Hilfe verfasst zu haben. Es wurden nur die angegebenen Quellen und Hilfsmittel verwendet. Aus der Literatur wörtlich oder inhaltlich entnommene Stellen sind als solche kenntlich gemacht. Ferner erkläre ich, die vorliegende Dissertation an keiner anderen Einrichtung eingereicht und ich mich noch nicht früher um einen Doktorgrad beworben zu haben

Date 09.03.2017

Halle (Saale), Germany

Mohanraj Gopalswamy

15 Acknowledgements

The Present work was carried out during my time as a PhD student at the Institute of Physics, Martin Luther University of Halle-Wittenberg, Halle (Saale), Germany.

First I sincerely thank Prof. Dr. Jochen Balbach for giving me an opportunity to work in his research group and to work on Hot topic "Parathyroid hormone-GPCR-membrane proteins-Calcium regulation-Osteoporosis". He has provided all the necessary facilities and exceptional level of supervision. His remarkable experience, a tremendous source of encouragement, fruitful discussions, devotion to science, smart ideas, patience, friendliness and his long term support was an inspiration for my own research perspective. With his motivation and help, I was able to participate and establish fruitful collaborations with other research groups. Especially I want to thank him for all his effort he made to check my slides and to teach "How to speak in a conference". He did not only teach Science, he has shown how to balance research and family. He is also good in sports and he was kind enough to teach me how to play volleyball, billiard, canoeing, etc. I am extremely lucky to work with him. I would proudly say, Jochen is the best person to work with and his group is the best lab in the world.

I would like to thank few people from Institute of biotechnology, MLU. First I thank Late Prof. Dr. Rainar Rudolph, who co-supervised me for some time period. I thank him for his excellent suggestions and lab facilities. I thank PD. Hauke Lilie for his supervision, time to time discussion and his generous technical support. He was always available and patient enough to clear all my doubts. I also thank Dr. Eva Bosse-Doenecke, who help in the making SUMO-PTH constructs and helped a lot for HPLC. I thank Prof. Dr. Milton Stubbs for his fruitful discussions and his permission to use his lab facilities.

Next, I would like to thank important former members of Jochen's group. Dr. Christian Löw, Dr. Rolf Sachs and Dr. Caroline Haupt are the one who introduced me to the proteins. Then Dr. Mathias Henze was kind enough to teach every single step in protein

purifications. Dr. Ulrich Weininger and Dr. Michael Kovermann were helped me in learning NMR assignments and NMR measurements. I am very grateful to you all.

I want to thank Dr. Amit Kumar for numerous reasons and the list is very big. We have been good collaborators, a good friend and a good sport man. We together initiated several projects and gave us nice publications. Thank you very much for all your help Amit jii.

I thank my Tamil friends Senthil, Karthi, Dinesh and Waran for their excellent support and guidance. Those coffee time and lunch time gave me good publications and the time we all spend together was unforgettable. I also thank other Indian friends in Halle.

I would like to thank my collaborators Prof. Dr. Steffen Abel, Prof. Dr. Dan Donnelly, Dr. Sven Pfeifer, Dr. Qi Zang, Prof. Dr. Marcus Fändrich, Prof. Dr. Daniel Huster and Dr. Vogal, A. for their time, suggestions, comments and wonderful cooperations.

My special thanks goes to former GRK coordinator Martina for her personal help. I thank other biophysics members Rica Patzschke, Tobias Gruber, Heike Böcker, Andi Klamt, Stefan Gröger, Susanne Link, Monika Baumann, Constanze Westphal, Matthias Altenstein, Katrin Waldheim and Prof. Dr. Detlef Reichert for providing me a nice environment.

I thank Prof. Dr. K. V. Ramanathan, IISc, Dr. G. Sekaran, CLRI, Dr. P. N. Sudha, DKM for their help to reach up to here.

Finally, I would like to thank my family members, Gopalswamy, Usharani, Kavi, Kani, Thenmozhi, Nanda, Priya, Naveen, Aniruthan, Agastia, divya, sivabalan and all my relatives. I also want to thank my best friend L. Ramesh Kumar and several other friends for their endless support. Special thanks to Dr. Chadrakala also.

I thank State of Sachsen Anhalt, DAAD, MLU, GRK1026, DFG and European Union for funding. I want to thank everyone who unknowingly helped me.